

EMERGENCE OF THERMODYNAMICS
FOR QUANTUM SYSTEMS
OUT OF EQUILIBRIUM

*im Fachbereich Physik der Freien Universität eingereichte Dissertation
zur Erlangung des Grades eines Doktors der Naturwissenschaften*

MARCEL GOIHL

eingereicht im August 2019

Dahlem Center for Complex Quantum Systems
QMIO
Freie Universität Berlin

Eidesstattliche Erklärung

Ich versichere hiermit an Eides Statt, dass diese Arbeit von niemand anderem als meiner Person verfasst worden ist. Alle verwendeten Hilfsmittel wie Berichte, Bücher, Internetseiten oder ähnliches sind im Literaturverzeichnis angegeben, Zitate aus fremden Arbeiten sind als solche kenntlich gemacht. Die Arbeit wurde bisher in gleicher oder ähnlicher Form keiner anderen Prüfungskommission vorgelegt und auch nicht veröffentlicht.

Marcel Goihl

Reviewers
Prof. Dr. Jens Eisert
Prof. Felix von Oppen, PhD.
Day of the defense: 15th of January 2020

CONTENTS

1	ABSTRACT	2
2	INTRODUCTION TO OUT-OF-EQUILIBRIUM DYNAMICS	6
2.1	Locality	6
2.2	Equilibration On Average	8
2.3	Equilibration Time Scales	10
2.4	Thermalisation	13
2.5	Integrability	14
2.6	Anderson Localisation	15
2.7	Many-Body Localisation	16
2.8	Open Problems	19
3	STABILITY OF MANY-BODY LOCALISATION	20
3.1	Griffiths effects	20
4	EXPERIMENTAL WITNESSES OF MANY-BODY LOCALISATION	30
4.1	Disordered Optical Lattices	30
5	CONSTRUCTING CONSTANTS OF MOTION FOR MANY-BODY LOCALISED SYSTEMS	46
5.1	Constructing Local Constants Of Motion	46
6	CONSTRUCTING EDGE MODE OPERATORS FOR SYSTEMS EXHIBITING SYMMETRY PROTECTED ORDER	56
6.1	The XZX-Cluster Hamiltonian	56
7	CONCLUSIONS	78
APPENDIX		
A	CLIMATE FOOTPRINT CALCULATION	86

“Localization was a different matter: very few believed it at the time, and even fewer saw its importance; among those who failed to fully understand it at first was certainly its author. It has yet to receive adequate mathematical treatment, and one has to resort to the indignity of numerical simulations to settle even the simplest questions about it.”

P. W. Anderson, Nobel Lecture, 1977

ABSTRACT

The ability of classical thermodynamics to predict phenomena using only handful of parameters is miraculous. Moreover, this framework contrasts with other theories with its ability to describe our day to day experience, i. e. we know intuitively that an ice cube melts in a cold beverage on a hot summer day. A similarly powerful yet significantly less intuitive theory is quantum mechanics which describes the world at its tiniest length scales. Given this foundational position, we would expect to be able to derive all physical theories from quantum mechanics only. Unfortunately this would require knowing the quantum state of all particles which is costly as quantum mechanics requires resources growing exponentially in the system size to describe even relatively innocent many-body systems. Given this uncontrollable growth of parameters, it is highly desirable to apply the principles of thermodynamics to quantum many-body systems as a means to describe them efficiently. Yet, the two theories are not obviously compatible. Subtle differences such as the definition of thermalisation already puzzled founding fathers like John von Neumann. While these have been understood by now, the focus shifted to gaining a thorough understanding of the process of thermalisation in the quantum regime, meaning that the state of the system can be described by a thermal ensemble locally after an initial out-of-equilibrium situation. In the recent past the field of quantum thermodynamics and specifically out-of-equilibrium dynamics has witnessed many successes notably the advent of highly controllable analogue quantum simulators which allow to probe out-of-equilibrium physics to an unprecedented precision. It has been established that thermalisation takes place in quantum many-body systems, but the underlying reasons and a comprehensive theory are still elusive.

Only very recently, a class of systems exhibiting many-body localisation has been identified that defy this paradigm of thermalisation by localising their constituent particles despite many-body interactions. This can be captured using an effective description in terms of local constants of motion. Understanding the emergence of these physically relevant operators that hinder thermalisation hopefully sheds light also on the mechanism of thermalisation itself.

In this thesis, we investigate the relation between thermodynamics and quantum mechanics in the context of out-of-equilibrium physics for many-body localisation. We give numerical evidence for the stability of localisation in large, closed one-dimensional chains. Furthermore, we connect the established phenomenology of many-body localisation to experiments with ultra-cold atoms in optical lattices and give a blue print of measurements that can be performed with existing technology to show that the simulator indeed exhibits many-body localisation. We then set out to obtain a deeper understanding of the underlying theory of many-body localisation by devising an algorithm that explicitly constructs exact constants of motion allowing us to put the existing theoretical framework of many-body localisation to the test. It is our firm belief that understanding local constants of motion is indispensable to not only understand thermalisation in quantum many-body systems but is also of great use in other fields. A connection of this type is displayed by an extension of our algorithm to finding edge modes in spin chains with symmetry protected order.

Klassische Thermodynamik erlaubt erstaunlich genaue Vorhersagen für physikalische Systeme basierend auf nur einer handvoll von Parametern. Darüber hinaus beschreibt sie ebenfalls unsere Alltagserfahrungen, beispielsweise einen schmelzenden Eiswürfel in einem kalten Getränk an einem heißen Sommertag. Eine vergleichbar mächtige, aber deutlich weniger intuitive Theorie ist die Quantenmechanik, die unsere Welt im Kleinen beschreibt und von vielen für die grundlegende Theorie gehalten wird. Es kommt uns jedoch teuer zu stehen, alle Details zu kennen, da die Zahl der Parameter die nötig sind, um ein Quantensystem zu beschreiben, exponentiell in dessen Größe wächst. Dies stellt bereits für verhältnismäßig kleine Quantensysteme ein großes Problem dar. Eine Lösung könnte darin liegen, die Prinzipien der Thermodynamik zu nutzen, um auch Quantensysteme effizient beschreiben zu können. Leider sind die beiden Theorien nicht auf Anhieb kompatibel. Kleinere Feinheiten, wie die Definition von Thermalisierung beschäftigten schon Gründungsväter wie John von Neumann, sind heutzutage aber gut verstanden. Unklar ist allerdings, wie ein Quantensystem nach einer initialen Störung einen lokal thermisch aussehenden Zustand erreicht. In der näheren Vergangenheit konnte das Feld der Quantenthermodynamik und insbesondere das der Nichtgleichgewichtsdynamik viele Erfolge feiern, insbesondere die Etablierung von Quantensimulatoren, die es erlauben Nichtgleichgewichtsphysik mit bisher unerreichter Präzision zu untersuchen. Es gilt als gesichert, dass Thermalisierung in Quantensystemen stattfindet, aber die Gründe oder eine umfassende Theorie dafür sind noch unbekannt.

Vielteilchenlokalisierung beschreibt eine neue Klasse von Systemen, die dieser Beobachtung widersprechend nicht thermalisieren, indem Teilchen in einem solchen System lokalisiert werden und dies obwohl das System wechselwirkend ist. Daher können diese Systeme durch lokale Konstanten der Bewegung beschrieben werden. Ein tiefgehendes Verständnis warum diese Operatoren in solchen Systemen auftauchen wird hoffentlich auch einen Beitrag zur Frage leisten, wie Thermalisierung in Quantensystemen eigentlich zustande kommt.

In dieser Doktorarbeit bringen wir Thermodynamik und Quantenmechanik einen kleinen Schritt näher zusammen. Wir legen unseren Fokus auf Nichtgleichgewichtsdynamik in Systemen mit Vielteilchenlokalisierung. Wir präsentieren numerische Resultate, die nahelegen, dass Vielteilchenlokalisierung in großen, geschlossenen, eindimensionalen Ketten stabil ist. Darüber hinaus bringen wir bekannte Effekte der Vielteilchenlokalisierung mit ultrakalten Atomen in optischen Gittern in Verbindung, indem wir skizzieren, wie man mit vorhandenen Techniken Vielteilchenlokalisierung in diesem Quantensimulator nachweist. Daraufhin wollen wir ein tieferes Verständnis für Vielteilchenlokalisierung erlangen, indem wir einen Algorithmus entwickeln, der exakte Konstanten der Bewegung konstruiert, anhand derer wir die Vorhersagen für Vielteilchenlokalisierung testen können. Wir glauben fest daran, dass es unausweichlich ist, lokale Konstanten der Bewegung zu verstehen, um Thermalisierung zu erklären, aber darüber hinaus auch weitere physikalische Effekte zugänglich zu machen. Wir schließen mit einer Anwendung einer Erweiterung unseres Algorithmus' für Spinketten mit symmetriegeschützter Ordnung, in der wir deren Randmoden konstruieren.

LIST OF PUBLICATIONS

This cumulative thesis contains the following first-author publications:

- Marcel Goihl, Marek Gluza, Christian Krumnow, and Jens Eisert
Construction of exact constants of motion and effective models for many-body localized systems,
Phys. Rev. B **97**, 134202 (2018), DOI: 10.1103/PhysRevB.97.134202
- Marcel Goihl, Jens Eisert, and Christian Krumnow
Exploration of the stability of many-body localized systems in the presence of a small bath,
Phys.Rev. B **99**, 195145 (2019), DOI: 10.1103/PhysRevB.99.195145
- Marcel Goihl, Marek Gluza, Christian Krumnow, Jens Eisert, and Nicolas Tarantino
Edge mode locality in perturbed symmetry protected topological order,
SciPost Phys. **6**, 072 (2019), DOI: 10.21468/SciPostPhys.6.6.072
- Marcel Goihl , Mathis Friesdorf, Albert H. Werner, Winton Brown, and Jens Eisert
Experimentally Accessible Witnesses of Many-Body Localization,
Quantum Reports **2019**, **1(1)**, 50-62, DOI: 10.3390/quantum1010006

Furthermore, during the completion of this doctoral research, the following other works were produced:

- Henrik Wilming, Marcel Goihl, Christian Krumnow, and Jens Eisert
Towards local equilibration in closed interacting quantum many-body systems,
arXiv:1704.06291
- Henrik Wilming, Marcel Goihl, Ingo Roth, and Jens Eisert
Entanglement-ergodic quantum systems equilibrate exponentially well,
arXiv:1802.02052

INTRODUCTION TO OUT-OF-EQUILIBRIUM DYNAMICS

While standard thermodynamics is mostly concerned with static systems, we here ask the question of how interacting, finite quantum systems can dynamically attain an equilibrium state when initially in an out-of-equilibrium situation. We will refer to a system as out of equilibrium, if the initial state has non-trivial dynamics when evolved with the Hamiltonian. This can be probed using local observables. If the expectation value of the local observable reaches a steady value with only small fluctuations in time, we will call the system equilibrated. We can then ask, whether the resulting equilibrium state can be described by its energy only, an approach referred to as thermalisation. We also investigate the rare occurrence of systems that do not thermalise and explain why this can happen. These questions are particularly timely as analogue quantum simulators such as ion traps, NV-centers and optical lattices are delivering experimental platforms which allow to probe out-of-equilibrium many-body physics at an unprecedented level of precision. These setups excel at creating initial states with low entanglement and evolving them under many-body interacting Hamiltonians - a domain which is very hard to access analytically or numerically as interacting systems generically require a treatment in the full Hilbert space, which is exponentially large in the number of constituents.

In this chapter, we lay out the theoretical framework required to understand equilibration and thermalisation for finite, interacting many-body systems, which are exactly those that can be simulated in analogue quantum simulators. Much of this introduction applies to any dimension, but this thesis will exclusively work with one dimensional systems. We will start by defining locality.

2.1 LOCALITY

Let us start by recalling what we mean by a quantum many-body system. We are interested in the collective behaviour of quantum particles confined to lattices, usually defined as a graph with vertices and edges. For most condensed matter systems, the vertices have associated Hilbert spaces and the edges describe the possible connections between vertices. Since one-dimensional systems are the main focus of our work, we restrict our attention to the special case of a finite chain of length L , where the vertices are referred to as sites and the edges connect neighbouring sites only. The natural definition of distance between sites applies. A chain is composed of local Hilbert spaces at each site that can be finite or infinite dimensional in general, though we will mostly use spin or fermionic degrees of freedom, which have a local dimension of two. The full space is then given by the Fock space, or in the spin case by a tensor product over all local spaces. This allows us to capture states in terms of their local occupation numbers according to the rules of second quantisation.

In order to speak about phenomena such as particle transport, it is necessary to have a notion of locality. Let us discuss this explicitly for the case of one dimen-

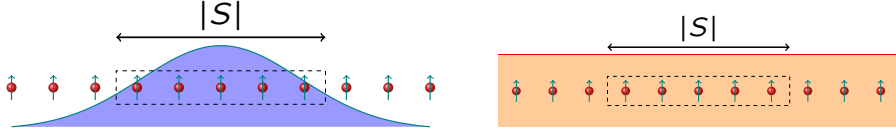


Figure 2.1: Sketch of a quasi-local operator (left) and a non-local operator (right). For the left operator, the weight of the terms depicted by the blue colour decays sufficiently quickly away from the center, rendering the operator quasi-local. For the operator on the right, the weights depicted by the red colour do not decay at all, rendering it non-local.

sional spin systems. Here, we have a natural local operator basis characterised by the Pauli matrices

$$\sigma^x = \begin{pmatrix} 0 & 1 \\ 1 & 0 \end{pmatrix}, \quad \sigma^y = \begin{pmatrix} 0 & 1 \\ -1 & 0 \end{pmatrix}, \quad \sigma^z = \begin{pmatrix} 1 & 0 \\ 0 & -1 \end{pmatrix},$$

and the identity $\sigma^1 = \mathbb{1}_2$. To promote this to an operator basis acting on the full chain, we take all possible tensor products of the basis elements for each site, yielding 4^L many operators. This can be formalised by introducing a vector $\mu \in \{\alpha\}^L$, where $\alpha \in \{x, y, z, 1\}$ determines the corresponding Pauli-operator which allows us to define

$$\sigma(\mu) = \bigotimes_{i=1}^L \sigma_i^{\mu(i)},$$

which we will refer to as a Pauli-string. The support of any operator \mathcal{O} can now be calculated by decomposing it into these Pauli-strings. We then consider all strings that contribute to \mathcal{O} and define the support as the set of all sites, on which the contributing strings act non-trivially. The range of the support is then given by the maximal distance between these sites. If \mathcal{O} is supported on a connected set of sites, the support is contiguous. With these definitions at hand, we are now in position to define the concept of locality.

In this work, we will consider local Hamiltonians, by which we mean that their terms only have finite and contiguous support. This distinguishes our definition from the one used in quantum information theory where the requirement of contiguous support is usually dropped. Many of the Hamiltonians considered are either nearest-neighbour local or next-nearest neighbour local, meaning that their terms only have a range of support of two or three sites, respectively. However, there are also operators that in a strict sense are supported on the full lattice, but whose weight distribution over the chain allows to call them quasi-local. Consider an operator \mathcal{O} whose decomposition has non-trivial terms on every lattice site. We will call it quasi-local if its reduction to a contiguous region $|S|$ fulfills

$$\|\mathcal{O} - \text{tr}_{S^c}(\mathcal{O}) \otimes \frac{\mathbb{1}_{S^c}}{|2^{S^c}|}\| \leq c_1 e^{-c_2 |S|},$$

in a suitable norm and with $c_1, c_2 > 0$. Here, we are comparing the reduced operator to the full operator. The reduction is obtained by performing the partial trace over the complement region of S denoted by S^c , i. e. all sites that do not belong to S . Since all non-trivial local basis operators are traceless, only those terms will remain that act as the identity on S^c . We then divide by the dimension of S^c to account for the factor of $2^{|S^c|}$ that is obtained from the partial trace. After the partial trace, the operator $\text{tr}_{S^c}(\mathcal{O})$ only acts on S and has the dimension $2^{|S|}$. We then extend

it by a tensor product with an identity of dimension $2^{|S^c|}$ such that $\text{tr}_{S^c}(\mathcal{O}) \otimes \mathbb{1}_{S^c}$ again acts on the full chain. This allows us to compare it to the full operator \mathcal{O} and we will call \mathcal{O} quasi-local, if its reduction to a region S approximates the full operator exponentially well in the size of S . This means that the cumulated weight on terms that are outside of S needs to decay exponentially. One can also define quasi-locality using other functions with different decay behaviour, but for the following work, the definition with an exponential decay is most suited. As an illustration, we show the weight distribution of a quasi-local operator and a non-local operator as a sketch in Fig. 2.1.

These formal tools will allow us to study and quantify locality properties in dynamics and more precisely out-of-equilibrium physics.

2.2 EQUILIBRATION ON AVERAGE

Having pushed our system out of equilibrium initially, we now want to understand under which circumstances it dynamically evolves to a steady state again. We will refer to this process as equilibration. In this section, we discuss the prerequisites for equilibration such as the initial state, the resulting equilibrium state and how to distinguish the two. We end by giving a theorem for equilibration in finite interacting many-body systems.

In quantum mechanics, the dynamics of closed systems are governed by the time evolution operator with the Hamiltonian acting as its generator. Given a Hamiltonian H and an initial pure state $|\psi\rangle$, the state at time t is given by the solution of Schrödinger's equation

$$|\psi(t)\rangle = e^{-itH} |\psi\rangle .$$

Since we are interested in non-trivial dynamics, this implies that the initial state cannot be a single eigenstate of the Hamiltonian governing the time evolution, but rather a superposition of eigenstates. Specifically, quantum simulators can prepare product and lowly entangled states such as local particle configurations in real space. Such lowly entangled states intuitively are supported on many eigenstates as these typically have an extensive amount of entanglement. It will turn out that the amount of overlap that the initial state has with the energy eigenbasis is crucial for equilibration to take place. The initial state is then subjected to the time evolution under an interacting Hamiltonian. In a physical system, measurable observables are mostly local, meaning that they only probe part of the system, which is why we consider local reductions in the following. A reduction to a subsystem S can be obtained by performing the partial trace

$$\rho(t) = \text{tr}_{S^c} |\psi(t)\rangle\langle\psi(t)| .$$

The resulting state $\rho(t)$ has a dimension of $2^{|S|} \times 2^{|S|}$ and contains all the information that is local to $|S|$ and dismisses everything else. While $|\psi(t)\rangle$ is a pure state, $\rho(t)$ may well be a mixed state due to the dynamical entanglement built-up.

Once a classical system attains equilibrium it stays close to it to a good approximation, i. e. it has not yet been reported and reproduced that a melted ice cube reassembles over time. However, there is a striking difference for finite quantum systems where the dynamics occurs on finitely many orbits given by the overlaps with the energy eigenbasis, which means that approximate and exact recurrences can occur at some point in time [1] (actually, recurrences also occur in classical

systems with discrete phase spaces, but we will not cover this here). For realistic materials the exact recurrence time is unphysically large, but this issue makes a rigorous definition of equilibration more subtle. One possible solution is to consider time intervals which exclude the recurrences [2]. Here, we could for example consider only the equilibration dynamics up to the recurrence time. Another approach that avoids the problem of recurrence is to consider time averages instead of points in time. If the system equilibrates, we expect it to be close to its equilibrium state for almost all times which makes averaging over the rarely occurring recurrences acceptable. In this chapter, we consider equilibration on average. One particularly useful concept is the infinite time average given by

$$\bar{\rho}^\infty = \lim_{T \rightarrow \infty} \frac{1}{T} \int_0^T d\tau \rho(\tau).$$

This already allows for an intuitive formulation of equilibration. If ρ equilibrates, it should be close to its infinite time averaged state $\bar{\rho}^\infty$ for almost all times. We will formalise this in the following. Let us start by calculating the infinite time averaged state for a given initial state $|\psi\rangle$. Using the eigendecomposition of H , namely the eigenvalues or energies e_k and corresponding eigenvectors $|k\rangle$, we can rewrite the time evolution of $|\psi\rangle$ as

$$|\psi(t)\rangle\langle\psi(t)| = \sum_{k,l} e^{it(e_l - e_k)} \langle\psi|l\rangle\langle k|\psi\rangle |k\rangle\langle l|.$$

by acting on $|\psi(t)\rangle\langle\psi(t)|$ with the unitary which diagonalises H . The equilibrium state ω is then given by the diagonal of the above operator

$$\begin{aligned} \omega := \bar{\rho}^\infty &= \lim_{T \rightarrow \infty} \frac{1}{T} \int_0^T d\tau \sum_{k,l} e^{i\tau(e_l - e_k)} \langle\psi|l\rangle\langle k|\psi\rangle |k\rangle\langle l| \\ &= \sum_k |\langle k|\psi\rangle|^2 |k\rangle\langle k|, \end{aligned}$$

where we used that the average over the phases $e^{it(e_l - e_k)}$ vanishes as long as $e_l - e_k \neq 0$. This non-degeneracy assumption is well justified for interacting systems, where energy levels repel one another. Non-interacting systems on the other hand come with large amounts of degeneracies and hence require a different theoretical treatment [3, 4].

As an interlude, we need to define a distance between two states ρ and ω . Since we are interested in the distinguishability with respect to observables \mathcal{O} we employ the 1-norm which is given by

$$\|\rho - \omega\|_1 := \sup_{\mathcal{O}: \mathcal{O} \text{ observable}} \text{tr}(\mathcal{O}(\rho - \omega)).$$

Without the supremum, this is only the expectation value of the observable \mathcal{O} and the difference of our states. Therefore, the 1-norm gives the maximal distinguishability of the two states using all possible observables. A natural relaxation of the 1-norm is to consider only a restricted set of allowed observables.

With this, we are now set to formulate a theorem for equilibration in interacting and local systems. It can be shown that in the infinite time average, the time evolved state $|\psi(t)\rangle$ is close to its equilibrium state ω when reduced to a local region S in the following sense [5, 6]

$$\overline{\|\text{tr}_{S^c}(|\psi(t)\rangle\langle\psi(t)| - \omega)\|_1}^\infty \leq \frac{d^{|S|}}{d_{\text{eff}}}, \quad (2.2.1)$$

where d is the local dimension of the system and d_{eff} , the effective dimension, counts how many eigenstates the initial state $|\psi\rangle$ has overlap with

$$d_{\text{eff}}^{-1} = \sum_{\mathbf{k}} \langle \mathbf{k} | \psi \rangle^4.$$

The effective dimension is $d_{\text{eff}} = 1$, if $|\psi\rangle$ is an eigenstate itself. On the other hand, if $|\psi\rangle$ is the equal superposition over all eigenstates, its effective dimension is $d_{\text{eff}} = d^L$, which is the maximal value possible. This means that if a state has overlap with many eigenstates, it equilibrates well in the infinite time average. We would like to note in passing that single eigenstates are by definition equilibrated since they have no dynamics but if the initial state has support on few eigenstates only, it will likely not equilibrate. Thankfully, it can be shown that experimentally preparable initial states in fact have a high effective dimension [7]. This result even holds when the eigenstates are themselves characterised by low entanglement content and can be approximated by matrix product states. We can therefore conclude that finite, generic initial states equilibrate locally in interacting quantum systems after being pushed out of equilibrium [8]. What is obscured by the infinite time average though, are the associated time scales. How much use does the above discussion have, when our system only reaches equilibrium for the first time on the advent of the heat death of the universe? In practise, we observe that for interacting many-body systems equilibration happens extremely rapidly. We set out to make this plausible in the next section.

2.3 EQUILIBRATION TIME SCALES

While the above framework constitutes an important milestone in understanding out-of-equilibrium dynamics in quantum systems from first principles, it is necessary to determine the time scales involved in the equilibration process, i. e. when does the system first approach equilibrium. Generically, this happens quite fast although there exist examples (aside from theoretically constructed systems [9, 10]) that take uncharacteristically long to equilibrate [11]. Essentially, not only do we need to take into account the effective dimension, i. e. the support on the eigenstates, but also the corresponding energies which inform us about the frequency of the orbits. The key mechanism to understand how fast a system can equilibrate is called dephasing [12, 13], describing how contributions from different eigenstates with different frequencies can cancel each other which we will detail below.

So far, we have basically neglected the role of the observable which we use to probe our system with. In our final bound on infinite time averaged equilibration given in Eq. (2.2.1), the 1-norm shows up, which is a supremum over all possible observables to distinguish the two states. To obtain reasonable time scale estimates however, such a general approach ignoring the structure that local observables offer cannot be pursued. It is known for example, that the off-diagonal elements of a local observable in the energy eigenbasis decay strongly [14, 15]. In the following, we will hence consider a fixed observable A . Let us take a closer look into how we can calculate the distinguishability of $|\psi\rangle\langle\psi|$ and ω using an observable A in the following denoted by $\Delta A(t)_\psi$

$$\begin{aligned} \Delta A(t)_\psi &:= \text{tr}(A(|\psi(t)\rangle\langle\psi(t)| - \omega)) \\ &= \sum_{\substack{\mathbf{k}, \mathbf{l} \\ \mathbf{k} \neq \mathbf{l}}} \langle \mathbf{k} | A | \mathbf{l} \rangle \langle \mathbf{l} | \psi \rangle \langle \psi | \mathbf{k} \rangle e^{-i(e_{\mathbf{k}} - e_{\mathbf{l}})t} = \sum_{\Delta \neq 0} z_{\Delta} e^{-i\Delta t}, \end{aligned}$$

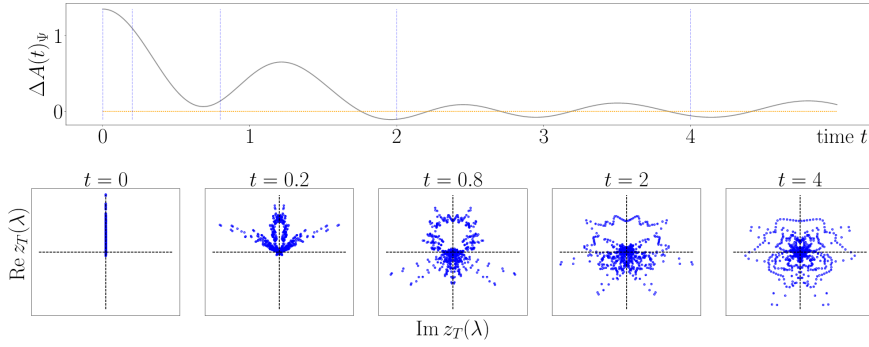


Figure 2.2: An investigation of the equilibration behaviour for a transverse field Ising model on the level local magnetisation $A = \sigma_{L/2}^z$ for a disordered unentangled initial state out of equilibrium [16]. Top: Distinguishability $\Delta A(t)_\psi$ in the transverse field Ising model on $L = 15$ sites (for details refer to Ref. [12]). The dashed orange line is the equilibrium value and the blue line corresponds to the actual value at time t . Rapid equilibration is observed. Bottom: Decomposition of $\Delta A(t)_\psi$ in its components on the complex plane for fixed points in time. The distribution quickly spreads over the complex plane, which is linked to the equilibration behaviour. Figure taken from Ref. [12].

where we used the energy representation in the first step and that ω is the diagonal of $|\psi\rangle\langle\psi|$ to exclude $k = l$. In the final step, we changed the summation from indices to energy differences $\Delta = e_k - e_l$ and furthermore defined $z_\Delta := \sum_{k,l:\Delta=e_k-e_l} \langle k|A|l\rangle \langle l|\psi\rangle\langle\psi||k\rangle$. When the system is prepared out of equilibrium at $t = 0$, the z_Δ are all positive and hence sum to a large value. We call the system equilibrated if this sum becomes very small. This happens when all the elements of the z_Δ distribution have phases $e^{-i\Delta t}$ such that they are almost isotropically spread out in the complex plane. Furthermore, if we assume non-degenerate energy gaps, which is also justified as soon as small random perturbations are added to a local Hamiltonian [5], all the velocities are distinct and therefore spreading has to occur at some point. This process is referred to as dephasing of the initial distribution. It can be thought of as a clock with many hands that move at different velocities. Equilibration takes place if the hands cover the full clock dial. Thus, we can see that equilibration time scales are governed by the energy representation of the observable and the state reflected in the distribution z_Δ .

We will now illustrate this point, by considering the evolution of the distinguishability $\Delta A(t)_\psi$ for a transverse field Ising model of the form

$$H_{\text{TIM}} = J \sum_i \sigma_i^x \sigma_{i+1}^x + h_x \sum_j \sigma_j^x + h_z \sum_j \sigma_j^z,$$

where the σ_i^α operators are the Pauli-matrices extended to the full chain by a tensor product with identities acting on all other sites than i . This example is taken from Ref. [12], where the mechanism of dephasing is laid out in detail. We consider two distinct scenarios with different initial states and different Hamiltonian parameters. Both initial states have a high effective dimension with their corresponding Hamiltonian and will therefore equilibrate in the infinite time average. When looking at the short time dynamics however, we find that one equilibrates rapidly and the other one does not equilibrate on the time scales considered. Fig. 2.2 shows the scenario which yields fast equilibration. Here, the Hamiltonian parameters are $J = 4$, $h_x = 1$ and $h_z = -2.1$ and the initial state is a random product state,

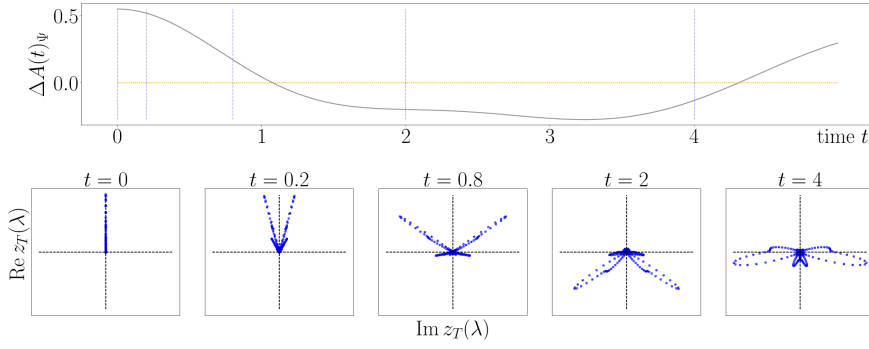


Figure 2.3: An investigation of the equilibration behaviour for a transverse field Ising model on the level local magnetisation $A = \sigma_{L/2}^z$ for an ordered unentangled initial state out of equilibrium situation [11]. Top: Distinguishability $\Delta A(t)_\psi$ in the transverse Ising model on $L = 15$ sites (for details refer to Ref. [12]). The dashed orange line is the equilibrium value and the blue line corresponds to the actual value at time t . There is no visible equilibration for the time interval considered. Bottom: Decomposition of $\Delta A(t)_\psi$ in its components on the complex plane for fixed points in time. The distribution stays concentrated throughout the evolution. Figure taken from Ref. [12].

meaning that for each site a random spin configuration is assigned. Originally, this setting is discussed in Ref. [16]. As described above, the initial distribution at $t = 0$ is aligned on the real axis of the complex plane yielding a large distinguishability $\Delta A(0)_\psi$. As time goes on, the phases rapidly cover the plane, resulting in a small $\Delta A(t)_\psi$ for $t \sim 4$. A rather different behaviour is found for similar Hamiltonian parameters $J = 1$, $h_x = 0.5$ and $h_z = -1.05$ but an initial state that consists only of spin ups on every site. In Fig. 2.3 we again show the corresponding distinguishability $\Delta A(t)_\psi$. When turning on time evolution, there are two distinct contributions whose phases only slowly split yielding a non-uniform distribution on the complex plane even for late times. This example shows that the underlying mechanism for equilibration apparently is dephasing. However, up to now it is unclear how to connect this to more physical assumptions, such as the precise form of the initial state or the observable. It seems plausible however, that the amount of randomness surrounding the observed region might play a role in the short time dynamics. For now, we leave this as an open question.

Lastly, we also would like to mention a complementary approach to finding fast equilibration time scales, namely typicality [17--19]. Here, an assumption on the unitaries transforming the bases of observable, state and Hamiltonian into one another is made, demanding those resemble Haar random matrices. While this approach beautifully reproduces the equilibration time scales found in experiments, it delivers little insight into the theoretical structures and mechanisms which yield this rapid equilibration.

With this, we would like to close our discussion on equilibration, again pointing out that interacting many-body systems do reach equilibrium after an initial perturbation. The time scales of when this happens are observed to be short in generic cases, but a rigorous proof or rather physical assumptions allowing to prove rapid equilibration are still lacking. We move on to describing the resulting equilibrium state - the question of thermalisation.

2.4 THERMALISATION

Describing quantum systems in terms of statistical ensembles is a two-step process. First, we need the system to actually equilibrate and only then can we attempt characterising this equilibrium state. We will call a system thermalised if the equilibrium ensemble depends on the energy of the initial state only. Thermalisation is the panacea to understanding why quantum mechanics may be the foundational theory of everything despite the classical appearance of our day to day world as it wipes out quantum coherence and leaves us only with thermal ensembles.

A principal feature of classical thermodynamics is dynamical entropy production, best exemplified by releasing a gas into an empty room. We say that the previously concentrated gas equilibrates by expanding to fill the available space. Given the final position of the gas particles, it is impossible to reconstruct the initial position of the gas can. The final state is an ensemble whose only parameters are macroscopic quantities such as the volume of the room and its temperature. Such a description is only possible, because the microscopic details are erased over time. In the corresponding quantum scenario, where a specific wavefunction as introduced above is evolved in time, there is no corresponding loss of information due to the time evolution being unitary and hence probability preserving. The final state will therefore always be pure and not mixed. This failure, which was already pointed out by von Neumann in his seminal work [20], hinges upon the knowledge of the full quantum state, which in practise is almost never accessible.

As in the equilibration problem discussed in the previous chapter, if we only assume knowledge of local expectation values, we can define thermalisation for quantum systems as well. The question at hand is whether expectation values of local observables in the equilibrium state can be predicted by using a thermal ensemble which only depends on the energy of the initial state. We say that a state ρ has thermalised if

$$\|\mathrm{tr}_{S^c}(\omega - \omega_{\mathrm{Gibbs}})\|_1 \leq \epsilon, \quad (2.4.1)$$

with

$$\omega_{\mathrm{Gibbs}} := e^{-\beta H} / Z,$$

where Z is the partition function of the system, $\epsilon > 0$ and β is the inverse temperature which is chosen such that the energies of ω and the thermal state agree. In the following and in agreement with the literature we will refer to ω_{Gibbs} as the Gibbs state of the system. From Eq. (2.4.1) we can deduce why thermalisation of many-body systems is potentially the most important open question in the field. If a system thermalises, the number of parameters necessary to faithfully represent its equilibrium ensemble reduces from d^L for generic quantum states to one - its energy. Needless to say, this renders the treatment of large quantum system feasible. As with equilibration time scales that generically are observed to be rapid, it is observed that thermalisation generically takes place [21] but the precise details of how it comes about are not fully settled. Nevertheless, a powerful conjecture used to explain thermalisation is the eigenstate thermalisation hypothesis which links thermalisation to a feature of the eigenstates [22--25]. It states that eigenstates in a microcanonical, i. e. small, energy window in the bulk of the spectrum already approximate a Gibbs state of this energy quite well. By this token, any initial state with high effective dimension whose support on the energy eigenbasis is peaked, will also equilibrate to this very Gibbs state. This hypothesis is powerful, but difficult to check. It also disregards prerequisites such as locality of the Hamiltonian

and it is not clear where in the spectrum its validity should end, as the boundary of the spectrum is - in some instances even provably so [26] - not thermal. Moreover, if the initial state has overlap with several energy segments, it is far from clear whether the superposition of several Gibbs states again yields a Gibbs state and if so which temperature we should assign in that case.

Given its totalising statement, it is important to understand when the eigenstate thermalisation hypothesis fails. This is often the case when the system has some additional local structure which we will discuss in the following under the headline of integrability.

2.5 INTEGRABILITY

In this section, we will consider requirements for a system to evade thermalisation. If a system features local memory, i. e. information in local regions is not being erased under the time evolution, this hinders thermalisation. The reason why we do not encounter a single report of a stable ice cube in the summer sun is that many of the systems with local memory are not robust. Let us now explore what local memory means for quantum systems.

It is conceivable that a quantum system retains most of its local structure if there are local operators which are preserved under the Hamiltonian evolution. In quantum mechanics, an operator Z which commutes with the Hamiltonian does not evolve in time and is hence called a constant of motion. In the classical case, each constant of motion comes with a cyclic coordinate and hence reduces the time evolution of that coordinate to a trivial motion. Moreover, the initial value of this constant of motion with respect to the initial state does not change and the coordinate is said to be integrable.

In the quantum world, there is again a problem with carrying over the classical definition [27] as any operator that is diagonal in energy space commutes with the Hamiltonian by definition. However, not all of these operators are physically meaningful. Some of them are global symmetries like particle conservation, which do restrict the dynamics but not on local scales. Others do not even have any local interpretation, i. e. energy eigenprojectors or arbitrary combinations of these. Only constants of motion with a local real space representation give rise to local memory, which in turn inhibits thermalisation. To illustrate this in more detail, consider a spin chain with fixed magnetisation and an initial state from the zero magnetisation sector. If the Hamiltonian flips adjacent spins, the equilibrium state will be a homogeneous spin distribution over the full chain. This is the case for any initial state from the zero magnetisation sector. Things change when we introduce local memory though. Let us assume the spin of one site is a constant of motion. Then the equilibrium state will necessarily have the same value as the initial state on this specific site and thereby only half of the initial states equilibrate to the same equilibrium state. But this means that the reduced equilibrium state to any region containing this site depends on the local initial conditions now, which clashes with the requirements for thermalisation, where only the energy is allowed as a parameter for the equilibrium state. To formalise this, let us assume that we have L many constants of motion Z_i that fulfil $[H, Z_i] = 0$, are functionally independent and have a local representation in real space. If we now want to find a description of our equilibrium ensemble ω for a given initial state $|\psi\rangle$, we must not only consider its energy but also the expectation values of all constants of motion $\langle\psi|Z_i|\psi\rangle$ as

these also do not change over time. States with different expectation values for the constants of motion can have the same energy, as the constants of motion blockdiagonalise the Hamiltonian and therefore the different blocks decouple. In practise, this implies that there is no level repulsion between the blocks as their states are decoupled, allowing for degenerate energies in an otherwise interacting system. To conclude, an equilibrium ensemble in such a system takes a more complicated form also referred to as generalised Gibbs ensemble ω_{GGE}

$$\omega_{\text{GGE}} := e^{-\beta H + \sum_i \mu_i \mathcal{Z}_i} / Z,$$

where the μ_i are the Lagrange multipliers that are optimised such that the expectation values of the \mathcal{Z}_i in ω_{GGE} and the initial state agree [28]. Much less is known about these ensembles, especially it is not clear whether higher orders of the constants of motion are also required to faithfully represent the initial state.

Integrability does inhibit thermalisation, but many of the known models exhibiting it are fine-tuned and therefore will hardly be observed in nature. A slight perturbation to their Hamiltonians usually restores thermalisation. At the start of this millennium however, a class of systems has been identified that are robustly integrable. The underlying mechanism at work is particle localisation which persists even in the presence of many-body interactions culminating in the name many-body localisation. The following section will give a brief introduction into this class of systems putting them into context with equilibration and thermalisation.

2.6 ANDERSON LOCALISATION

The field of particle localisation dates back to the endeavours of P. W. Anderson investigating the impact of impurities onto a conducting material [29]. The model he was considering was non-interacting, but it is still instructive to briefly sketch the physics of the Anderson model before moving on to its interacting generalisation to understand the concept of particle localisation in a tractable model.

A conductor consists of a rigid lattice of positive ions with electrons orbiting them. Charge effects are mediated by the electrons tunneling from ion to ion. Furthermore, electrons are fermions, which implies that they cannot be in the same quantum state simultaneously. Assuming that interactions between electrons are strongly screened, an analytically tractable starting point to model the electron movement in a conductor is a model that only involves hopping terms and neglects interactions. Since Anderson was interested in the effect of local impurities, as they naturally occur in the production of any material for example by imperfect lattice geometry or defect ions, we furthermore add a random onsite potential such that the resulting Hamiltonian takes the form

$$H_{\text{And}} = J \sum_i \left(f_i^\dagger f_{i+1} + \text{h.c.} \right) + \sum_j h_j f_j^\dagger f_j,$$

where f_i^\dagger, f_i are the canonical fermionic creation and annihilation operators, J is the hopping strength (mostly we will set $J = 1$ and rescale all other Hamiltonian parameters) and h_j are random numbers drawn independently from an interval $[-\Delta, \Delta]$, where Δ is referred to as the disorder strength.

The surprising discovery by Anderson was that while in the absence of disorder $\Delta = 0$ this model is a perfect conductor, conductance breaks down in the thermodynamic limit as soon as any nonzero disorder is added to the model. What is more, it

was later discovered that not only particle but also information propagation is suppressed beyond a certain length scale, that depends on the disorder strength and is called localisation length [30]. Phrased in the language of quantum information theory this means, that if we give an Anderson localised chain to two parties Alex and Brook, it is not possible for them to transfer information between the two by encoding it at one end, say Alex', with a local unitary and trying to read it out on Brook's end with a measurement. This is a consequence of the eigenstates of the Anderson model being localised in real space in contrast to the extended eigenstates in the absence of disorder. In essence, the Anderson insulator is a perfect insulator in that it does neither transport particles nor information. Furthermore, the system cannot equilibrate via dephasing because it is non-interacting but also due to the absence of transport it does not equilibrate in any other way and without equilibration it does not make sense to talk about thermalisation. At the time of Anderson, it was strongly expected that localisation would break down as soon as arbitrarily small interactions are added to the Hamiltonian. Almost 50 years later however, this question was finally followed up with a different result, namely that even in the presence of many-body interactions, localisation can persist [31]. This effect was therefore named many-body localisation and sparked a new field of research. In the following, we will summarise those results that are particularly relevant for out-of-equilibrium dynamics.

2.7 MANY-BODY LOCALISATION

In this section, we investigate how localisation responds to the addition of many-body interactions. Anderson (and others at the time) conjectured, that localisation would cease to exist as soon as many-body interactions are introduced to the model. Intuitively, this was based on the idea that particles which are trapped in the system now can exchange energy with other particles and thereby overcome the energy barriers of the potential landscape. By now it is established that this is not the full answer to this question. Rather, a complicated interplay of interactions and disorder governs the physics of many-body localised systems resulting in both a localised and an ergodic parameter regime.

The plethora of approaches and results related to many-body localisation cannot comprehensively be presented in this thesis and hence we try to find a middle ground of delivering a concise theoretical description, while still covering the cornerstones of the field.

The essential ingredients to observe localisation physics are Hamiltonian terms which facilitate particle transport, interactions between particles and a source of randomness [32]. We would like to remind the reader, that we put emphasis on one-dimensional systems. A prototypical Hamiltonian used as a model for a many-body localised system is the spinless, disordered Fermi-Hubbard model

$$H_{\text{FH}} = J \sum_i \left(f_i^\dagger f_{i+1} + \text{h.c.} \right) + \sum_j h_j n_j + U \sum_k n_k n_{k+1}, \quad (2.7.1)$$

where $n_j = f_j^\dagger f_j$ are particle number operators acting on site j . This is an interacting generalisation of the Anderson model with interaction strength U , where again we draw the disorder fields from a bounded interval $h_j \in [-\Delta, \Delta]$, where Δ is the

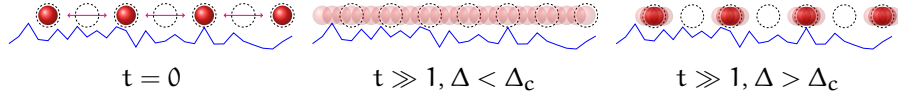


Figure 2.4: Sketch of the experiment in Ref. [33]. The left panel shows the initial state $|\psi_{\text{CDW}}\rangle$ at time $t = 0$. The panel in the center shows the equilibrium state if the disorder strength Δ is smaller than the critical disorder strength Δ_c . Here, the particles can spread through the system and hence the equilibrium state is homogeneous with no trace of the initial configuration. The right panel shows the equilibrium state if the disorder strength Δ is larger than the critical disorder strength Δ_c . In this case, the disorder will keep the particles localised to their initial site. Therefore, the initial charge density wave pattern is still visible in the equilibrium state.

disorder strength. In one dimension, this model can be mapped to a random field XXZ spin model using the Jordan-Wigner transform.

$$H_{\text{XXZ}} = \tilde{J} \sum_i \sigma_i^x \sigma_{i+1}^x + \sigma_i^y \sigma_{i+1}^y + \sum_j \tilde{h}_j \sigma_j^z + \tilde{U} \sum_k \sigma_k^z \sigma_{k+1}^z, \quad (2.7.2)$$

where the σ^α operators are the Pauli-matrices and the constants are shifted with respect to the fermionic variant.

The seminal result giving birth to the field of many-body localisation shows vanishing conductivity when the disorder is sufficiently strong. [31]. Only later was it possible to demonstrate this particle localisation experimentally [33]. Here, the authors prepared an initial state with a charge density wave pattern, i. e.

$$|\psi_{\text{CDW}}\rangle = |10101010 \dots 1010\rangle,$$

in the real space particle occupation basis. This state was then evolved in time under a bosonic variant of the above Hamiltonian with a quasi-random potential. In the absence of localisation, particles spread over the full system and eventually the system equilibrates to a homogeneous state. This has actually been observed before in a different context in Ref. [34]. If particles are localised, they remain close to their initial position, which results in the preservation of the charge density wave pattern in its equilibrium state [35]. To track how well this pattern is preserved over time, one can measure an observable called the imbalance \mathcal{J} , which takes the form

$$\mathcal{J} = \frac{N_{\text{odd}} - N_{\text{even}}}{N_{\text{odd}} + N_{\text{even}}},$$

where N_x is the summed particle number on odd and even sites, respectively. Its expectation value with $|\psi_{\text{CDW}}\rangle$ is 1, which is actually also its maximum. When calculating the imbalance of a homogeneous state, one finds that it vanishes.

In Ref. [33] it was reported that for zero disorder strength Δ , the imbalance plummets to zero very fast, a signal of particle transport. As soon as the disorder strength exceeded a critical disorder strength $\Delta > \Delta_c$, the imbalance saturated at a non-zero value. A sketch of the initial states and the equilibrium states for low and high disorder is given in Fig. 2.4. This directly implies that the system does not thermalise, as the system has local memory of the initial particle configuration, which is not thermal. This was the first experimental realisation of a system that provably does not thermalise.

Another particular feature of many-body localised systems is the formation of dynamical correlations. The spread of information in generic ergodic local systems

is linear in time [36--38]. When putting many-body localised systems to a test by preparing a random product state and evolving it in time, they show a logarithmic in time growth of the halfchain entanglement [39,40]. Recall that in Anderson localised systems, information propagation is bounded. In essence, particle localisation and logarithmic in time growth of correlations clearly delineate many-body localised systems from thermalising systems, where particles move in unconstrained fashion and Anderson localisation, where the correlation growth in time saturates.

We will now introduce an effective model incorporating the phenomenology discussed above. For this purpose, it is useful to define an operators basis of L many operators \mathcal{Z}_i , which fulfil $[H, \mathcal{Z}_i] = 0$ and are functionally independent. Decomposing our Hamiltonian in terms of these yields

$$H_{\text{eff}} = \sum_i \mu_i \mathcal{Z}_i + \sum_{i,j} \mu_{i,j} \mathcal{Z}_i \mathcal{Z}_j + \sum_{i,j,k} \mu_{i,j,k} \mathcal{Z}_i \mathcal{Z}_j \mathcal{Z}_k + \mathcal{O}(\mathcal{Z}_i^4),$$

where the $\mu_{\{a\}} = \text{tr}(H \prod_{i \in \{a\}} \mathcal{Z}_i)$ are the coefficients from the expansion in the new basis. So far, everything we have done is still exact and applicable to any Hamiltonian, but also not very useful. For generic Hamiltonians, these operators are likely non-local and in accordance with our discussion of integrability in Chapter 2 not relevant for the local dynamics. However, to capture localisation physics, we look for constants of motion that do constrain the local dynamics, i. e. that are responsible for particle localisation. Therefore, we will now assume that there is a set of \mathcal{Z}_i operators that are furthermore quasi-local, meaning that their support in real space decays strongly. These can now be thought of as the localisation regions that particles in our lattice are confined to. Taking into account their commutation with the Hamiltonian, these are L many quasi-local constants of motion. Furthermore, they are expected to be connected to the real space particle number operators by a unitary transformation of decaying support, making them quasi-local [41, 42]. This constitutes a form of emergent integrability, which is one of the necessary conditions to represent localised systems.

Let us consider the first order of H_{eff} denoted by H_{eff}^1 . It only consists of localisation regions and no coupling between those. This can be seen as an effective model of an Anderson insulator, where the \mathcal{Z}_i describe the localisation regions. Occupations cannot be exchanged between these regions, which is why there are no \mathcal{X}_i -type terms. Moreover, there is no term coupling these regions so information cannot be transferred between them. If we want to extend the model to also cover the physics of many-body localised systems, we need to include terms that do couple different localisation regions in order to have information propagation. However, we want correlations to only spread logarithmically in time, which entails that the effective interaction between distant sites needs to decay exponentially in that distance. Essentially, we want the sum over all interaction terms that connect the two sites to decay exponentially in the distance between the sites [42]. To formalise this, we can write down the more cumbersome expression $\| \sum_{\{a\}} \mathcal{Z}_i (\prod_{k \in \{a\}} \mathcal{Z}_k) \mathcal{Z}_j \| \leq e^{-\text{dist}(i,j)}$, where $\{a\}$ is a (possibly empty) set of sites between site i and site j . Hence, the simplest model that is capable of mimicking the physics of a many-body localised system is H_{eff}^2 . Such an effective model, which is fully commuting, has been shown to exhibit the logarithmic in time spread of entanglement [43]. An exact mapping, which would also allow to prove stability of localisation is still elusive despite impressive efforts [44]. Having established the phenomenology and presented a fruitful attempt of capturing it formally, we will now point out the open questions that will be tackled in this thesis.

2.8 OPEN PROBLEMS

To our understanding, many-body localisation is a physical effect that prevents thermalisation in spite of interactions in a robust way. The following chapters will address the natural questions of stability, experimental realisability and computability of this effect.

One pressing question when studying a physical effect is its stability to various perturbations. In the end, we would like to understand how and where an effect can be realised in nature. Investigating its stability gives insights into whether it can exist and in which circumstances. We already pointed out that many-body localisation is stable to perturbations of the Hamiltonian parameters. As with many effects in phases of matter, the dimension of the system has a strong impact on the observed physics. There is experimental evidence for localisation in two dimensions [45], but also arguments that predict the breakdown of many-body localisation in dimensions higher than two at long times [46]. In fact, there is a recent numerical study claiming that even in one dimension a many-body localised system thermalises at late times [47]. In Chapter 3, we will ask a similar question by considering the stability of localisation with respect to unlikely disorder configurations. We numerically study systems, that deliberately include a region of low disorder, allowing for local thermalisation. If a locally thermalised region is able to destroy the localisation of its surroundings, this would be indicative of an instability for larger systems, where such disorder configurations are likely to occur.

Another important question is whether the effect can be realised in experiments. A real material exhibiting many-body localisation is yet to be found, but analogue quantum simulators such as trapped ions [48], superconducting qubits [49] or optical lattices [33] allow to probe theoretical predictions to a high accuracy. While it is possible to show particle localisation in these setups, it is still desirable to also measure interaction induced effects such as the logarithmic in time growth of entanglement. Since the entanglement entropy is not an experimentally accessible quantity, one needs to find measurable quantities that serve the same purpose. In Chapter 4, we set out to design measures, which witness the interaction induced effects in many-body localised optical lattices based only on technology present in these setups.

Lastly, we also put the theoretical framework to a test by devising an algorithm which constructs quasi-local constants of motion in Chapter 5. We put emphasis on the algebraic properties of the obtained operators, allowing us to furthermore compute the weights of the effective model in a small system. We then extend this algorithm to an application in a spin chain with symmetry protected order in Chapter 6, where local constants of motion emerge naturally as edge modes of the system.

STABILITY OF MANY-BODY LOCALISATION

Stability is a natural question to ask about phases in physical systems. Generically one is interested in how certain phase properties change when the system size is changed. In the context of many-body localisation one of the most pressing questions is whether localisation persists for large systems and long times. This is a very difficult question to tackle since the dynamics in many-body localised systems are extremely slow. It follows that a local perturbation will need a long time to explore the full system and hence stability can only be assessed for very late times. In this chapter, we focus on delocalising effects of regions which have an uncharacteristically small disorder variance. While they are in general very unlikely, there is a non-vanishing probability of finding those in large systems. In this sense, we probe the long time and large system physics of many-body localisation.

3.1 GRIFFITHS EFFECTS

Since the local potentials of the disordered Hamiltonians we consider are drawn at random, it is unlikely but possible to draw potentials of comparable size in a region of neighbouring sites. In principle it is even possible that we obtain a completely flat potential landscape and the system is thermalising. Although the probability of this situation decays extremely quickly when increasing the system size, small regions of locally flat disorder landscape are not unreasonable. If the local potential difference is small enough, the particles in this region can thermalise in this small region. Depending on the number and size of such thermalised regions, it is conceivable that they also thermalise the remaining localised system. In the end, this most likely is the mechanism which drives the transition between the thermalising and the many-body localised phase when the disorder strength is changed.

The situation where a system is in a certain phase but small local regions are in a different phase and the resulting dynamics are called Griffiths effect [50]. Essentially, it is interesting to understand in which phase the resulting equilibrium state will be in. Here, we are interested in a localised system with small local patches which are thermal and whether these are able to thermalise the full system or not. This is not very well understood theoretically and an active open question of the field of many-body localisation. There exists an argument that a single thermal region can delocalise the full system if it is two-dimensional or its interactions do not decay fast enough in one dimension [46]. This however does not cover the setting which is most commonly considered, namely a one-dimensional system with strictly local interactions as described in Eq. (2.7.1).

Another way of testing the stability of many-body localisation with respect to thermal inclusions is to directly engineer models that include a small thermal region. In Ref. [51], the authors build a model based on the effective description of many-body localisation. They consider the following Hamiltonian, which consists of a

thermal region on the first three sites and an effective description of a localised chain on the rest of the system

$$H = R \otimes \mathbb{1}_{L-3} + \sum_{i=4}^L \mu_i \sigma_i^z + \sum_{j=4}^L \frac{g_0 \alpha^{j-4}}{4} \sigma_3^x \sigma_j^x,$$

where R is a random matrix of dimension $2^3 \times 2^3$ drawn from the generalised orthogonal ensemble. Such random matrices have spectral features that resemble those of thermalising Hamiltonians and hence are often used to model thermalised systems. The coupling to the localised chain is mediated via spin flip terms that decay in distance, where α takes the role of the effective disorder strength by limiting the range of the coupling. The authors find that there is a critical value of the coupling, where the local region is able to thermalise the localised chain irrespective of its size. This is a very interesting finding as it suggests that a finite thermal inclusion is able to thermalise its localised surroundings. Some more remarks about this work are in order. The model implemented is actually an Anderson insulator since higher order σ^z terms are missing. The authors claim that adding higher order terms would only increase the thermalising power of the bath and hence propose that their finding is morally a lower bound for the thermalisation of a many-body localised system. Also, the coupling implemented appears to be very powerful as it can flip constants of motion even at long ranges and is not included in the typical description of the effective model.

In this chapter, we put this finding to a test using the disordered XXZ model defined in Eq. (2.7.2) instead of an effective description. We model the thermal region by drawing a number of potentials from an extremely small window independent of the disorder strength for all other sites finding that many-body localisation is stable for a finite thermal region and unstable for extensive thermal regions.


CLIMATE FOOTPRINT ESTIMATE

Total Kernel hours [h]	8260
Total Energy consumption [kWh]	82
Total CO ₂ -emission [kg]	45

Table 3.1: Estimated climate footprint of the numerical calculations performed for the paper “Exploration of the stability of many-body localized systems in the presence of a small bath”. Estimates are based on the data presented in the manuscript and exclude prototyping. CO₂-emission estimates are based on the German average emission of 0.56 kg/kWh. A similar emission is caused by manufacturing a smartphone (≈ 30 kg) [52]. Calculations were performed on the `leonard` and `tron` cluster equipped with Intel® Xeon® Processor X5570 and Intel® Xeon® Processor E5-2680 v2 nodes with a thermal design power of 95 W and 115 W, respectively. Further details on the estimation can be found in Appendix A.

Exploration of the stability of many-body localized systems in the presence of a small bath

Marcel Goihl, Jens Eisert, and Christian Krumnow

Dahlem Center for Complex Quantum Systems, Freie Universität Berlin, 14195 Berlin, Germany (Received 13 February 2019; revised manuscript received 13 May 2019; published 24 May 2019)

When pushed out of equilibrium, generic interacting quantum systems equilibrate locally and are expected to evolve towards a locally thermal description despite their unitary time evolution. Systems in which disorder competes with interactions and transport can violate this expectation by exhibiting many-body localization. The strength of the disorder with respect to the other two parameters drives a transition from a thermalizing system towards a nonthermalizing one. The existence of this transition is well established both in experimental and numerical studies for finite systems. However, the stability of many-body localization in the thermodynamic limit is largely unclear. With increasing system size, a generic disordered system will contain with high probability areas of low disorder variation. If large and frequent enough, those areas constitute ergodic grains which can hybridize and thus compete with localization. While the details of this process are not yet settled, it is conceivable that if such regions appear sufficiently often, they might be powerful enough to restore thermalization. We set out to shed light on this problem by constructing potential landscapes with low disorder regions and numerically investigating their localization behavior in the Heisenberg model. Our findings suggest that many-body localization may be more stable than anticipated in other recent theoretical works.

DOI: [10.1103/PhysRevB.99.195145](https://doi.org/10.1103/PhysRevB.99.195145)**I. INTRODUCTION**

One of the long-standing puzzles of physics is how the postulates of quantum statistical mechanics and thermodynamics can be made compatible with the unitary time evolution of quantum systems. It is increasingly becoming clear that generic interacting quantum systems—once pushed out of equilibrium—are expected to dynamically evolve towards a locally thermal description again [1–5]. This constitutes an interesting state of affairs, since it reconciles the apparent contradiction between the description of time-evolving states and of equilibrium ensembles. Such an interpretive scheme also provides a picture in which interacting systems can be described by only a small number of parameters for almost all time intervals, thus avoiding the curse of dimensionality. A few exceptions are known to exist but these are fine-tuned *integrable* systems featuring local constants of motion that prohibit a general description in terms of thermal ensembles.

At the turn of the millennium, a new class of quasi-integrable systems emerged which fail to thermalize over a wide range of parameters. As this effect is caused by the interplay of transport, interactions, and disorder, it has been dubbed *many-body localization* (MBL) [6–8]. A many-body localized system does not exhibit transport of particlelike quantities and therefore can be effectively described by an extensive set of quasilocally conserved constants of motion (qLCOMs) [9,10]. This leads to local memory of particle configurations [11]. Note that unlike the noninteracting Anderson insulator, systems exhibiting MBL may well transport informationlike quantities such as correlations between particles. This is reflected, e.g., in the logarithmic growth of the entanglement entropy in time [12,13].

While many of the properties ascribed to MBL have been observed either experimentally or numerically in finite

systems, the question of the stability of MBL in the thermodynamic limit is as of yet unresolved. The expected leading sources of instability are rare regions of low disorder that might conceivably thermalize the rest of the system [14–17]. Questions regarding the effect of local regions that are localized in the otherwise ergodic phase or ergodic regions in the otherwise localized phase have been investigated in the field of *Griffiths effects* [18–23] (for a review, see Ref. [24]). The question of whether a closed MBL system is stable to uncharacteristic disorder potentials is hence part of this subfield.

In this work, we deliberately construct potential landscapes with regions of improbably low disorder and study their influence on a localized chain surrounding them. A previous study has reported that a constant size thermal region is able to thermalize a localized chain coupled to it independent of its size if the constants of motion do not decay sufficiently strongly [16]. The study has been conducted within an effective description of MBL [9,10], one in which the localized part has been modelled by constants of motion and the bath by a suitable random matrix. The postulated coupling between the bath and the localized part is characterized by a decay length which is related to the localization length of the constants of motion.

Here, instead we use its real-space equivalent: the disordered Heisenberg chain. Employing exact diagonalization, we analyze the statistics of local expectation values of the eigenstates which allows us to draw conclusions about the locality of the constants of motion of the system. Our results are not entirely compatible with those of Ref. [16], as we find MBL is not compromised by the presence of low disorder regions of constant size. When the size of the region is allowed to scale with system size however, we find that localization vanishes when extrapolating our results to large systems.

II. SETTING

A. Hamiltonian model

We consider the ‘‘drosophila’’ of MBL, the disordered spin-1/2 Heisenberg chain. In order to study the effect of small subregions of low disorder, we investigate systems for which the potential on the sites $1, \dots, s$ is close to zero. Consequently, for a system of L sites, our Hamiltonian reads

$$H = \sum_{i=1}^L (\sigma_i^x \sigma_{i+1}^x + \sigma_i^y \sigma_{i+1}^y + \sigma_i^z \sigma_{i+1}^z) + \sum_{i=1}^t \epsilon h_i \sigma_i^z + \sum_{i=t+1}^L \Delta h_i \sigma_i^z, \quad (1)$$

where the h_i are drawn uniformly and independently from the interval $[-1, 1]$, ϵ and Δ denote the disorder strength in the low and high disorder region and σ_i^a is the Pauli- a operator acting on the i th site. The fully disordered model (without ergodic subregion) is expected to undergo a localization transition at a critical disorder strength $\Delta_c \approx 7$ (note that since we use Pauli instead of spin operators, the transition is shifted with respect to other literature). Moreover, we use periodic boundary conditions and work in the zero magnetization sector. We set $\epsilon = 10^{-6}$ independent of the disorder strength Δ . This creates the situation that the local flatness of the potential may thermalize the subsystem, which is expected to compete with localization effects in the remaining system. In the following, we will hence refer to the first t sites as the thermal sites and refer to the remaining $L - t$ sites as the disordered sites or part of the system. This model is very close to state-of-the-art experimental realizations of MBL in, e.g., optical lattice architectures [11]. However, it bears the problem that for the zero on-site field, it becomes Bethe-ansatz integrable which arguably inhibits the thermalizing effect of the thermal sites. This is why we also investigated a similar model which includes integrability breaking terms

$$H = \sum_{i=1}^L (\sigma_i^x \sigma_{i+1}^x + \sigma_i^y \sigma_{i+1}^y + \sigma_i^z \sigma_{i+1}^z) + \sum_{i=1}^t \epsilon h_i \sigma_i^z + \sum_{i=t+1}^L \Delta h_i \sigma_i^z + \sum_{i=1}^{L-1} J_{nm} (\sigma_i^x \sigma_{i+1}^z \sigma_{i+2}^x + \sigma_i^y \sigma_{i+1}^z \sigma_{i+2}^y), \quad (2)$$

where the last term upon Jordan-Wigner transformation yields a next-nearest-neighbor hopping, which breaks integrability [8]. For all simulations of this model, we use $J_{nm} = 0.2$. We consider two different scenarios: In the first, the number of thermal sites is independent of the system size ($t = 3$). In the second setting, we take a fixed fraction of the full size to be thermal ($t = L/2$).

B. Distribution of disorder

Within this model, we investigate below the effect of a local cluster with uncharacteristically small disorder on its

environment. The formation of such a cluster should be understood as a rare instance of a generic MBL model and is specifically relevant when considering the stability of an interacting localized phase in the thermodynamic limit, where the effect of these rare regions is not fully understood yet. For large systems, the probability of having small thermal regions increases and poses the question if these are able to compromise localization of the full chain as well. As a prerequisite, these must first thermalize their neighbors which can also be checked in small systems and which is precisely the context of this work. In a system so large that it cannot be treated numerically, there will be small subsystems which resemble the systems we consider in this work with high probability, namely there will be regions of low disorder. It is reasonable to assume that before such a small region could delocalize the full chain, it would delocalize its surroundings. However, we would like to point out that here we seek for hints of this physics in the Heisenberg model without assuming further structure such as the representation of the bath. The minimal model for the delocalization scenario for us is the local flatness of the potential and this is the only prerequisite. Note that we only consider local observables as global quantities such as energy levels commonly used to detect MBL [8,25] will likely not be faithfully recovered in our small system and are hence not considered here.

III. MEASURE OF LOCALIZATION

The proposed *effective integrability* of MBL comes about due to the presence of extensively many quasilocal conserved operators \mathcal{Z}_i [9,10]. This is seen most readily in the infinite disorder limit ($\Delta \rightarrow \infty$) where these are given by the local fields $\mathcal{Z}_i = \sigma_i^z$ and hence act on a single site only. Moreover, they allow us to label the eigenstates by the occupation of the \mathcal{Z}_i . When one moves away from the infinite disorder case, energy space and real space no longer coincide and the above identity becomes more intricate. The Hamiltonian formulated in real space is then diagonalized by a unitary U_D which relates energy and real space. The real-space representation of the \mathcal{Z}_i is given by a decomposition in which all possible Pauli operator combinations can appear,

$$U_D \mathcal{Z}_i U_D^\dagger = \alpha_i \sigma_i^z + \sum_{\mu, \nu \in C} \beta_i(\mu, \nu) \Sigma^z(\mu) \Sigma^x(\nu), \quad (3)$$

where Σ^z, Σ^x are Pauli words consisting of local Pauli- z and Pauli- x operators respectively and $\mu, \nu \in \{0, 1\}^L$ indicate the position of the Pauli operators in the chain, e.g., $\Sigma^a(\mu) = \otimes_i (\sigma_i^a)^{\mu_i}$. We deliberately singled out the weight on σ_i^z corresponding to the infinite disorder conserved operator. All remaining weights are subsumed by the index set C which contains all possible μ, ν configurations except the one which would yield $\Sigma^z(\mu) \Sigma^x(\nu) = \sigma_i^z$. In practice, $\alpha_i, \beta_i(\mu, \nu)$ can be calculated using the Hilbert-Schmidt scalar product $\beta_i(\mu, \nu) = \text{Tr}[U_D \mathcal{Z}_i U_D^\dagger \sigma^z(\mu) \sigma^x(\nu)]/2^L$. This representation might seem cumbersome at first glance, but also allows one to understand how a transition between strictly local constants of motion in the infinite disorder case to nonlocal constants of motion in the ergodic regime can be captured formally in terms of the structure of the constants of motion. In fact

this is nothing but a formalization of the “dressing” process [9,10]. The above decomposition is completely general in the sense that the constants of motion of any system of qubits can be expanded as in Eq. (2) and can hence be applied to the localized as well as to ergodic phase of an MBL system.

The behavior of the conserved operators can be tracked by analyzing the statistics of α_i . In the localized regime the \mathcal{Z}_i are expected to be quasilocal such that the corresponding weights need to decay strongly for operators that have support outside of the localization length, an intuition that has been confirmed numerically [26–33]. The largest weight will hence still be given by $\alpha_i \sim 1$ and all other weights should be significantly smaller. In the ergodic regime, however, \mathcal{Z}_i are not local at all causing the weights to smear out over many different operators and therefore α_i will be essentially random and small.

To access the statistics of α_i , our main numerical tool is constituted by local magnetizations of eigenstates, i.e., $\langle E|\sigma_i^z|E\rangle$ [16,34]. As the eigenstates can be expressed in terms of the projectors $(1 \pm \mathcal{Z}_i)/2$ onto the (un)occupied sectors of the qLCOM, calculating the expectation value with σ_i^z yields $\pm\alpha_i$ depending on the occupation. Therefore, we analyze the histograms over all eigenstates, expecting two very distinct regimes. A localized phase is expected to exhibit a bimodal distribution peaked at ± 1 . This holds whenever the constants of motion are quasilocal and hence most of the operator weight is still on the on-site magnetization implying $\alpha_i \sim 1$.

For ergodic systems however, the distribution of the α_i values should feature a close-to-Gaussian shape with zero mean. Here, the constant of motion will be spread out over many different operators and therefore the weight on σ_i^z is essentially random. Note that in principle, one could also check the other weights $\beta_i(\mu, \nu)$ which certainly yield further insights into the decomposition of the qLCOMs. There are however $4^L - 1$ many of these and without prior knowledge about which one should be sampled, this task is computationally infeasible.

IV. RESULTS

In this section, we show and discuss the obtained results. We worked with system sizes $L \in \{8, 10, 12, 14, 16\}$ and various disorder strengths. Each point is an average over at least 2000 realizations. Errors have been calculated either using the standard deviation or bootstrapping which amounts to resampling from the obtained data to obtain a distribution of the quantity of interest. In all plots, the error bars are smaller than the symbols used. We either set $t = 3$ or $t = L/2$ sites to be thermal to cover the system size independent and dependent case. Moreover, we work with next-nearest-neighbor strengths $J_{mn} \in \{0, 0.2\}$ to also understand the effect of closeness to integrability. We first discuss the case of the constant size thermal region.

A. Constant size thermal region

In the model considered in this section, we set $t = 3$, i.e., three sites are thermal independent of the system size. The

two plots on the left in Fig. 1 show the histogram of the local expectation values of magnetization operators $\langle E|\sigma_i^z|E\rangle$ for different sites i encoded in color. We use a system of size $L = 16$ and $J_{mn} = 0$. As pointed out above, this amounts to sampling the weight of the constants of motion on the σ_i^z operator and hence is an indirect measure for their locality. For low disorder $\Delta = 3$, the distributions show a distinct peak at zero and feature strongly decaying tails consistent with the predictions for the thermal region. When comparing the thermal sites to the ones that experience the full disorder strength, we find that the decay for sites inside the thermal region is stronger—as one would intuitively expect. This implies that the constants of motion are not very dominantly supported on the respective σ_i^z operator but presumably rather spread over all remaining operators and hence nonlocal.

The picture changes drastically with increasing disorder. For $\Delta = 9$, the distributions originating from sites in the disordered part of the chain show a distinct bimodality. This shows that the σ_i^z are very close to the exact constants of motion as they inherit their occupation statistics which is a sign of quasilocality. For sites in the thermal region, we find that their distributions feature a peak around zero and small peaks in their heavy tails as well. Since the disorder that these sites experience directly is of order $\epsilon = 10^{-6}$, the peaks and the heavy tails should be ascribed to the proximity to the localized chain. When turning on next-nearest-neighbor hopping $J_{mn} = 0.2$ (data not shown), we recover the same qualitative behavior but the overall localization is slightly weaker, as one would expect from the increased capability of the bath.

We will now turn to a system size scaling of the observed locality behavior of the constants of motion again with $J_{mn} = 0$. Since the standard deviation measures the width of a distribution, it is a genuine measure to compare the distributions for different system sizes [16]. This is shown in the two plots on the right in Fig. 1, where we plot the standard deviation for all available system sizes encoded in color as a function of disorder strength in the Heisenberg model with three thermal sites. As a guide to the eye, the ergodic region is hatched in red. For both weak and strong disorder, we find in Fig. 1 that the distributions of local expectation values of energy eigenstates are narrower for sites in the thermal region than in the disordered one. In the ergodic regime for $\Delta = 3$, we see that in both regions the standard deviation decreases on all sites with increasing system size. This is an indicator that the system tends towards thermalization as even in the disordered part of the system the distributions become more narrow upon increasing the system size, which is to be expected for $\Delta < \Delta_c$. However, for $\Delta = 9$, we find that the standard deviation shows no systematic shift with increasing system size, instead a saturation seems to be the most accurate description. This suggests that localization is not compromised by a constant size thermal region.

To detail this observation, we show the standard deviation of a site in the middle of the disordered part of the system at $i = L - \lfloor(L - 3)/2\rfloor$ as a function of disorder strength in Fig. 3 (left panels). Here, we also include the data for the next-nearest-neighbor hopping model. In the ergodic regime $\Delta < \Delta_c$, the standard deviation of the middle site decays with increasing system size which is an indication that the

constants of motion become less local when increasing the system size. This decrease is enhanced by the next-nearest-neighbor hopping. Upon increasing the disorder strength, we observe a crossing behavior of the standard deviation for disorder values higher than the critical disorder $\Delta > \Delta_c$ in both models. This shows that in the localized phase there is a (admittedly weak) tendency towards higher standard deviation for increasing system sizes indicating that the model is driven towards localization upon increasing system size in the sense that the constants of motion become more and more localized. The effect of the next-nearest-neighbor hopping is a slight decrease in the maximal value obtained for $\Delta = 15$. These results indicate that the presence of a fixed size region of low disorder acting as ergodic grain does not alter the qualitative behavior of the full system—depending on the disorder present we find it to be in the ergodic or localized phase without a shift of the transition point compared to the standard disordered Heisenberg chain.

In the next section, we will increase the size of the thermal region with the system size and carry out the same analysis.

B. Constant fraction thermal region

Let us now consider the case $s = L/2$ such that the thermal region covers half of the system and is thus extensive. Again data for the next-nearest-neighbor model is not shown, but agrees qualitatively albeit with slightly weaker localization. The two plots on the left in Fig. 2 show the histogram of the local expectation values of magnetization operators $\langle E|\sigma_i^z|E\rangle$ for different sites i in a system of size $L = 16$. For low disorder $\Delta = 3$ the distribution essentially has the same shape as for the three site thermal region with the only exception being that now the eight thermal sites show the strong decay and the eight disordered sites decay less strongly. Again, this implies that the constants of motion are not very dominantly supported on the respective σ_i^z operator. For $\Delta = 9$ the distributions originating from sites in the disordered part of the chain show the expected bimodality but furthermore also feature a peak centered around zero indicating the proximity of the thermal

region. For the distribution of the thermal sites, we also notice the difference to the fixed size setting discussed above that they do not show a bimodality anymore but only heavier tails than in the case of low disorder.

To investigate these effects in a system size scaling, we again analyze the standard deviation of the distributions in the two plots on the right of Fig. 2. Here, we find that the two regimes show the same qualitative behavior, namely a decaying standard deviation with increasing system size. As this is also the case for both parts of the chain, it strongly suggests that the system tends towards narrower distributions and hence delocalization upon increasing the system size.

Let us emphasize this last observation by showing the standard deviation of a site in the middle of the disordered part of the chain at $i = L - \lfloor L/4 \rfloor$ as a function of disorder strength in Fig. 3 (right panels). We find that the gap between standard deviations for different system sizes is diminished at higher disorder but there is no crossover as in the case of a constant size thermal region for both models. For finite systems this implies that significantly stronger disorder scaling with the system size is needed in order to localize even the disordered part of the system. Furthermore, the extrapolation from the available system sizes leads to the conclusion that localization vanishes in the large system limit for this model as constants of motion become more nonlocal even in the regime of high disorder.

Let us summarize the results. We find that constant thermal regions which are independent of the system size seemingly cannot hinder localization and their influence is suppressed by increasing the system size. An ergodic region that scales with the system size, however, changes the physics of the model and apparently delocalizes the system. This observation holds for both models with and without next-nearest-neighbor hopping. It is important to note that an ergodic bubble of the order of the system size is exponentially unlikely to appear. It is, however, unclear, if already a weaker scaling of the size of the thermal region with the system size would be sufficient to delocalize the system which is not reasonable to test with the system sizes available to exact diagonalization based schemes.

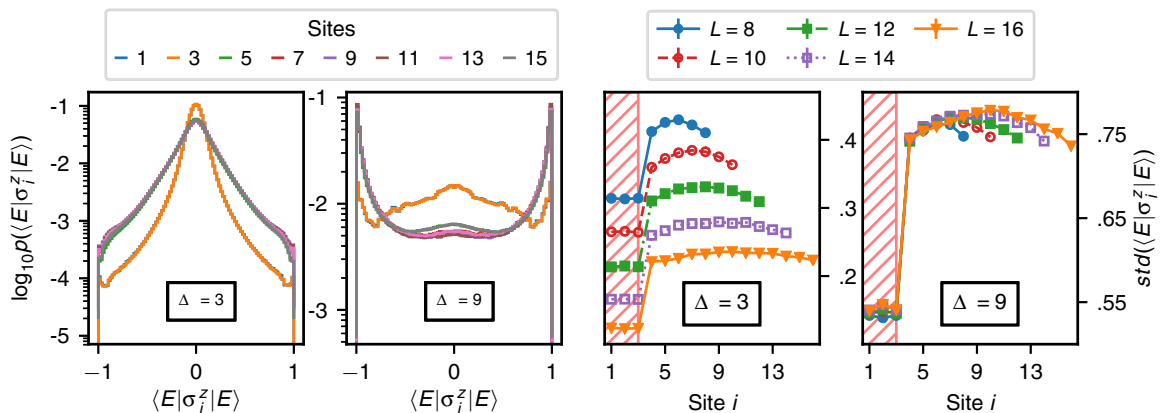


FIG. 1. Local expectation values of the eigenstates of the model with three thermal sites for weak ($\Delta = 3$) and strong disorder ($\Delta = 9$). Left: Histograms of $\langle E|\sigma_i^z|E\rangle$ in the Heisenberg model on $L = 16$ sites for $i \in \{1, 3, \dots, 15\}$ encoded by color. Each histogram is an average over all eigenstates in the zero magnetization sector and 2000 realizations. Right: Standard deviation of the histograms of $\langle E|\sigma_i^z|E\rangle$ in the Heisenberg model for different system sizes. Red hatches show the thermal part of the system. Each data point is an average over at least 2000 realizations.

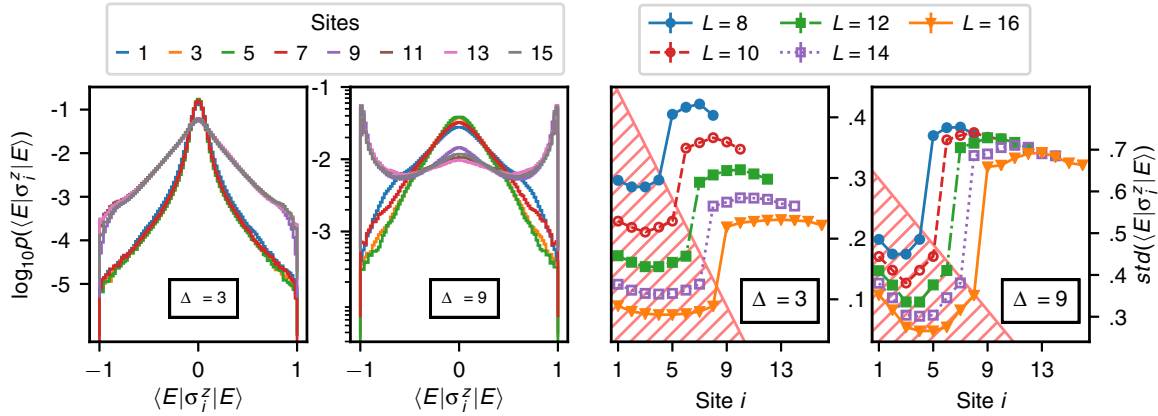


FIG. 2. Local expectation values of the eigenstates of the model with $L/2$ thermal sites for weak ($\Delta = 3$) and strong ($\Delta = 9$) disorder. Left: Histograms of $\langle E|\sigma_i^z|E\rangle$ in the Heisenberg model on $L = 16$ sites for $i \in \{1, 3, \dots, 15\}$ encoded by color. Each histogram is an average over all eigenstates in the zero magnetization sector and 2000 realizations. Right: Standard deviation of the histograms of $\langle E|\sigma_i^z|E\rangle$ in the Heisenberg model for different system sizes. The red hatched part of each curve indicates the thermal region of the system. Each data point is an average over at least 2000 realizations.

Let us relate our findings to results obtained in Ref. [16] where the authors predict and numerically show a parameter region in which a localized chain can be thermalized by a constant thermal bath. There the authors work in the effective description of MBL and present theoretical arguments for a possible mechanism of instability of MBL phases. Note however, that the disorder strength in their model is only implicitly defined. They use an effective model of the disordered part of the system in terms of quasilocal constants of motions. The disorder strength as used in our work controls the locality of these constants of motion and by this changes the decay length of the coupling of the bath to different qLCOMs. Upon changing this decay length the authors of Ref. [16] identify a critical value whereupon a small thermal grain thermalizes the full system. Based on the fact that we only find such an instability for thermal regions which scale with the system size, we present two explanations for this apparent contradiction.

The first one is that the two Hamiltonians do not exhibit similar physical signatures. Both display features of MBL, but the structure of the bath and coupling to the disordered part of the system might be incompatible. On the level of effective models and not the Hamiltonians as such, it may be that the two effective models in terms of qLCOMs may be incompatible. Since it is not clear how to transform the Heisenberg model into the effective description, we cannot directly connect and compare the two results. In Ref. [16] the authors employ off-diagonal terms which couple the bath and MBL chain; we instead suggest that the important ingredient governing the localization effects is solely the support of the qLCOMs and hence the diagonalizing unitary U_D . In the setting in which the bath is constant, the unitary U_D should still qualify to be quasilocal with an increased localization length inside the bath, whereas for the extensive bath the unitary will not be local at all in sufficiently large systems.

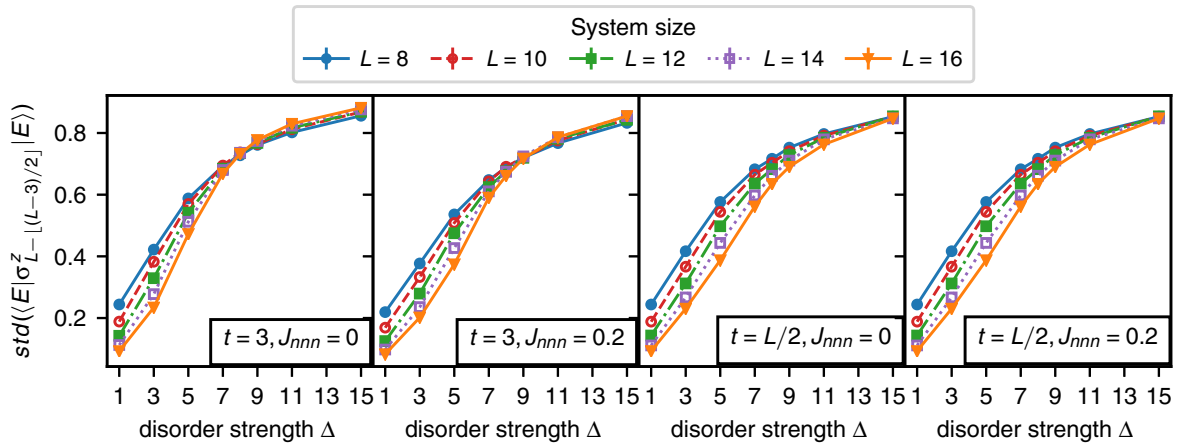


FIG. 3. Standard deviation of the histograms of $\langle E|\sigma_{L-\lfloor(L-3)/2\rfloor}^z|E\rangle$ of the center site in the disordered part positioned at $i = L - \lfloor(L-3)/2\rfloor$ in the Heisenberg model for different system sizes. Each data point is an average over at least 2000 realizations. The number of thermal sites t and the strength of the next-nearest-neighbor hopping J_{nnn} are indicated in the plots.

The second and more plausible explanation is that the critical coupling decay length at the transition found in Ref. [16] might actually correspond to the critical disorder strength separating the ergodic and MBL phase, giving rise to the detected instability. Since no comprehensive theory for this transition exists as well, it might be fruitful to combine our findings with the arguments of Ref. [16] in order to possibly establish a better understanding for the ergodic to MBL transition.

V. CONCLUSIONS

In this work, we have investigated the fate of the qLCOMs in the disordered Heisenberg model with and without next-nearest-neighbor hopping in the presence of a small thermal region modelled by improbably low disorder. We have examined the influence of these regions on the localization behavior. As such regions occur with high probability in large systems this allows us insights into the stability of the MBL phase in the large system limit. As a measure of the locality of the qLCOMs we have employed the expectation value of local magnetization operators obtained from exact diagonalization. In the system sizes accessible to us, we find that the qLCOMs and thereby the MBL phase is indeed expected to be stable when coupled to a finite bath for both models considered. This observation does not exclude the possibility that if the thermal region is much larger it could actually suffice to thermalize its

surroundings. If the thermal region is allowed to scale with the system size, however, our findings suggest that MBL will vanish when approaching the thermodynamic limit.

These results suggest that an isolated MBL system is stable upon increasing the system size. If, in contrast, coupled to an external bath, the question of the stability of MBL may depend on more subtle details as the precise size and shape of the bath may have a strong influence. An interesting further research direction would be to carry out a similar analysis for two-dimensional systems and devise local probes for delocalization which could then be used in state-of-the-art experimental realizations of MBL.

ACKNOWLEDGMENTS

M.G. is grateful for the feedback on the manuscript by N. Tarantino as well as numerous discussion with the participants of the *Anderson Localization and Interactions* workshop at the MPIPKS—specifically with W. De Roeck, A. Morningstar, A. Goremykina, and M. Serbyn as well as A. R. Abadal and J. Rui at MPQ. Moreover, we would like to thank H. Wilming for many discussions at earlier stages of this work. This work has been supported by the ERC (TAQ), the DFG (FOR 2724, CRC 183, EI 519/14-1), and the Templeton Foundation. This work has also received funding from the European Union’s Horizon 2020 research and innovation program under Grant Agreement No. 817482 (PASQuanS).

-
- [1] M. Rigol, V. Dunjko, and M. Olshanii, *Nature (London)* **452**, 854 (2008).
 - [2] A. Polkovnikov, K. Sengupta, A. Silva, and M. Vengalattore, *Rev. Mod. Phys.* **83**, 863 (2011).
 - [3] J. Eisert, M. Friesdorf, and C. Gogolin, *Nat. Phys.* **11**, 124 (2015).
 - [4] C. Gogolin and J. Eisert, *Rep. Prog. Phys.* **79**, 056001 (2016).
 - [5] T. Langen, S. Erne, R. Geiger, B. Rauer, T. Schweigler, M. Kuhnert, W. Rohringer, I. E. Mazets, T. Gasenzer, and J. Schmiedmayer, *Science* **348**, 207 (2015).
 - [6] I. V. Gornyi, A. D. Mirlin, and D. G. Polyakov, *Phys. Rev. Lett.* **95**, 206603 (2005).
 - [7] D. M. Basko, I. L. Aleiner, and B. L. Altshuler, *Ann. Phys.* **321**, 1126 (2006).
 - [8] V. Oganesyan and D. A. Huse, *Phys. Rev. B* **75**, 155111 (2007).
 - [9] M. Serbyn, Z. Papić, and D. A. Abanin, *Phys. Rev. Lett.* **111**, 127201 (2013).
 - [10] D. A. Huse, R. Nandkishore, and V. Oganesyan, *Phys. Rev. B* **90**, 174202 (2014).
 - [11] M. Schreiber, S. S. Hodgman, P. Bordia, H. P. Lüschen, M. H. Fischer, R. Vosk, E. Altman, U. Schneider, and I. Bloch, *Science* **349**, 842 (2015).
 - [12] M. Žnidarič, T. Prosen, and P. Prelovšek, *Phys. Rev. B* **77**, 064426 (2008).
 - [13] J. H. Bardarson, F. Pollmann, and J. E. Moore, *Phys. Rev. Lett.* **109**, 017202 (2012).
 - [14] P. Ponte, C. R. Laumann, D. A. Huse, and A. Chandran, *Philos. Trans. R. Soc. A* **375**, 20160428 (2017).
 - [15] W. De Roeck and F. Huveneers, *Phys. Rev. B* **95**, 155129 (2017).
 - [16] D. J. Luitz, F. Huveneers, and W. De Roeck, *Phys. Rev. Lett.* **119**, 150602 (2017).
 - [17] T. Thiery, F. Huveneers, M. Müller, and W. De Roeck, *Phys. Rev. Lett.* **121**, 140601 (2018).
 - [18] R. Nandkishore, S. Gopalakrishnan, and D. A. Huse, *Phys. Rev. B* **90**, 064203 (2014).
 - [19] S. Gopalakrishnan, M. Müller, V. Khemani, M. Knap, E. Demler, and D. A. Huse, *Phys. Rev. B* **92**, 104202 (2015).
 - [20] K. Agarwal, S. Gopalakrishnan, M. Knap, M. Müller, and E. Demler, *Phys. Rev. Lett.* **114**, 160401 (2015).
 - [21] D. J. Luitz and Y. B. Lev, *Ann. Phys.* **529**, 1600350 (2017).
 - [22] R. Nandkishore and S. Gopalakrishnan, *Ann. Phys.* **529**, 1600181 (2017).
 - [23] S. Gopalakrishnan and D. A. Huse, *Phys. Rev. B* **99**, 134305 (2019).
 - [24] K. Agarwal, E. Altman, E. Demler, S. Gopalakrishnan, D. A. Huse, and M. Knap, *Ann. Phys.* **529**, 1600326 (2017).
 - [25] D. J. Luitz, N. Laflorencie, and F. Alet, *Phys. Rev. B* **91**, 081103(R) (2015).
 - [26] A. Chandran, I. H. Kim, G. Vidal, and D. A. Abanin, *Phys. Rev. B* **91**, 085425 (2015).
 - [27] R.-Q. He and Z.-Y. Lu, *Chin. Phys. Lett.* **35**, 027101 (2018).
 - [28] L. Rademaker and M. Ortuño, *Phys. Rev. Lett.* **116**, 010404 (2016).

- [29] M. Mierzejewski, M. Kozarzewski, and P. Prelovšek, *Phys. Rev. B* **97**, 064204 (2018).
- [30] S. J. Thomson and M. Schiró, *Phys. Rev. B* **97**, 060201(R) (2018).
- [31] A. K. Kulshreshtha, A. Pal, T. B. Wahl, and S. H. Simon, *Phys. Rev. B* **98**, 184201 (2018).
- [32] M. Goihl, M. Gluza, C. Krumnow, and J. Eisert, *Phys. Rev. B* **97**, 134202 (2018).
- [33] M. Goihl, C. Krumnow, M. Gluza, J. Eisert, and N. Tarantino, [arXiv:1901.02891v3](https://arxiv.org/abs/1901.02891v3).
- [34] A. Pal and D. A. Huse, *Phys. Rev. B* **82**, 174411 (2010).

EXPERIMENTAL WITNESSES OF MANY-BODY LOCALISATION

Any physical effect should ideally be described theoretically and measured experimentally. Only the combined effort of verifying a theoretical framework by means of experimental data gives evidence for the validity of the theory and the existence of the physical effect at hand.

The seminal experiment on many-body localisation was carried out in an optical lattice experiment showing particle localisation for an interacting Hamiltonian [33]. Nevertheless, it was not yet possible to measure interaction induced effects such as the logarithmic in time growth of correlations. In this chapter, we present a road map of how to measure interaction induced effects in a many-body localised system employing only such tools which are available in optical lattice architectures.

4.1 DISORDERED OPTICAL LATTICES

While a real world material exhibiting many-body localisation still has to be found, there are experimental platforms which allow to probe the physics of the Hamiltonians of interest. In the spirit of Richard Feynman's idea of simulating the behaviour of a quantum system by using another quantum system which likens the system of interest in its physics but is more accessible and easier to control, many-body localisation can be realised in several of these quantum simulators. We will here focus specifically on realisations in ultra-cold atoms in optical lattices [53]. Let us start by reviewing the basic principles and feasible measurements in an optical lattice.

First of all, ions are cooled in a dipole trap. These can be fermionic or bosonic. Their hyperfine states can serve as the spin of the particles simulated. The lattice is built up from counterpropagating laser fields. Interfering two of these laser fields in an orthogonal orientation yields a two-dimensional lattice structure of light (see Fig. 4.1). Illuminating the ions with this optical lattice forces them into the minima of the laser field. Utilising additional high precision lasers to remove unwanted ions, a desired initial state is created. The amplitude of the laser field now acts as the potential barrier height between sites and hence governs the mobility of the particles and their ability to interact. Additionally, it is possible to manipulate the interaction strength directly using a magnetic field, which gives individual control of hopping and interaction strength. The potential landscape can be manipulated by adding another incommensurate laser field. This is referred to as a quasi-random potential and is most easily implemented. The frequency used for the additional laser determines the structure of the disorder landscape. In the absence of interactions, this is referred to as the Aubry-André model. In contrast to the Anderson model, where the single particle eigenstates are localised for arbitrarily low disorder, the Aubry-André model exhibits a transition at $\Delta/J = 2$ from delocalised to localised single particle eigenstates. This suggests that localisation is stronger when the potential is truly random. Such a truly random potential is also available in optical lattices via a programmable mirror setup. When projecting the lattice with such a potential, the disorder landscape becomes slightly correlated but only locally. Combining all

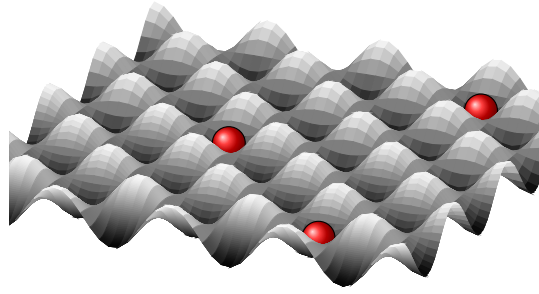


Figure 4.1: Sketch of an optical lattice. The gray surfaces represent the laser field, into which the ultra cold atoms (red balls) are evaporated. Tuning the wavelength then allows to tune Hamiltonian parameters.

these features, optical lattices simulate Hubbard-type Hamiltonians with on-site interactions. In Table 4.1, we summarise how the different Hamiltonian terms can be tuned.

The available measurements are time-of-flight and in-situ. In a time-of-flight measurement, the lattice and the trap are turned off, releasing the ions into free fall. They are then projected onto a screen, which essentially yields a Fourier transformed particle-particle correlator. In the in-situ methods, the local parity can be probed using an additional laser that addresses each site. Based on the reflected light, it can be deduced whether an odd or even amount of particles was present at the site.

Based on these measurements, we design probes that are capable of measuring the interaction induced effects of many-body localisation such as the logarithmic in time growth of correlations or the equilibration behaviour.

Hamiltonian property	Implemented via
Particle species	Ion species
Particle spin	Ion hyperfine states
Hopping strength	Laser field amplitude
Interaction strength	Laser field amplitude & Magnetic field
Quasi-random potential landscape	Frequency of additional laser field
Arbitrary potential landscape	Programmable mirror setup

Table 4.1: Tunable Hamiltonian parameters in an optical lattice architecture and their implementation.

CLIMATE FOOTPRINT ESTIMATE

Unfortunately, the data to calculate the CO₂-emission of this work could not be recovered and hence is not taken into consideration for further calculations.

Article

Experimentally Accessible Witnesses of Many-Body Localization

Marcel Goihl ^{1,*} , Mathis Friesdorf ¹, Albert H. Werner ², Winton Brown ³ and Jens Eisert ¹

¹ Dahlem Center for Complex Quantum Systems, Freie Universität Berlin, 14195 Berlin, Germany; fries@physik.fu-berlin.de (M.F.); jense@zedat.fu-berlin.de (J.E.)

² Department of Mathematical Sciences, University of Copenhagen, DK-2100 København, Denmark; ahw@physik.fu-berlin.de

³ Northrop Grumman Corporation, Baltimore, MD 21240, USA; wb@physik.fu-berlin.de

* Correspondence: mgoihl@physik.fu-berlin.de

Received: 28 May 2019; Accepted: 13 June 2019; Published: 17 June 2019



Abstract: The phenomenon of many-body localized (MBL) systems has attracted significant interest in recent years, for its intriguing implications from a perspective of both condensed-matter and statistical physics: they are insulators even at non-zero temperature and fail to thermalize, violating expectations from quantum statistical mechanics. What is more, recent seminal experimental developments with ultra-cold atoms in optical lattices constituting analog quantum simulators have pushed many-body localized systems into the realm of physical systems that can be measured with high accuracy. In this work, we introduce experimentally accessible witnesses that directly probe distinct features of MBL, distinguishing it from its Anderson counterpart. We insist on building our toolbox from techniques available in the laboratory, including on-site addressing, super-lattices, and time-of-flight measurements, identifying witnesses based on fluctuations, density–density correlators, densities, and entanglement. We build upon the theory of out of equilibrium quantum systems, in conjunction with tensor network and exact simulations, showing the effectiveness of the tools for realistic models.

Keywords: many-body localized (MBL); equilibrium quantum systems; simulations; realistic models

1. Introduction

Many-body localization provides a puzzling and exciting paradigm within quantum many-body physics and is for good reasons attracting significant attention in recent years. Influential theoretical work [1] building upon the seminal insights by Anderson on disordered models [2] suggests that localization would survive the presence of interactions. Such many-body localized models, as they are dubbed, would be insulators even at non-zero temperature and exhibit no particle transport. Maybe more strikingly from the perspective of statistical physics, these many-body localized models would fail to thermalize following out of equilibrium dynamics [3–5], challenging common expectations how systems “form their own heat bath” and hence tend to be locally well described by the familiar canonical Gibbs ensemble [6–8]. Following these fundamental observations, a “gold rush” of theoretical work followed, identifying a plethora of phenomenology of such many-body localized models. They would exhibit a distinct and peculiar logarithmic scaling of entanglement in time [9,10], the total correlations of time averages have a distinct scaling [11], many Hamiltonian eigenstates fulfill area laws [12] for the entanglement entropy [13,14] and hence violate what is called the eigenstate thermalization hypothesis [15]. The precise connection and interrelation between these various aspects of many-body localization is just beginning to be understood [14,16–20], giving rise to a vivid discussion in theoretical physics.

These theoretical studies have recently been complemented by seminal experimental activity, allowing to probe models that are expected to be many-body localized in the laboratory under remarkably controlled conditions [21,22]. This work goes much beyond earlier demonstrations of Anderson localization in a number of models [23], in that now actual interactions are expected to be relevant. Such ultra-cold atomic systems indeed provide a pivotal arena to probe the physics that is at stake here [24]. What is still missing, however, is a direct detection of the rich phenomenology of many-body localization in the laboratory. Rather than seeing localization and taking the presence of interactions for granted, it seems highly desirable to make use of these novel exciting possibilities to directly see the above features, distinctly separating the observations from those expected from non-interacting Anderson insulators. Such a mindset is that of “witnessing” a property, somewhat inspired by how properties such as entanglement are witnessed [25–27] in quantum information.

In this work, we aim at capturing precisely those aspects of the rich phenomenology of many-body localization that are directly accessible with present experimental tools. We would like to provide a “dictionary” of possible tools, as a list or a classification of features that can be probed making use of only in situ site resolved measurements, including the measurement of density–density correlations and time of flight measurements, in conjunction with a variation of densities. In this way, we aim at identifying a comprehensive list of features that “could be held responsible” for MBL, based on data alone. While all we explicitly state is directly related to cold atoms in optical lattices, a similar approach is expected to be feasible in continuous cold bosonic atoms on atom chips [28,29], where correlation functions of all orders can readily be directly measured. We leave this as an exciting perspective.

2. Probing Disordered Optical Lattice Systems

The setting we focus on is that of interacting (spin-less) fermions placed into a one-dimensional optical lattice, a setting that prominently allows to probe the physics under consideration [21,24]. Such systems are well described by

$$H = \sum_j \left(f_j^\dagger f_{j+1} + \text{h.c.} \right) + \sum_j w_j n_j + U \sum_j n_j n_{j+1}, \quad (1)$$

where f_j denotes a fermionic annihilation operator on site j and $n_j = f_j^\dagger f_j$ is the local particle number operator. The disorder in the model is carried by the local potential-strength w_j , which is drawn independently at each lattice site j according to a suitable probability distribution. Experimentally, the disorder can either be realized by superposing the lattice with an incommensurate laser or by speckle patterns [21]. From Equation (1), one obtains the disordered Heisenberg chain [30] by setting $U = 2$ and scaling the disorder by a factor two. To keep the discussion conceptually clear, as in Ref. [30], we make use of a uniform distribution on the interval $[-I, I]$, where we refer to I as the disorder strength. Thus, for $U = 2$ the ergodic to MBL phase transition is approximately at $I \approx 7$ [30]. Most of the known experiments of MBL have been carried out in a related model of on-site interacting bosons for which we show data in Appendix B.

The phase diagram of these models is best known for $U = 0$ corresponding to the non-interacting Anderson insulator and for $U = 2$, the MBL phase. To add a flavor of usual phase transitions order parameters such as total correlations [11], fluctuations of local observables [31] or the structure of the eigenstates [32] have been suggested. While these quantities impressively signal the transition, it is not a priori clear whether they can be implemented in an actual experiment. Recent numerical studies [33] show that pump–probe type setups and novel instances of spin noise spectroscopy [34] as well as utilizing MBL systems as a bath [35] are indeed suited to distinguish the above phases, albeit experimental realizations of this endeavor appear to need substantial changes and innovations in realistic setups. Another possibility for the phase distinction, which has prominently been carried out experimentally [22], is given by observing the behavior of quasi two-dimensional systems in comparison to their one dimensional counterparts. While this impressively demonstrates the

capabilities of optical lattices as platforms for quantum simulations, it does not test the properties of MBL in one dimension as such. We set out to find comparably strong and direct signatures of one dimensional MBL, which however rely on simple established measurement operations. Hence, we start by summarizing the measurements, which we conceive to be feasible in an optical lattice experiment.

3. Measurements Considered Feasible

We now turn to specifying what measurements we consider feasible in optical lattices with state-of-the-art techniques. For this, we focus on the following two types of measurements:

In-situ: An in-situ measurement detects the occupation of individual lattice sites. This technique only allows resolving the parity of the particle number on each site, which for fermions constitutes no limitation, however. Using the fact that single-shot measurements are performed, higher moments such as density–density correlators can also be extracted from this kind of measurements. Both ramifications are used. This measurement has been used to determine onsite parities in Ref. [36] to show particle localization in two-dimensional disordered optical lattices. Here, we try to additionally witness the interactions necessary to distinguish Anderson from MBL systems.

Time-of-flight: The time-of-flight (ToF) measurement extracts position-averaged momentum information of the form

$$\langle n(q, t_{\text{ToF}}) \rangle = |\hat{w}_0(q)|^2 \sum_{j,k} e^{iq(r_j - r_k) - i \frac{c(r_j^2 + r_k^2)}{t_{\text{ToF}}}} \langle f_j^\dagger f_k \rangle ,$$

where $\{r_j\}$ are the positions of the lattice sites, \hat{w}_0 reflects the Wannier functions in momentum space, and $c > 0$ is a constant derived from the mass of the particles and the lattice constant. This measurement was used in Ref. [21] to determine the imbalance—a measure of localization.

The main goal of this work is to identify key quantities that indicate that the system indeed is many-body localized based on measurement information extracted using these two techniques. Here, we want to show both that the system is localized and that it is interacting. Thus, we also want to convincingly detect the difference between an MBL system and a non-interacting Anderson insulator. To approach this task, we look at the time evolution of an initial state that is particularly easy to prepare experimentally relying on optical super-lattices [21,37], namely an alternating pattern of the form

$$|\psi(t = 0)\rangle = |0, 1, 0, 1, \dots, 0, 1\rangle . \quad (2)$$

This initial product state will, during time evolution, build up entanglement and become correlated [9,10]. Naturally, this is far from being the only choice for an initial state and alterations in this pattern and, correspondingly, locally changing particle and hole densities would surely be insightful, specifically since a modulation of the density already points towards interactions in the MBL phase being significant. In this work, we put emphasis on measurements, although preparation procedures such as the above-mentioned density variations are an interesting problem in their own right. However, as we demonstrate, the above-defined initial state already captures the colorful phenomenology of MBL in all of its salient aspects.

4. Phenomenology of Many-Body Localization

A fundamental characteristic of MBL is the presence of local constants of motion [3]. They are approximately local operators $\tilde{\sigma}_j^z$ whose support is centered on lattice site j , but which nevertheless commute with the Hamiltonian, i.e., $[H, \tilde{\sigma}_j] = 0$. These operators are mainly supported on a region with diameter ξ , corresponding to the localization length scale of the system. In fact, in the MBL

regime, the dynamics can be captured by a phenomenological model in terms of a set of mutually commuting quasi-local constants of motion,

$$H_{l\text{-Bit}}^{(2)} = \sum_i \mu_i \tilde{\sigma}_i^z + \sum_{j<i} J_{i,j} \tilde{\sigma}_i^z \tilde{\sigma}_j^z . \quad (3)$$

Such a Hamiltonian constitutes a second order approximation of what is known as the l -bit model [19,20,38] to exemplify the dynamics. Here, $\tilde{\sigma}_i^z$ again denotes a quasi-local integral of motion centered on site i , μ_i is a random onsite potential and the coupling strength $J_{i,j}$ between constants of motion is assumed to decay suitably fast in their distance $d(i,j)$. In particular, it is expected that the dynamics generated by the Hamiltonian defined in Equation (1) in the MBL regime corresponding to $U = 2$ and $I > 7$ can be well captured by the l -bit model.

This phenomenological model gives rise to a separation of time scales in the evolution into two regimes. Initially, there is a fast regime, where the evolution takes place mainly inside the support of each local constant of motion $\tilde{\sigma}_i^z$. Hence, for this time scale, transport is unconstrained and particles and energies can move freely inside the localization length. Correspondingly, information can spread ballistically. Beyond the localization length, the dynamics is dominated by the coupling of the constants of motion, given by the second term in Equation (3) [20]. The intuition is that this evolution does not facilitate particle or energy propagation, leading to a complete break-down of thermal and electric conductivity. Nevertheless, the couplings between distant constants of motion allow for the creation of correlations over arbitrary length scales given sufficient time. This dephasing mechanism in turn makes it possible to send information and yields an explanatory mechanism for the observed slow growth of entanglement [9,10,16], measured as the von Neumann entropy of the half chain of an infinite system $S(t) = \Theta(\log(t))$ (in Landau notation).

Mathematically, these two dynamical regimes are best distinguished by the effect of a local unitary excitation on distant measurements. More precisely, given a local measurement O_A supported in a spatial region A and a unitary V_B corresponding to a local excitation in a region B , we wish to bound the change in expectation value of $O_A(t)$ induced by the unitary excitation. This can be cast into a Lieb–Robinson bound [14,39] of the form

$$\left| \langle V_B O_A(t) V_B^\dagger \rangle - \langle O_A(t) \rangle \right| \leq C(A) \begin{cases} e^{-\mu(d(A,B)-v|t|)} & \mathbf{I}, \\ t e^{-\mu d(A,B)} & \mathbf{II}, \end{cases} \quad (4)$$

where $C(A)$ a constant depending on the support of O_A . For the connection between different zero velocity Lieb–Robinson bounds and the necessity of a linear t -dependence in **II**, see Ref. [14]. Here, **I** corresponds to the ballistic regime and **II** captures the slower dephasing. In the context of optical lattices, local excitations seem difficult to implement. Hence, in the following, we focus on the observation of indirect effects on the dynamical evolution in MBL systems.

5. Feasible Witnesses

In the following, we demonstrate that local memory of initial conditions, slow spreading of correlations and equilibration of local densities provide clear measures to distinguish MBL systems from both the non-interacting Anderson insulators and the ergodic systems, i.e., those where local measurements, after a short relaxation time, can be captured by thermal ensembles. To carry out our analysis, we complement the intuitive guideline provided by the phenomenological l -bit model by a numerical tensor network TEBD simulation [40] (for details, see Appendix A). The chosen parameters for the simulation are a disorder strength of $I = 8$ and interaction strengths of $U = 2$ or $U = 0$ for the MBL and Anderson case, respectively. An overview of the measures and their capabilities is given in Figure 1. We begin by considering the influence of the suppression of particle propagation.

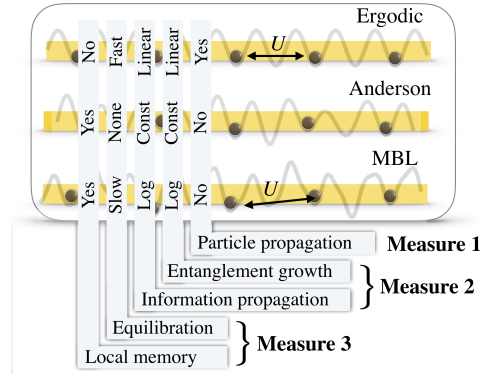


Figure 1. An overview over the dynamical behavior of MBL systems versus their ergodic and thermalizing and Anderson localized counterparts. **Measure 1** detects particle propagation and phase correlations and can be implemented using time-of-flight imaging. **Measure 2** and **Measure 3** utilize in-situ imaging to observe density–density correlations and equilibration behavior.

5.1. Absence of Particle Transport

A defining feature of localized systems is that independent of the interaction strength, particles and energies do not spread over the entire system, but remain confined to local regions. They merely redistribute inside the localization length, which can be extracted from the constants of motion. Therefore, even for long times, the particle density profile of an MBL system will not move to its thermal form, but rather retain some memory of its initial configuration. This gives rise to the following particle localization measure.

Measure 1 (Particle propagation and phase correlations). We define the following measure $y_{\text{Phase}}(t)$, which probes particle propagation for a system of length L

$$f_{\text{Phase}}(k, t) := \left| \langle f_{L/2}^\dagger(t) f_{L/2+k}(t) \rangle \right|, \quad (5)$$

$$y_{\text{Phase}}(t) = \sum_k f_{\text{Phase}}(k, t) k^2. \quad (6)$$

On an intuitive level, this measure directly probes the spread of particles, including weights based on the distance to the initial position $L/2$ such that distant contributions are amplified.

Numerically, we find that $y_{\text{Phase}}(t)$ initially shows a steep linear increase, indicative of the ergodic dynamics governed by the onsite term of Equation (3) (Figure 2). In the second regime, it fluctuates without visible growth, indicating a break-down of particle transport on length scales beyond the localization length. Thus, the length scale of the phase correlations established in the system can be bounded independent of time $y_{\text{Phase}}(t) = O(1)$. For ergodic systems, where particles and energies spread ballistically, the measure would grow in an unconstrained fashion over time. Based on this insight, we deduce that time-of-flight images, while clearly distinguishing between localized and ergodic phase, are not useful for the distinction between interacting and non-interacting localized systems.

Again, more formally, this measure can be understood by considering the time evolution of the correlation matrix given by the matrix elements

$$\gamma_{j,k}(t) := \langle f_j^\dagger(t) f_k(t) \rangle, \quad (7)$$

where $\langle f_j^\dagger f_k \rangle = \text{Tr}(f_j^\dagger(t) f_k(t) \rho)$. For the non-interacting case of an Anderson insulator, this evolution is unitary $\gamma(t) = U(t) \gamma(0) U^\dagger(t)$, where $f_j^\dagger(t) = \sum_l U_{j,l}(t) f_l^\dagger$ is the evolution of the fermionic mode operators. For an Anderson insulator, dynamical localization precisely corresponds to locality of the

unitary evolution [41], meaning that the matrix elements of U are expected to decay exponentially $|U_{j,k}(t)| \leq Ce^{-d(j,k)}$ for some constant C with high probability [42].

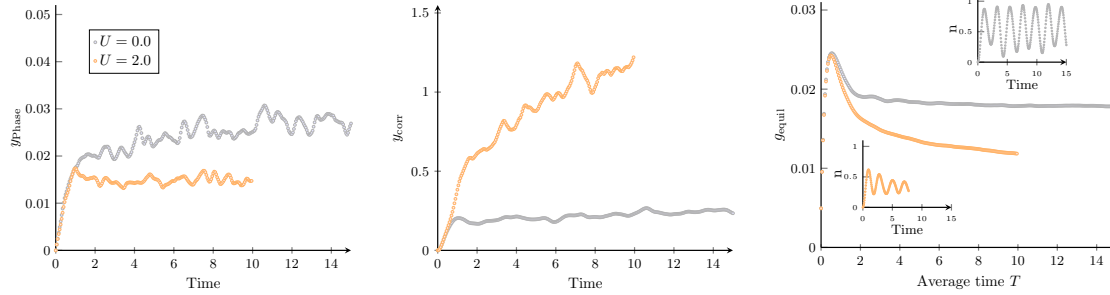


Figure 2. Plotted are the results of a TEBD simulation [43] of the dynamical evolution of the initial state ψ from Equation (2) under the Hamiltonian in Equation (1) for the case of an Anderson insulators with $U = 0$ and MBL with $U = 2$. The disorder strength is $I = 8$. The three plots are averaged over 100 disorder realizations. **(Left)** Shown is the time evolution of y_{Phase} defined in **Measure 1** demonstrating that the phase correlation behavior saturates both for MBL and Anderson localization. **(Middle)** The plot shows the dynamical evolution of y_{Corr} defined in **Measure 2**. Information propagation is fully suppressed in an Anderson insulator, resulting in a saturation of this quantity. In contrast, correlations continue to spread in the MBL system beyond all bounds, giving rise to a remarkably strong signal feasible to be detected in experiments. **(Right)** Shown are the averaged fluctuations g_{Eq} defined in **Measure 3** as a function of the time T over which the average is performed. The insets show the time evolution of the particle density at the position $L/2$, which enters the calculation of g_{Eq} for one disorder realization, which is identical for the MBL and Anderson localized model. As the insets also show, the local fluctuations continue indefinitely for the Anderson insulator, corresponding to a saturation of g_{Eq} , while the MBL system equilibrates and g_{Eq} continues to decrease accordingly.

In the case of interacting Hamiltonians that conserve the particle number, this time evolution can be captured in form of a quantum channel

$$\gamma(t) = \sum_{l=1}^{L^2} K_l(\rho_0, t) \gamma(0) K_l^\dagger(\rho_0, t), \quad (8)$$

where the Kraus operators $K_l(\rho_0, t)$ depend on the full initial state. As particle propagation in an MBL system is expected to also be localized, it is assumed that the individual Kraus operators obey $|K_{j,k}(\rho_0, t)| \leq C_K e^{-d(j,k)}$. Starting from an initial product state of the form in Equation (2), we obtain

$$\begin{aligned} \gamma_{z_1, z_2}(t) &= \langle f_{z_1}^\dagger(t) f_{z_2}(t) \rangle \\ &= \sum_{j,l} \langle z_1 | K(\rho_0, t) | j \rangle \gamma(0)_{j,l} \langle l | K(\rho_0, t) | z_2 \rangle \\ &= \sum_{j \text{ even}} C_K^2 e^{-d(j,0) - d(z_1 + j, z_2)}. \end{aligned} \quad (9)$$

This again results in a suppression with the distance between z_1 and z_2 , causing a saturation of the phase correlation measure $f_{\text{Phase}}(k, t)$ independent of time.

5.2. Slow Spreading of Information

While particles and energies remain confined in interacting localized systems, correlations are expected to show an unbounded increase over time [9,10], although slower than in the ergodic counterpart. In stark contrast, Anderson localized many-body systems will not build up any correlations that go beyond the localization length. To probe the spreading of correlations in the

system, we focus on a quantity easily accessible in the context of optical lattices, using in-situ images for different evolution times. As it turns out, this kind of simple density–density correlator is already sufficient to separate Anderson localization from MBL systems.

Measure 2 (Logarithmic information propagation). *To examine the spatial spreading of density–density correlations, we define the quantity $y_{\text{Corr}}(t)$,*

$$f_{\text{Corr}}(k, t) := |\langle n_{L/2} n_{L/2+k} \rangle - \langle n_{L/2} \rangle \langle n_{L/2+k} \rangle|, \quad (10)$$

$$y_{\text{Corr}}(t) := \sum_k f_{\text{Corr}}(k, t) k^2. \quad (11)$$

y_{Corr} is a direct indicator for the length scale over which density–density correlations are established without having to resort to assuming an explicit form, such as a decay in terms of an exponential function.

Comparable to the dynamics of the phase correlations, we numerically find a steep initial increase followed by a saturation for the non-interacting case (Figure 2). The MBL system, however, continues to build up density–density correlations for the times simulated. There is a transition in propagation speed, which we ascribe to the two dynamical regimes discussed before. Hence, we conclude that density–density correlations can be used to discriminate MBL from its non-interacting counterpart.

An intuitive explanation for the spread of density–density correlations despite spatial localization of particles is that, after exploring the localization length, the particles feel the presence of neighboring particles. Mediated by this interaction, the local movement of particles, governed by the respective constant of motion, becomes correlated, even over large distances. In contrast, in the Anderson insulator where constants of motion are completely decoupled, this communication cannot take place.

We can connect this intuitive explanation to the more rigorous setting of Lieb–Robinson bounds. In the Anderson insulator in one dimension, it is possible to prove that there exists a zero-velocity Lieb–Robinson bound, where the correlator on the left hand side of Equation (4) is bounded by a time independent factor $e^{-\mu d(A,B)}$ [44]. This means that the detectability of an excitation created in region A decreases exponentially with the distance to B . On the contrary, in the MBL regime we expect a logarithmic Lieb–Robinson cone of the form of Equation (4) II. Hence, an unbounded growth of correlations between distant regions is in principle possible, given sufficient time. Furthermore, we have shown that this built-up of correlations also happens on observable time scales, as can be seen from the evolution of density–density correlations captured by **Measure 2**.

5.3. Dephasing and Equilibration

It is also instructive to study the differences between the Anderson and MBL-regime with respect to their equilibration properties. Due to the interactions present, we expect equilibration of fluctuations to take place in MBL systems, whereas in Anderson insulators the effective subspaces explored by single particles remain small for all times and hence fluctuations remain large. This in turn implies that fluctuations of local expectation values die out in the interacting model, but persist in an Anderson insulator. This qualitative difference has already been identified as a signifier of interactions in a disordered system [21]. Here, we build upon this idea and propose to consider the average change rate of local expectation values in order to detect the decreasing fluctuations in the MBL phase.

Measure 3 (Density evolution: Equilibration of fluctuations). *We consider the expectation value $f_{\text{Eq}}(t) = \langle n_{L/2} \rangle(t)$ of a local density operator in the middle of the system. As a measure of local equilibration, we introduce the averaged rate of change of this density as a function of time $T > 0$*

$$g_{\text{Eq}}(T) := \frac{1}{T} \int_0^T dt |f'_{\text{Eq}}(t)|. \quad (12)$$

As laid out in Figure 2, again, this function over time indeed shows a remarkably smooth behavior that allows for the clear distinction between an Anderson localized system and its MBL counterpart in that, after a mutual increase, the Anderson system saturates at a constant value, whereas, in the MBL phase, g_{Eq} shrinks successively.

If we again resort to the Lieb–Robinson bound picture, we find that in the Anderson case a local excitation is confined to a distinct spatial region given by the zero-velocity Lieb–Robinson bound introduced in the previous section. This implies that the effective subspace explored is constant and specifically, the excitation cannot build up long distance correlations and fluctuations remain large. This can also be seen from the results of **Measure 2**. If we now, however, turn to the interacting model, a local excitation will slowly explore larger and larger parts of the Hilbert space, leading to a slow, but persistent decrease of the fluctuations.

5.4. Present and Future Experimental Realizations

For an optical lattice architecture, the limitations of implementing the given measures are governed by the achievable repetition rate of the experiment and the quality of the initial state preparation. First, several repetitions are needed to get the expectation value of the measurements. Due to the disorder present in the system, it is furthermore necessary to repeat the first step with changing disorder to obtain a disorder averaged quantity. Lastly, since dynamics are in the focus of our measures, the described procedure needs to be carried out at any point in time. For linear quantities, such as **Measure 1**, **Measure 3** or the imbalance, which is a measure of particle localization as well [21], the quantum average does in principle commute with the disorder average allowing for simultaneous averaging with fewer realizations. This is however not the case for non-linear quantities such as **Measure 2**. Here, the full procedure described above needs to be carried out. The repetition rates of optical lattices are on the order of seconds and leading experimentalists assured us that taking reliable data for all our measures is indeed feasible [45].

Recently, there was an impressive progress in measuring quantities very much related to the entanglement entropy in small one-dimensional optical lattices [46,47]. In both these works, quantities similar to our **Measure 2** are used as well. In Ref. [47], the authors defined a quantity called transport distance which basically coincides with our **Measure 2**. The difference being that their scaling function is only linear instead of quadratic. However, they do not employ this measure to show the many-body correlations in these systems. Rather, they calculated the number and configurational entanglement [46]. The system sizes used are very restricted, possibly due to the complicated procedure of obtaining these entropies.

We think that an implementation of **Measure 2** or **Measure 3** might complement these results nicely by overcoming these problems and hence being applicable also for larger systems and potentially also higher dimensional systems, where the fate of MBL is still debated.

6. Conclusions and Outlook

In this work, we proposed an operational procedure for distinguishing MBL phases building upon realistic measurements, which can be performed in the realm of optical lattices with present technology. Utilizing a phenomenological model and the concept of Lieb–Robinson bounds, we explained the effects numerically investigated employing tensor network methods. The equilibration of local observables allows for the distinction of Anderson and MBL localized models. Density–density correlations allow for the same information bit extraction, while also reproducing the expected phenomenology. Further investigating this quantity might yield information about the localization length via the duration of the first evolution regime.

Phase correlations, which are directly connected to ToF imaging, cannot detect interactions in a localized system due to their correspondence to particle transport. There is yet other information the ToF reveals: One can also lower bound the spatial entanglement of bosons in optical lattices [48], building upon the ideas of constructing quantitative entanglement witnesses [25–27], a notion

of multi-partite entanglement $M(t)$ detecting a deviation from a best separable approximation, as $M(t) \geq \max(0, \langle n \rangle - \langle n(q) \rangle / |\hat{w}_0(q)|^2)$ for all q . This quantity detects a reasonable notion of multi-particle entanglement, which is yet different from the bi-partite entanglement discussed above. Since this measure is only onsite local, we would expect that it cannot distinguish the long-range correlations of an interacting disordered model from the dynamics inside the constant of motion. This further motivates the quest to engineer appropriate entanglement witnesses both accessible in optical lattice architectures as well as probing key features of MBL, a quest that is in turn expected to contribute to our understanding of MBL as such.

Author Contributions: Conceptualization: M.F., W.B., A.H.W. and J.E. Investigation: M.G. and M.F. Writing—Original Draft Preparation: M.G. and M.F. Writing—Review and Editing: A.H.W. and J.E. Validation: A.H.W. and J.E. Visualization: M.F. and J.E. Supervision: J.E. Project Administration: J.E. Funding Acquisition: J.E.

Funding: This research was funded by the DFG grant number FOR2724, CRC 183, EI 519/14-1, EI 519/7-1, EI 519/15-1, the European Commission grant number AQUUS, SIQS, RAQUEL, the Templeton Foundation, the ERC grant number TAQ, the European Union’s Horizon 2020 research and innovation programme under grant agreement No. 817482 (PASQuaS).

Acknowledgments: We warmly thank A. Rubio Abadal, U. Schneider, C. Gross, I. Bloch, A. Scardicchio, and R. Vasseur for discussions. *Note added:* This work was first submitted as a preprint as a blueprint for a joint experimental-theoretical effort in progress. We now decided to properly publish this work in Quantum Reports as a scientific venue that is sympathetic to preprints. We insist that this work is still timely and guiding present and future experiments.

Conflicts of Interest: The authors declare no conflict of interest

Appendix A. Numerical Details

In this appendix, we present the details of our numerical simulations. Our results mainly rely on a matrix-product state simulation based on a TEBD code [43], thus an instance of a tensor network state simulation. To corroborate the results, we further employ an exact diagonalization code [49] that uses the particle number symmetry and keeps track of the time evolution with a Runge–Kutta integration scheme. For the non-interacting case, further checks are performed by an explicit simulation of the dynamical evolution of the covariance matrix, which takes a particularly easy form in this case.

For short times and the system sizes that can be achieved with exact diagonalization, the codes agree up to a negligible error, thus also demonstrating that the chosen step size in the fifth-order Trotter decomposition used in TEBD [43] of τ_{step} does not produce significant errors. This leaves only two potential error sources: the fact that numerics necessarily simulate a finite system and the possibility of discarded weights accumulating over time.

Performing a finite size scaling, we find that comparably small systems are already indistinguishable from the thermodynamic limit for the quantities considered here (see Figure A1). This is in agreement with the very slow growth of Lieb–Robinson cones expected in these disordered systems. To be on the safe side, we have nevertheless carried out our numerical analysis on systems with $L = 80$ sites and open boundary conditions.

Having demonstrated that the considered system size is indistinguishable from the thermodynamic limit only leaves the discarded weight as potential error source (see Figure A2). The time evolution of this quantity, which is directly connected to spatial entanglement entropies, depends strongly on the chosen disorder realization. To keep this discarded weight small enough, we increase the bond dimension in the simulation in a three-step procedure up to $d_{\text{Bond}} = 350$, which is sufficient to guarantee a discarded weight smaller than 2×10^{-5} for all disorder realizations.

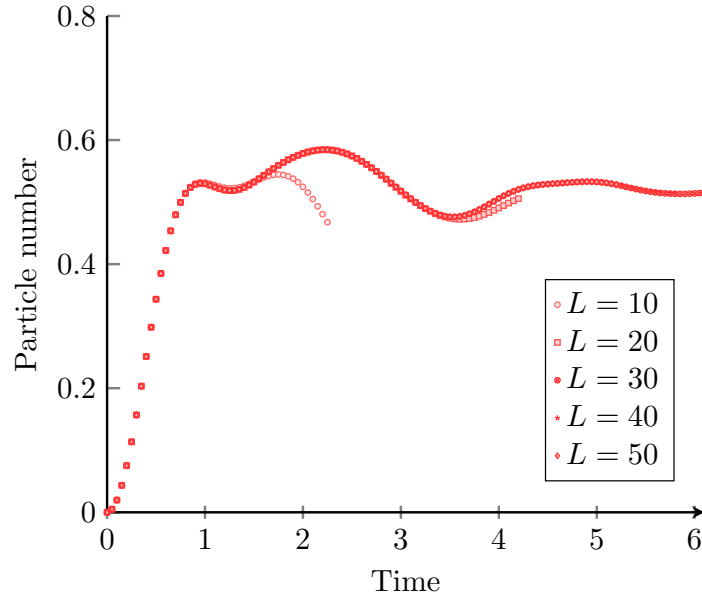


Figure A1. Finite size scaling for the evolution of particle density in the middle of the chain for a typical disorder realization. For $L = 10, 20$, an exact diagonalization code was used. The other system sizes are simulated with a TEBD code [43].

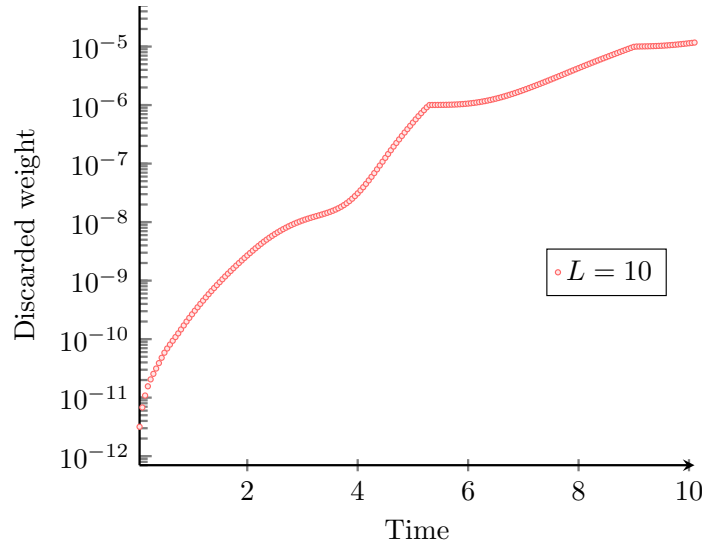


Figure A2. Evolution of the discarded weight. This plot varies strongly depending on the chosen disorder realization. From the 100 realizations used for the averaged plots, the realization with the largest discarded weights is shown here.

Appendix B. Bosonic Model with On-Site Interactions

In this appendix, we show additional simulation data for a measure similar to **Measure 2** for a related model that is used in some of the experimental realizations of MBL. This is the disordered Bose–Hubbard model with on-site interactions given by

$$H = \sum_j (b_j^\dagger b_{j+1} + \text{h.c.}) + \sum_j w_j n_j + U \sum_j n_j n_j, \quad (\text{A1})$$

where b_j denotes a bosonic operator on site j , $n_j = b_j^\dagger b_j$ is the local particle number operator and, again, we draw the w_j from the uniform distribution on the interval $[-I, I]$. In contrast to the fermionic variant in the main text, we here need to restrict the local Hilbert space to be able to perform numerics.

We restrict the local particle number to $k = 3$ particles per site, but also make sure that enlarging the local dimension would not change our results qualitatively. Moreover, our initial state is again an MIS state as defined in Equation (2), featuring an average particle number of 0.5 per site. The measure we employ for bosons is identical to **Measure 2** with the exception that the number operators were replaced by parity operators.

Measure 4 (Logarithmic information propagation). *To examine the spatial spreading of parity–parity correlations, we define the quantity $P_{\text{Corr}}(t)$,*

$$f_{\text{Corr}}(k, t) := |\langle p_{L/2} p_{L/2+k} \rangle - \langle p_{L/2} \rangle \langle p_{L/2+k} \rangle|, \quad (\text{A2})$$

$$P_{\text{Corr}}(t) := \sum_k f_{\text{Corr}}(k, t) k^2, \quad (\text{A3})$$

where p is the local parity operator.

In Figure A3, we show **Measure 4** for the Anderson ($U = 0$) and MBL ($U = 2$) case. Similar to the main text, we find that, in the non-interacting case, the measure saturates after few tunneling times. In contrast, for the interacting model, we found that the measure grew in comparable fashion to the fermionic counterpart (grey stars). This suggests that the correlation measure can be employed in similar models as well.

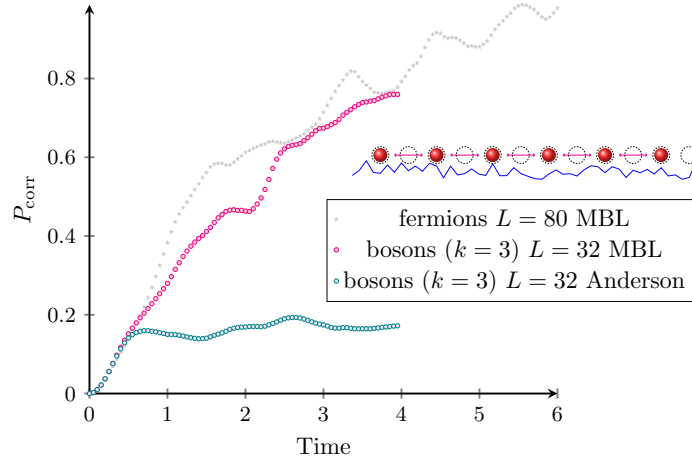


Figure A3. Plotted are the results of a TEBD simulation of the dynamical evolution of the parity–parity correlations P_{corr} . The initial state ψ is again found in Equation (2) under the Hamiltonian in Equation (A1) for the case of an Anderson insulator with $U = 0$ and MBL with $U = 2$. We compared the results of the fermionic MBL setting and the bosonic MBL and Anderson setting with a local Hilbert space dimension truncation $k = 3$. Every data point corresponds to an average of over 100 realizations.

References

1. Basko, D.M.; Aleiner, I.L.; Altshuler, B.L. Metal-insulator transition in a weakly interacting many-electron system with localized single-particle states. *Ann. Phys.* **2006**, *321*, 1126. [[CrossRef](#)]
2. Anderson, P.W. Absence of Diffusion in Certain Random Lattices. *Phys. Rev.* **1958**, *109*, 1492. [[CrossRef](#)]
3. Nandkishore, R.; Huse, D.A. Many-Body Localization and Thermalization in Quantum Statistical Mechanics. *Ann. Rev. Cond. Mat. Phys.* **2015**, *6*, 15–38. [[CrossRef](#)]
4. Pal, A.; Huse, D.A. The many-body localization transition. *Phys. Rev. B* **2010**, *82*, 174411. [[CrossRef](#)]
5. Oganesyan, V.; Huse, D.A. Localization of interacting fermions at high temperature. *Phys. Rev. B* **2007**, *75*, 155111. [[CrossRef](#)]
6. Polkovnikov, A.; Sengupta, K.; Silva, A.; Vengalattore, M. Non-equilibrium dynamics of closed interacting quantum systems. *Rev. Mod. Phys.* **2011**, *83*, 863. [[CrossRef](#)]

7. Eisert, J.; Friesdorf, M.; Gogolin, C. Quantum many-body systems out of equilibrium. *Nat. Phys.* **2015**, *11*, 124–130. [[CrossRef](#)]
8. Gogolin, C.; Eisert, J. Equilibration, thermalisation, and the emergence of statistical mechanics in closed quantum systems. *Rep. Prog. Phys.* **2016**, *79*, 056001. [[CrossRef](#)]
9. Znidaric, M.; Prosen, T.; Prelovsek, P. Many-body localization in the Heisenberg XXZ magnet in a random field. *Phys. Rev. B* **2008**, *77*, 064426. [[CrossRef](#)]
10. Bardarson, J.H.; Pollmann, F.; Moore, J.E. Unbounded Growth of Entanglement in Models of Many-Body Localization. *Phys. Rev. Lett.* **2012**, *109*, 017202. [[CrossRef](#)]
11. Goold, J.; Clark, S.R.; Gogolin, C.; Eisert, J.; Scardicchio, A.; Silva, A. Total correlations of the diagonal ensemble herald the many-body localisation transition. *Phys. Rev. B* **2015**, *92*, 180202(R). [[CrossRef](#)]
12. Eisert, J.; Cramer, M.; Plenio, M.B. Area laws for the entanglement entropy. *Rev. Mod. Phys.* **2010**, *82*, 277. [[CrossRef](#)]
13. Bauer, B.; Nayak, C. Area laws in a many-body localised state and its implications for topological order. *J. Stat. Mech.* **2013**, *2013*, P09005. [[CrossRef](#)]
14. Friesdorf, M.; Werner, A.H.; Brown, W.; Scholz, V.B.; Eisert, J. Many-body localisation implies that eigenvectors are matrix-product states. *Phys. Rev. Lett.* **2015**, *114*, 170505. [[CrossRef](#)] [[PubMed](#)]
15. Srednicki, M. Chaos and quantum thermalization. *Phys. Rev. E* **1994**, *50*, 888–901. [[CrossRef](#)]
16. Kim, I.H.; Chandran, A.; Abanin, D.A. Local integrals of motion and the logarithmic light cone in many-body localised systems. *Phys. Rev. B* **2015**, *91*, 085425.
17. Chandran, A.; Carrasquilla, J.; Kim, I.H.; Abanin, D.A.; Vidal, G. Spectral tensor networks for many-body localisation. *Phys. Rev. B* **2015**, *92*, 024201. [[CrossRef](#)]
18. Friesdorf, M.; Werner, A.H.; Goihl, M.; Eisert, J.; Brown, W. Local constants of motion imply transport. *New J. Phys.* **2015**, *17*, 113054. [[CrossRef](#)]
19. Serbyn, M.; Papić, Z.; Abanin, D.A. Local Conservation Laws and the Structure of the Many-Body Localized States. *Phys. Rev. Lett.* **2013**, *111*, 127201. [[CrossRef](#)] [[PubMed](#)]
20. Huse, D.A.; Nandkishore, R.; Oganesyan, V. Phenomenology of fully many-body-localized systems. *Phys. Rev. B* **2014**, *90*, 174202. [[CrossRef](#)]
21. Schreiber, M.; Hodgman, S.S.; Bordia, P.; Lüschen, H.P.; Fischer, M.H.; Vosk, R.; Altman, E.; Schneider, U.; Bloch, I. Observation of many-body localization of interacting fermions in a quasi-random optical lattice. *Science* **2015**, *349*, 842. [[CrossRef](#)] [[PubMed](#)]
22. Bordia, P.; Lüschen, H.P.; Hodgman, S.S.; Schreiber, M.; Bloch, I.; Schneider, U. Coupling Identical one-dimensional Many-Body Localized Systems. *Phys. Rev. Lett.* **2016**, *116*, 140401. [[CrossRef](#)] [[PubMed](#)]
23. Wiersma, D.S.; Bartolini, P.; Lagendijk, A.; Righini, R. Localization of light in a disordered medium. *Nature* **1997**, *390*, 671–673. [[CrossRef](#)]
24. Bloch, I.; Dalibard, J.; Nascimbene, S. Quantum simulations with ultracold quantum gases. *Nat. Phys.* **2012**, *8*, 267. [[CrossRef](#)]
25. Eisert, J.; Brandao, F.G.; Audenaert, K.M. Quantitative entanglement witnesses. *New J. Phys.* **2007**, *9*, 46. [[CrossRef](#)]
26. Audenaert, K.M.R.; Plenio, M.B. When are correlations quantum? *New J. Phys.* **2006**, *8*, 266. [[CrossRef](#)]
27. Guehne, O.; Reimpell, M.; Werner, R.F. Estimating entanglement measures in experiments. *Phys. Rev. Lett.* **2007**, *98*, 110502. [[CrossRef](#)]
28. Gring, M.; Kuhnert, M.; Langen, T.; Kitagawa, T.; Rauer, B.; Schreitl, M.; Mazets, I.; Smith, D.A.; Demler, E.; Schmiedmayer, J. Relaxation and Prethermalization in an Isolated Quantum System. *Science* **2012**, *337*, 1318. [[CrossRef](#)]
29. Steffens, A.; Friesdorf, M.; Langen, T.; Rauer, B.; Schweigler, T.; Hübener, R.; Schmiedmayer, J.; Riofrio, C.A.; Eisert, J. Towards experimental quantum field tomography with ultracold atoms. *Nat. Commun.* **2015**, *6*, 7663. [[CrossRef](#)]
30. Luitz, D.J.; Laflorencie, N.; Alet, F. Many-body localisation edge in the random-field Heisenberg chain. *Phys. Rev. B* **2015**, *91*, 081103. [[CrossRef](#)]
31. Singh, R.; Bardarson, J.H.; Pollmann, F. Signatures of the many-body localization transition in the dynamics of entanglement and bipartite fluctuations. *New J. Phys.* **2016**, *18*, 023046. [[CrossRef](#)]
32. Serbyn, M.; Papić, Z.; Abanin, D.A. Criterion for many-body localization-delocalization phase transition. *Phys. Rev. X* **2015**, *5*, 041047. [[CrossRef](#)]

33. Serbyn, M.; Knap, M.; Gopalakrishnan, S.; Papic, Z.; Yao, N.Y.; Laumann, C.R.; Abanin, D.A.; Lukin, M.D.; Demler, E.A. Interferometric Probes of Many-Body Localization. *Phys. Rev. Lett.* **2014**, *113*, 147204. [[CrossRef](#)] [[PubMed](#)]
34. Roy, D.; Singh, R.; Moessner, R. Probing many-body localisation by spin noise spectroscopy. *Phys. Rev. B* **2015**, *92*, 180205. [[CrossRef](#)]
35. Vasseur, R.; Parameswaran, S.A.; Moore, J.E. Quantum revivals and many-body localization. *Phys. Rev. B* **2015**, *91*, 140202. [[CrossRef](#)]
36. Choi, J.Y.; Hild, S.; Zeiher, J.; Schauß, P.; Rubio-Abadal, A.; Yefsah, T.; Khemani, V.; Huse, D.A.; Bloch, I.; Gross, C. Exploring the many-body localization transition in two dimensions. *Science* **2016**, *352*, 1547–1552. [[CrossRef](#)]
37. Trotzky, S.; Chen, Y.A.; Flesch, A.; McCulloch, I.P.; Schollwoeck, U.; Eisert, J.; Bloch, I. Probing the relaxation towards equilibrium in an isolated strongly correlated one-dimensional Bose gas. *Nat. Phys.* **2012**, *8*, 325. [[CrossRef](#)]
38. Ros, V.; Müller, M.; Scardicchio, A. Integrals of motion in the many-body localized phase. *Nucl. Phys. B* **2015**, *891*, 420–465. [[CrossRef](#)]
39. Lieb, E.H.; Robinson, D.W. The finite group velocity of quantum spin systems. *Commun. Math. Phys.* **1972**, *28*, 251–257. [[CrossRef](#)]
40. Daley, A.J.; Kollath, C.; Schollwoeck, U.; Vidal, G. Time-dependent density-matrix renormalization- group using adaptive effective Hilbert spaces. *J. Stat. Mech.* **2004**, *2004*, P04005. 04/P04005. [[CrossRef](#)]
41. Kirsch, W. An invitation to random Schroedinger operators. *arXiv* **2007**, arXiv:0709.3707.
42. Germinet, F.; Klein, A. Bootstrap multi-scale analysis and localization in random media. *Commun. Math. Phys.* **2001**, *222*, 415. [[CrossRef](#)]
43. Wall, M.L.; Carr, L.D. Open Source TEBD. 2013. Available online: [http://physics.mines.edu/downloads/software/tebd\(2009\)](http://physics.mines.edu/downloads/software/tebd(2009)) (accessed on 12 June 2019).
44. Burrell, C.K.; Eisert, J.; Osborne, T.J. Information propagation through quantum chains with fluctuating disorder. *Phys. Rev. A* **2009**, *80*, 052319. [[CrossRef](#)]
45. Gross, C.; Bloch, I. (Max-Planck-Institut für Quantenoptik, Garching, Germany). Personal communication, 2018.
46. Lukin, A.; Rispoli, M.; Schittko, R.; Tai, M.E.; Kaufman, A.M.; Choi, S.; Khemani, V.; Leonard, J.; Greiner, M. Probing entanglement in a many-body-localized system. *arXiv* **2018**, arXiv:1805.09819.
47. Rispoli, M.; Lukin, A.; Schittko, R.; Kim, S.; Tai, M.E.; Léonard, J.; Greiner, M. Quantum critical behavior at the many-body-localization transition. *arXiv* **2018**, arXiv:1812.06959.
48. Cramer, M.; Bernard, A.; Fabbri, N.; Fallani, L.; Fort, C.; Rosi, S.; Caruso, F.; Inguscio, M.; Plenio, M. Spatial entanglement of bosons in optical lattices. *Nat. Commun.* **2013**, *4*, 2161. [[CrossRef](#)]
49. Jones, E.; Oliphant, T.; Peterson, P. *SciPy: Open Source Scientific Tools for Python*; ResearchGate: Berlin, Germany, 2001.



© 2019 by the authors. Licensee MDPI, Basel, Switzerland. This article is an open access article distributed under the terms and conditions of the Creative Commons Attribution (CC BY) license (<http://creativecommons.org/licenses/by/4.0/>).

CONSTRUCTING CONSTANTS OF MOTION FOR MANY-BODY LOCALISED SYSTEMS

Finding constants of motion for quantum systems is deceptively simple. Given the diagonalising unitary, any operator that is diagonal in the same basis as the Hamiltonian commutes with it by construction. However, for many-body localised systems we are interested in those constants of motion that actually have an impact onto the local dynamics of the system. This allows to measure their presence with local observables. In the following, we lay out a procedure that heuristically constructs local constants of motion given the diagonalising unitary.

5.1 CONSTRUCTING LOCAL CONSTANTS OF MOTION

In the case of many-body localisation, we are looking for L many functionally independent constants of motion. Intuitively, these should be a quasi-local unitary transformation of particle number operators to promote them to localisation regions. This is why many approaches take local particle numbers as initial operators and try to achieve commutation with the Hamiltonian perturbatively [54--56]. This however makes it very difficult to ensure that the operators remain functionally independent. Moreover, the final operators usually do not commute exactly with the Hamiltonian.

We instead propose an inverse approach in which we start with the energy space representation of the operators, where we exactly know what they should look like and then optimise the diagonalisation unitary to get their real space representation while still preserving all wanted algebraic properties. The obtained operators are therefore commuting exactly with the Hamiltonian and are still functionally independent. The remaining task is to optimise their locality in real space.

Consider L many Pauli-Z operators Z_i that are defined in energy space. These naturally form a basis for this diagonal space and it is hence possible to decompose the full Hamiltonian in terms of those, as shown in Chapter 2. Furthermore, they by definition commute with H and are functionally independent. Assume furthermore, we are given the unitary U_D which diagonalises the Hamiltonian $H = U_D \Lambda U_D^\dagger$, where $\Lambda = \sum_i e_i |i\rangle\langle i|$. The real space representation of the Z_i is accordingly given by $U_D Z_i U_D^\dagger$. If we reorder eigenvalues of the Hamiltonian H and the corresponding eigenvectors in the diagonalisation unitary U_D , we leave the Hamiltonian invariant. However, we are allowed to change the mapping between eigenvalues of Z_i and the eigenvectors of U_D . In fact, this is the only freedom we still have for optimising the locality of the Z_i . Essentially, this amounts to finding a new set of constants of motion \tilde{Z}_i that is related to the old set by $\tilde{Z}_i = P Z_i P$, where P is a permutation matrix. But since there are 2^L many entries in each Z_i , a brute force approach would require checking $2^L!$ many permutations. While this is practically infeasible, not all hope is lost as long as there is a useful heuristic that aids the optimisation.

In a many-body localised system, we expect the real space representation of the constants of motion to resemble the local particle number operator as their physical

interpretation should be that of a localisation region. This can be employed to find an heuristic ordering of the eigenvectors in \mathcal{U}_D . In the following, we will put this approach to a test in a many-body localised system.

CLIMATE FOOTPRINT ESTIMATE

Total Kernel hours [h]	576000
Total Energy consumption [kWh]	16560
Total CO ₂ -emission [kg]	9274

Table 5.1: Estimated climate footprint of the numerical calculations performed for the paper “Construction of exact constants of motion and effective models for many-body localized systems”. Estimates are based only on the data for the interacting system of size $L = 13$ presented in the manuscript and exclude prototyping. CO₂-emission estimates are based on the German average emission of 0.56 kg/kWh. A comparable emission is the average annual German emission per capita (11.000 kg) [57]. Calculations were performed on the `leonard` cluster equipped with Intel® Xeon® Processor X5570 and nodes with a thermal design power of 95 W. Further details on the estimation can be found in Appendix A

Construction of exact constants of motion and effective models for many-body localized systems

M. Goihl, M. Gluza, C. Krumnow, and J. Eisert

Dahlem Center for Complex Quantum Systems, Freie Universität Berlin, 14195 Berlin, Germany

(Received 7 August 2017; published 16 April 2018)

One of the defining features of many-body localization is the presence of many quasilocal conserved quantities. These constants of motion constitute a cornerstone to an intuitive understanding of much of the phenomenology of many-body localized systems arising from effective Hamiltonians. They may be seen as local magnetization operators smeared out by a quasilocal unitary. However, accurately identifying such constants of motion remains a challenging problem. Current numerical constructions often capture the conserved operators only approximately, thus restricting a conclusive understanding of many-body localization. In this work, we use methods from the theory of quantum many-body systems out of equilibrium to establish an alternative approach for finding a complete set of exact constants of motion which are in addition guaranteed to represent Pauli- z operators. By this we are able to construct and investigate the proposed effective Hamiltonian using exact diagonalization. Hence, our work provides an important tool expected to further boost inquiries into the breakdown of transport due to quenched disorder.

DOI: [10.1103/PhysRevB.97.134202](https://doi.org/10.1103/PhysRevB.97.134202)**I. INTRODUCTION**

The question of the precise mechanism of thermalization of closed quantum many-body systems lies at the heart of the foundations of quantum statistical mechanics. For generic systems, one generally expects that the unitary time evolution evolves the system into states that can locally be captured by a thermodynamic ensemble using only few parameters such as the total energy or particle number [1–3]. This expectation will be violated if additional structure is present in the system that enforces a *local* memory of initial conditions by confining, for instance, particles to local regions. Such a nonthermalizing behavior caused by localization is most famously observed due to quenched disorder in Anderson insulators [4] and prevails under the addition of interactions in the form of *many-body localization* (MBL) as predicted theoretically [5–7] and observed experimentally [8,9].

These systems are expected to feature extensively many *quasilocal constants of motion* (qLCOMs) which prevent a thermodynamic description. In stark contrast to the Anderson insulator, many-body localized systems feature a slow, *unbounded growth of entanglement* due to interactions [10,11]. Moreover, all MBL eigenstates are expected to fulfill an entanglement area law [12–14], which delineates them from the eigenstates of thermalizing systems while making them amenable to *tensor network approaches* [14–19]. Due to their special structure, MBL systems are candidates for understanding fundamental aspects of quantum mechanics, microscopic transport properties, and interacting systems as their efficient description appears to be in reach.

One of the most successful explanations of the intriguing behavior of MBL systems has been through a proposed effective Hamiltonian valid in the strong disorder limit, stated by employing a complete set of qLCOMs [20,21]. This description explains the logarithmic entanglement growth [10,22,23]. For the case of disordered spin chains the qLCOMs are considered to be dressed local magnetization operators, i.e.,

local spin operators conjugated by a unitary transformation smearing their support within an exponential envelope but at the same time promoting them to constants of motion. Under reasonable assumptions these operators can actually be calculated analytically for a specific MBL model [24] that is disordered in all parameters. For models which contain disorder only in the form of local potentials, much in the spirit of current experimental investigations, no analytical results are known as of today. It is hence unclear if more physical models of MBL, such as the disordered Heisenberg chain, can actually be mapped to the effective Hamiltonian of Refs. [20,21]. We report on progress in developing a machinery to numerically construct exact quasilocal constants of motion.

Among the strategies established so far are several variants of transformation schemes which focus on decoupling the Hamiltonian [25–29] and by this implicitly define qLCOMs. These approaches have the advantage of being able to treat larger systems at the cost of making specific approximations, whose exact effects need to be understood [30,31]. For small systems exact diagonalization based methods can be used [32–34]. While in general quite arbitrary operators qualify as constants of motion, one aims to ensure specific attributes when constructing them numerically. The qLCOMs are supposed to be quasilocal, resemble Pauli- z operators by being traceless with only two degenerate eigenvalues, and mutually commute among each other and of course with the Hamiltonian of the system. Different numerical schemes trade these properties differently against each other. Whenever exact diagonalization is feasible then qLCOMs can be constructed directly, e.g., via optimizing the commutant matrix [33,34] or performing the infinite-time average [32] which also inspired our work. The latter methods perturb the spectrum and the qLCOMs are not dressed spins anymore and the former study shows that when a local region is embedded into a larger one then the optimal qLCOMs conditioned on the subsystem size could be a superposition of several dressed spin operators because of tail cancellation. In neither of these

exact diagonalization (ED) studies it was possible to construct the effective Hamiltonian of Refs. [20,21] in order to support the large-scale transformation schemes.

In this work we present a scheme for computing constants of motion that allows us to study the effective Hamiltonian. The idea behind our construction follows a clear physical intuition: Quasilocality conservation of the local magnetization implies that the corresponding local Pauli- z operators remain approximately local under time evolution. We show numerically that infinite time-averaged magnetization operators can be promoted to true Pauli- z operators, while keeping the locality properties intact and gaining the desired spectrum by construction. Our construction fails to be local if the time evolution ergodically spreads local excitations and is hence physically directly connected to the breakdown of MBL. Equipped with a full set of exact qLCOMs we go a step further and study the effective model of Refs. [20,21] for the disordered Heisenberg chain, which is based on obtained qLCOMs.

II. SETTING

We consider the prototypical model of MBL, the disordered spin-1/2-Heisenberg chain on L sites

$$H = \sum_{i=1}^L (\sigma_i^x \sigma_{i+1}^x + \sigma_i^y \sigma_{i+1}^y + \sigma_i^z \sigma_{i+1}^z + \Delta h_i \sigma_i^z), \quad (1)$$

where the h_i are drawn from the interval $h_i \in [-1, 1]$ and Δ denotes the disorder strength. This model is expected to undergo a localization transition at $\Delta \approx 7.5$. Moreover, we use periodic boundary conditions in order to have a meaningful definition of support for all lattice sites and denote with $\text{dist}(\cdot, \cdot)$ the natural distance of two sites for a ring configuration. The Pauli operators above in the Hamiltonian denote real space spin operators acting on lattice sites $i = 1, \dots, L$ by $\sigma_i^\alpha := \mathbb{1}_{2^{i-1}} \otimes \sigma^\alpha \otimes \mathbb{1}_{2^{L-i}}$, where σ^α for $\alpha = x, y, z$ denotes the spin-1/2 Pauli matrices and $\mathbb{1}_n$ the identity on \mathbb{C}^n . These operators are formulated within the standard real space basis $\{|i_1 \dots i_L\rangle | i_j = 0, 1\}$ which we abbreviate by $|\widetilde{j}\rangle$ with $j = 1, \dots, 2^L$ and $|\widetilde{j}\rangle = |(j-1)_2\rangle$, where x_2 denotes the binary representation of $x \in \mathbb{N}$ and we add leading 0's on the left such that x_2 has always L bits. For the following, it is useful to note that the σ_i^z operators for $i = 1, \dots, L$ can be written as

$$\sigma_i^z = \sum_{j=1}^{2^L} (-1)^{\lfloor (j-1)/2^{L-i} \rfloor} |\widetilde{j}\rangle \langle \widetilde{j}| \quad (2)$$

with $\lfloor \dots \rfloor$ denoting the floor function.

Similarly, we introduce Pauli operators defined in energy space. Given an eigenbasis $\{|k\rangle\}$ of H , we specify another set of Pauli- z operators through the relation

$$\mathcal{Z}_i = \sum_{k=1}^{2^L} (-1)^{\lfloor (k-1)/2^{L-i} \rfloor} |k\rangle \langle k|. \quad (3)$$

In the infinite disorder limit ($\Delta \rightarrow \infty$), the Hamiltonian becomes diagonal in the real space basis and hence these operators become equal to the $\{\sigma_i^z\}$ operators. For the general case with finite Δ , however, the $\{\mathcal{Z}_i\}$ and $\{\sigma_i^z\}$ are formulated in

different bases and differ from each other. Written in the given eigenbasis of H it holds then that $\mathcal{Z}_i = \mathbb{1}_{2^{i-1}} \otimes \sigma^z \otimes \mathbb{1}_{2^{L-i}}$ which corresponds to a formal decomposition $\mathcal{H} = \mathbb{C}^{2^L} \simeq \otimes_{i=1}^L \mathbb{C}^2$ that is implicitly fixed by an arbitrarily chosen order of energy eigenvalues and eigenvectors. As this is crucial for the following we emphasize that the $\mathcal{Z}_i = \mathbb{1}_{2^{i-1}} \otimes \sigma^z \otimes \mathbb{1}_{2^{L-i}}$ operators are formulated in energy space, meaning that the σ^z operators here are diagonal in energy space and in principle unrelated to their real space versions. Hence, there are two decompositions of the Hilbert space into $\otimes_{i=1}^L \mathbb{C}^2$, one in real and the other in energy space. Identifying a decomposition of \mathcal{H} in energy space which preserves locality in real space lies at the heart of the construction of the set of qLCOMs.

Throughout this work, the MBL constants of motion will be denoted by τ_i^z . Let us summarize their desired properties:

(i) *Independent conserved quantities.* The $\{\tau_i^z\}$ operators must commute with H and each other

$$[H, \tau_i^z] = 0 \quad \text{and} \quad [\tau_i^z, \tau_j^z] = 0 \quad \forall i, j. \quad (4)$$

(In fact, they should be functionally independent, i.e., no constant of motion can be expressed as a function of the other.)

(ii) *Dressed spins.* The qLCOMs are expected to have a spectrum resembling Pauli- z operators, i.e., there exists a dressing unitary U_D^\dagger transforming the energy to real space

$$\tau_i^z = U_D \mathcal{Z}_i U_D^\dagger. \quad (5)$$

(iii) *Quasilocality.* For each i let us denote by S a “buffer” region of odd cardinality $|S|$, i.e., $S := \{j : \text{dist}(i, j) \leq (|S| - 1)/2\}$. Then we demand that the conserved quantities must be quasilocal, meaning each τ_i^z is centered around site i , and its local reductions fulfill

$$1 - \frac{1}{2^{|S|+2|S^c|}} \|\text{Tr}_{S^c}(\tau_i^z)\|_2^2 \leq f(|S|), \quad (6)$$

where $\text{Tr}_{S^c}(\cdot)$ denotes the partial trace over the complement of S , and $f: \mathbb{N} \rightarrow \mathbb{R}^+$ is a suitably—presumably exponentially—decaying function. Acknowledging that $\|A\|_2^2 = \text{Tr}(A^\dagger A)$, this is exactly the quantity-measuring locality discussed in Ref. [32], and it implies the locality discussed in Ref. [35]. Note that there are several possible definitions for measuring the locality of the qLCOMs. It is interesting to see that this notion of quasilocality based on the Hilbert-Schmidt norm is the sense in which it is discussed for integrable models [36–38].

Note that constructing a set of constants of motion fulfilling only properties (i) and (ii) can be easily done for systems which allow for exact diagonalization, as any set of $\{\mathcal{Z}_i\}$ operators constructed from any eigenbasis of H will automatically satisfy (i) and (ii). Ensuring (iii), however, is nontrivial in this case and can only be obtained by choosing a correct ordering of eigenvectors of H in the eigenbasis.

III. EFFECTIVE DESCRIPTION OF LOCALIZATION

Assuming the precise knowledge of the set of qLCOMs, it is possible to identify an effective Hamiltonian in terms of the $\{\tau_i^z\}$ operators because by properties (i) and (ii), the collection of $\{\tau_i^z\}$ and products thereof form a basis for all matrices diagonal in the chosen eigenbasis $\{|k\rangle\}$ of H . Given

a set of qLCOMs the effective model [20,21] takes the form

$$H_{\text{eff}}^{(N_{\text{eff}})} = \sum_i \omega_i^{(1)} \tau_i^z + \sum_{i,j} \omega_{i,j}^{(2)} \tau_i^z \tau_j^z + \dots, \quad (7)$$

where \dots subsumes terms up to a truncation order N_{eff} , and $H_{\text{eff}}^{(L)} = H$ if the order of the expansion reaches the system size $N_{\text{eff}} = L$. Let us introduce a subscript $\mu \in \{0,1\}^L$, a binary word of length L , which determines the position of the $\{\tau_i^z\}$ operators in the chain and define $\tau(\mu) = \prod_{i=1}^L (\tau_i^z)^{\mu_i}$. There are 2^L many of these configurations covering all possible combinations of the τ_i^z operators acting on the chain. Then, for any

$$H = \sum_{e=1}^{2^L} E_e |e\rangle\langle e|, \quad (8)$$

we may write the full expansion of Eq. (7) to order $N_{\text{eff}} = L$ as

$$H = \sum_{\mu} \omega_{\mu} \tau(\mu), \quad (9)$$

with $\omega_{\mu} = 2^{-L} \text{Tr}[H \tau(\mu)]$. Note that according to Eq. (5) the ω_{μ} can be calculated in energy space via $\omega_{\mu} = 2^{-L} \text{Tr}[\text{diag}(E) \mathcal{Z}(\mu)]$ if the energies in $\text{diag}(E)$ are ordered according to the ordering of the eigenbasis constructing the $\{\mathcal{Z}_i\}$ operators. This construction can be interpreted as a *Boolean Fourier transform* of the spectrum E [39,40]. For a specific model the weights $\{\omega_{\mu}\}$ can only be calculated that way if the different $\{\mathcal{Z}_i\}$ are orthogonal with respect to the Hilbert-Schmidt scalar product, which follows from property (ii). In the localizing case putatively realized by MBL systems, two additional restrictions are expected to hold for the couplings $\{\omega_{\mu}\}$:

(iv) *Convergence*. The couplings of different orders are expected to fulfill $\omega_{\eta} \ll \omega_{\xi}$, whenever

$$\sum_{k=1}^L \eta_k > \sum_{l=1}^L \xi_l. \quad (10)$$

This would imply that Eq. (7) is expected to be a good approximation of the full Hamiltonian for low $N_{\text{eff}} \ll L$.

(v) *Locality*. It is expected that the weights $\{\omega_{\mu}\}$ decay with the maximal distance of two τ_i^z , $|\omega_{\mu}| \leq g(d(\mu))$, where again $g: \mathbb{N} \rightarrow \mathbb{R}^+$ is a suitably decaying function and $d(\mu) := \max\{\text{dist}(i, j) : \mu_i = \mu_j = 1\}$.

In later parts of this work, we explicitly construct H_{eff} and investigate the validity these two properties using ED.

IV. MINDSET OF THE APPROACH

The physical intuition behind the algorithm for identifying qLCOMs proposed below is simply that real space spin operators should merely change under the infinite time average if the system is localized. Their time average will hence be diagonal in the energy eigenbasis and at the same time quasilocal in real space. We then set out to find a permutation of the eigenvectors of H such that the time averages of the real space Pauli- z operators best resemble Pauli- z operators in energy space from which we can then construct the qLCOMs $\{\tau_i^z\}$.

The new method to construct the qLCOMs we propose here starts from the energy eigenbasis $\{|e\rangle\}$, expressed in an

arbitrary but fixed ordering. For each ordering of the eigenbasis $|k\rangle = |\pi(e)\rangle$, where $\pi \in S_{2^L}$ is a permutation of the spectrum, we can define $\{\mathcal{Z}_i\}$ as above and relate them to real space $\{\tau_i^z\}$ operators as in Eq. (5). As already pointed out above, these operators by construction fulfill properties (i) and (ii). Any energy ordering $\pi \in S_{2^L}$ can be used to define a set of $\{\mathcal{Z}_i\}$, but this in general does not yield quasilocal constants of motion $\{\tau_i^z\}$ in real space. Demanding property (iii) in localized systems, the task is to identify permutations $\pi \in S_{2^L}$ that yield local constants of motion. However, there are $2^L!$ possible permutations, hence achieving global optimality over all permutations is computationally not feasible. Having said that, we can find a solution giving rise to sufficiently local constants of motion heuristically, by exploiting the physical insight above: We order the eigenbasis such that the spectra of the dephased local magnetization operators *simultaneously* resemble Pauli- z spectra of $\{\mathcal{Z}_i\}$. This turns out to be sufficient for ensuring locality of the qLCOMs $\{\tau_i^z\}$.

V. CONSTRUCTING THE SET OF qLCOMS

We begin by mapping each real space spin operator $\{\sigma_i^z\}$ to its infinite time average $\mathbb{E}(\sigma_i^z) = \sum_e \langle e | \sigma_i^z | e \rangle |e\rangle\langle e|$, where the sum goes over all eigenvectors $\{|e\rangle\}$ of H . This operation stems from *equilibration theory* [1,41] and for nondegenerate Hamiltonians one has $\mathbb{E}(\sigma_i^z) = \lim_{T \rightarrow \infty} (1/T) \int_0^T \sigma_i^z(t) dt$. This yields L operators diagonal in energy space which commute among each other and with H [property (i)] and are found to be quasilocal [32] [property (iii)]. However, due to the nonunitary dephasing, the spectrum of $\mathbb{E}(\sigma_i^z)$ does not satisfy (ii) and hence is only approximately Pauli- z -like. We now set out to reorder the eigenbasis $\{|e\rangle\}$ of each $\{\mathbb{E}(\sigma_i^z)\}$ with a permutation $\pi \in S_{2^L}$ such that $\{\mathbb{E}(\sigma_i^z)\}$ written in the reordered basis $\{|k = \pi(e)\rangle\}$ best resemble $\{\mathcal{Z}_i\}$ in the sense that the entrywise difference between each $\mathbb{E}(\sigma_i^z)$ and \mathcal{Z}_i is small. We construct the reordered basis $\{|k\rangle\}$ using a heuristic scheme in multiple steps by considering each $\mathbb{E}(\sigma_i^z)$ successively.

The structure of all $\{\mathcal{Z}_i\}$ is by construction known (see for instance the black dashed line in Fig. 1 which indicates the diagonal of $\mathcal{Z}_1, \mathcal{Z}_2, \mathcal{Z}_3$, and \mathcal{Z}_4 in the different panels from top to bottom). For each $\mathbb{E}(\sigma_i^z)$, we then identify a permutation by which $\mathbb{E}(\sigma_i^z)$ best approximates \mathcal{Z}_i without altering the result identified for previous $\mathbb{E}(\sigma_j^z)$ with $j < i$ by sorting the eigenvectors only in the degenerate subspaces of \mathcal{Z}_{i-1} according to the size of the eigenvalues of $\mathbb{E}(\sigma_i^z)$ and not allowing for a mixing between those subspaces. To illustrate the concept, consider the operator $\mathcal{Z}_1 = \sigma^z \otimes \mathbb{1}_{2^{L-1}}$ in the energy eigenbasis. It is diagonal in the desired basis $\{|k\rangle\}$ and takes the form $\mathcal{Z}_1 = \mathbb{1}_{2^{L-1}} \oplus -\mathbb{1}_{2^{L-1}}$. Hence, the entrywise closest permutation of $\mathbb{E}(\sigma_1^z)$ is simply sorting its spectrum by size (cf. Fig. 1, first row). Note that this choice is highly nonunique, as it allows for an arbitrary order inside the two degenerate sectors. We will use this ambiguity to optimize the remaining qLCOMs. Next, \mathcal{Z}_2 has the form $\mathcal{Z}_2 = \mathbb{1}_{2^{L-2}} \oplus -\mathbb{1}_{2^{L-2}} \oplus \mathbb{1}_{2^{L-2}} \oplus -\mathbb{1}_{2^{L-2}}$. The infinite time average $\mathbb{E}(\sigma_2^z)$ gives us a new spectrum to optimize. We then exploit the fact that in the degenerate sectors of \mathcal{Z}_1 our ordering is at the moment arbitrary, i.e., not fixed by $\mathbb{E}(\sigma_1^z)$. In the second step, we therefore sort each of the two sectors by size of the spectrum of $\mathbb{E}(\sigma_2^z)$ (cf. Fig. 1, second row). It is important to note that we

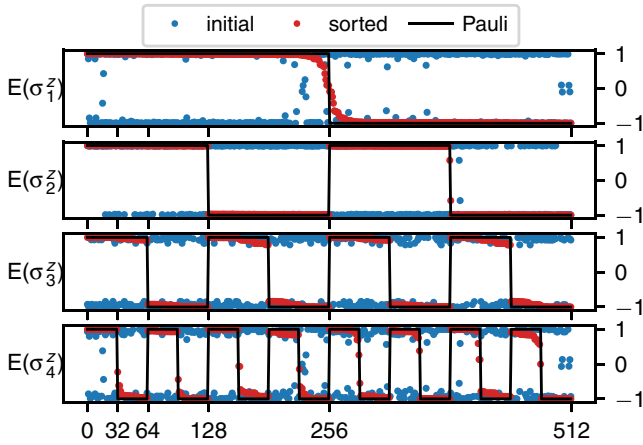


FIG. 1. Energy eigenbasis obtained from ED calculations is defined up to a permutation basis which may obscure the physical content available in the infinite time average of local spin operators. Here we show data for a specific disorder realization with $\Delta = 20$ on $L = 9$ sites. The plots show the size of the eigenvalues of the infinite time-averaged real space Pauli operators $\mathbb{E}(\sigma_i^z)$. We illustrate our procedure of permuting the eigenvalues of the set $\mathbb{E}(\sigma_i^z)$ to obtain a particular diagonalization unitary U_D that ensures locality properties of Pauli- z operators \mathcal{Z}_i when rotated into the real space basis τ_i^z . The difference of $\mathbb{E}(\sigma_i^z)$ to \mathcal{Z}_i comes from the discrepancy of the spectra due to the dephasing.

must not swap entries from the different sectors with one another as this would spoil the formerly established permutations. This procedure is iterated for the remaining $\mathbb{E}(\sigma_i^z)$ as shown in Fig. 1. Ultimately, for fixing the last permutation $\pi_L \in S_{2^L}$, we only have the freedom to sort in $2^L/2$ many blocks of size 2, namely, to perform swaps for neighboring eigenvectors only. As a result we find the final ordering $\pi = \pi_L \circ \dots \circ \pi_1$ and we collect the resulting basis to the unitary U_D of Eq. (5) that can be used to represent the qLCOMs in real space. To be precise, we now use the obtained U_D to transform the $\{\mathcal{Z}_i\}$ which by construction fulfill properties (i) and (ii) into real space. The

following pseudocode describes a possible way to implement this procedure numerically. We use a notation close to PYTHON and denote, for instance, for a list l of numbers $1, \dots, N$ in an arbitrary order, a vector $v \in \mathbb{C}^N$ and a matrix $U \in \mathbb{C}^{N \times N}$ by $v[l]$ and $U[:, l]$ the vector and matrix for which the elements of the vector and columns of the matrix are reordered according to l , i.e., $v[l]_i = v_{l_i}$ and $U[:, l]_{i,j} = U_{i,l_j}$. Similarly, we denote for $v \in \mathbb{C}^N$ and $1 \leq n < m \leq N$ by $v[n : m]$ the vector $v[n : m] \in \mathbb{C}^{m-n}$ with entries $v[n : m]_i = v_{n+i-1}$.

```

1  input: diagonalizing unitary  $U$  (as obtained from ED)
2  input:  $L$  real space Pauli operators  $\sigma_i^z$ 
3  output: quasi-local diagonalization unitary  $U_D$ 
4
5  define infinite_time_average( $V, O$ ):
6      return  $\text{diag}(VOV^\dagger)$ 
7
8  perm =  $[1, \dots, 2^L]$ 
9  for  $n$  in  $\{1, \dots, L\}$ :
10     spec = infinite_time_average( $U, \sigma_1^z$ )
11     permuted_spec = spec[perm]
12     for  $j$  in  $\{1, \dots, 2^{L-n}\}$ :
13         perm[( $j-1$ ) *  $2^{L-n} + 1 : j * 2^{L-n}$ ] =
14             (perm[( $j-1$ ) *  $2^{L-n} + 1 : j * 2^{L-n}$ ])[argsort(
15                 permuted_spec[( $j-1$ ) *  $2^{L-n} + 1 : j * 2^{L-n}$ ])]
16
17  return  $U[:, \text{perm}]$ 

```

VI. NUMERICAL RESULTS

We now examine the properties of the qLCOMs constructed according to the above scheme. First, we make sure that the obtained operators are indeed quasilocl and hence fulfill property (iii). We find that the qLCOMs constructed with our algorithm are local to a few sites only at high enough disorder, an observation which reproduces the theoretical predictions. In Fig. 2 we plot the support of the first, last, and averaged over all constructed $\{\tau_i^z\}$ of the 13-site lattice as a function of disorder strength Δ averaged over 300 realizations. The quantifier for the support is the truncation error to a subsystem S in 2-norm defined as $1 - \|\text{Tr}_{S^c}(\tau_i^z)\|_2^2 / (2^{|S|+2|S^c|})$. If the value is close to unity, the spectrum of the operator deviates

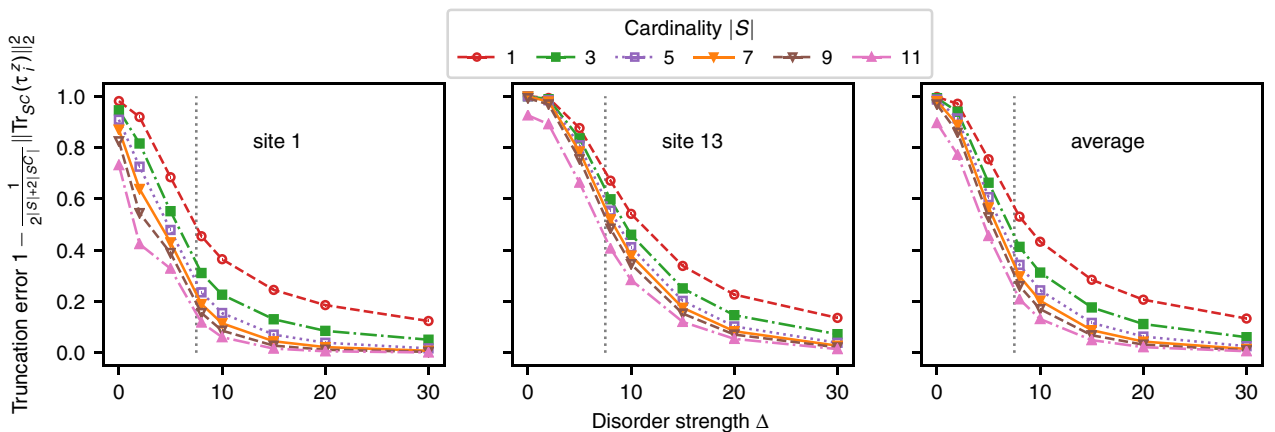


FIG. 2. Support of the first (left panel) and the last (center) qLCOMs as well as the averaged support of all constructed qLCOMs (right panel) of the disorder Heisenberg chain over the disorder strength Δ . As a measure of support, we use the truncation error $1 - \|\text{Tr}_{S^c}(\tau_i^z)\|_2^2 / (2^{|S|+2|S^c|})$ for buffer regions S of increasing cardinality $|S|$. Error bars show statistical deviations over 300 realizations. We use the Heisenberg Hamiltonian on $L = 13$ with periodic boundary conditions. The dashed lines at $\Delta = 7.5$ are a guide to the eye indicating the region of the expected phase transition.

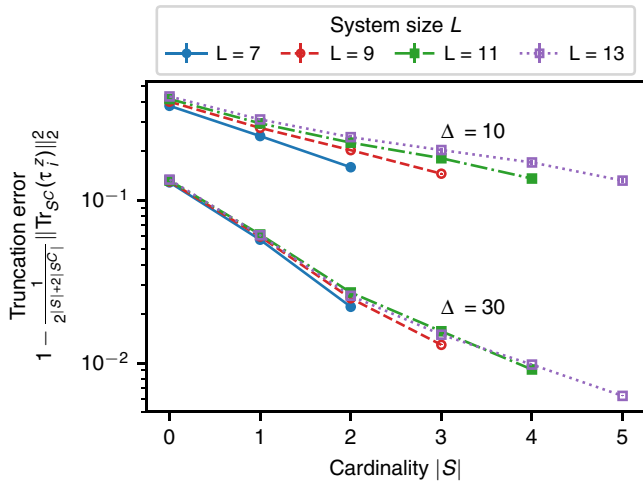


FIG. 3. Average truncation error with random disorder for $L \in \{7,9,11,13\}$ with $\{1000,1000,1000,300\}$ realizations. We use the Heisenberg Hamiltonian with the disorder strength $\Delta \in \{10,30\}$. Moreover we employ periodic boundary conditions. The plot shows the average truncation error $1 - \|\text{Tr}_{SC}(\tau_i^z)\|_2^2 / (2^{|S|+2|S^c|})$ of the qLCOMs when truncated onto a “buffer” region of off cardinality $|S|$ averaged over all qLCOMs. The plot is on a log scale. Lines are guide to the eye. Error bars show statistical deviations.

strongly from the Pauli- z spectrum. If the value is zero, the operator is in this sense well characterized by its reduction to the subsystem S . We find that increasing disorder localizes the obtained operators. Additionally, one observes a crossover in the region of the proposed phase transition. It can furthermore be seen that despite the recursive nature of our approach, which allows more variational freedom in the first initial qLCOMs, there is only a small systematic error between the first and last qLCOM, and all qLCOMs are well localized for Δ large enough. A finite size scaling is discussed in the following indicating that while our method works for the system sizes considered, it suggests inconclusive results for the locality of the operators for larger systems. Figure 4 displays the averaged decay of the qLCOMs and shows that in the localized phase $1 - \|\text{Tr}_{SC}(\tau_i^z)\|_2^2 / (2^{|S|+2|S^c|})$ decays exponentially showing that the $\{\tau_i^z\}$ are local up to exponential tails. Here we average both over realizations and qLCOMs per realization. Additionally one observes a stronger decay for larger disorder. This scaling with the disorder strength is very much expected and consistent with theoretical predictions. Next, we study the finite size dependence of the locality results. Fig. 3 shows the system size dependence of the truncation error $1 - \|\text{Tr}_{SC}(\tau_i^z)\|_2^2 / (2^{|S|+2|S^c|})$ of the qLCOMs for moderate ($\Delta = 10$) and strong ($\Delta = 30$) disorder. The qualitative behavior between the disorder strengths is consistent with Fig. 4. When considering increasing system sizes, we observe that the decay slows down. Nevertheless, we see that for all system sizes we obtain a strong decay with the distance. For the system sizes accessible, we find a still sufficient decay to call the obtained qLCOMs quasilocal. However, it seems hard to predict the trend for larger systems based on the given data. Let us now turn to insights about the transition between the MBL and the ergodic phase.

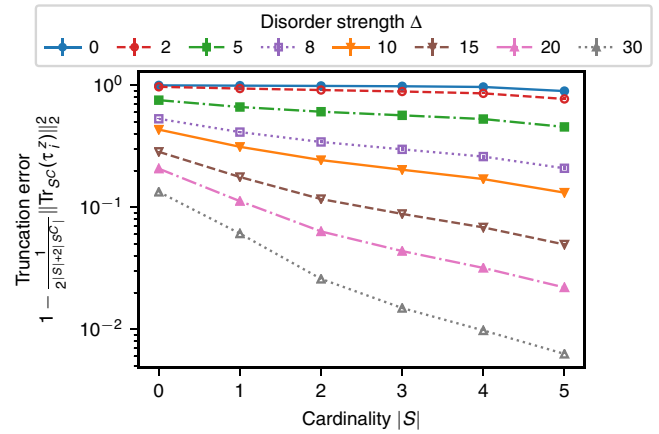


FIG. 4. Decay of the average truncation error over all constants of motion displayed in Fig. 3 on a log scale for different disorder strengths. The error bars indicate the standard deviation of the average and lines are a guide to the eye.

An interesting open question is how precisely the picture of the qLCOMs breaks down once the transition toward the ergodic phase is being approached. Intuitively, one expects a broadening of the qLCOMs upon delocalizing, which ultimately leads to completely nonlocal constants of motion. Here, we set out to observe this transition in the locality of the calculated qLCOMs. The measure we employ is the the cardinality of the minimal buffer region S (see above) needed to support as much as a threshold α of the weight of the operator. We again work with the squared two-norm of the reduced operator as a quantifier of support. We show the results in Fig. 5 for different thresholds $\alpha \in \{0.5,0.6,0.7,0.8\}$. While the resulting curve clearly depends on the chosen threshold, a transition between a phase, where the operator is supported

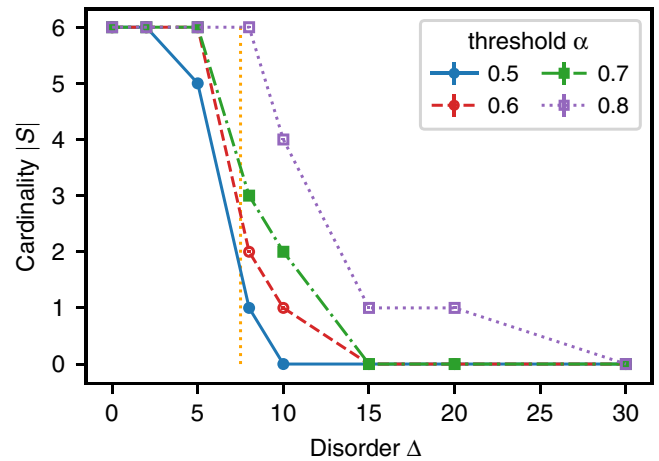


FIG. 5. Cardinality of the minimal buffer region for threshold values $\alpha \in \{0.5,0.6,0.7,0.8\}$. Values are obtained for the disordered Heisenberg model on $L = 13$ with periodic boundary conditions. Each data point comprises 300 realizations averaged over all qLCOMs. Lines are guide to the eye. Error bars show statistical deviations. The orange dotted line indicates the expected transition at $\Delta = 7.5$.

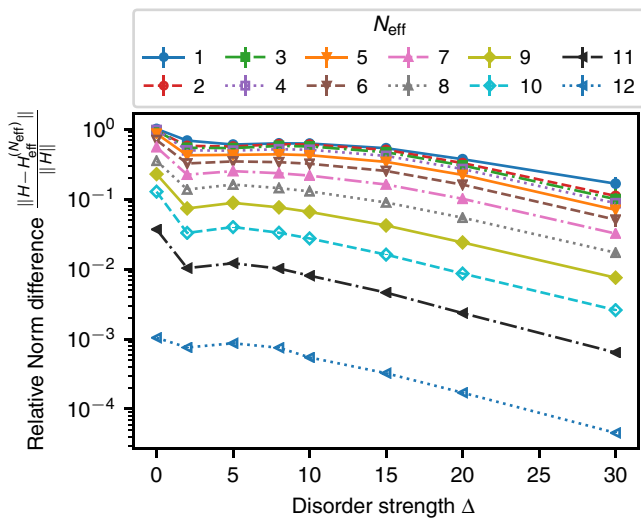


FIG. 6. Relative norm difference between effective model and actual Hamiltonian $\|H - H_{\text{eff}}^{(N_{\text{eff}})}\|/\|H\|$ on $L = 13$ with random disorder on a log scale. Different colors indicate the order of the approximation N_{eff} . Error bars show statistical deviations. The average is performed over 300 realizations. Lines are a guide to the eye.

on the full system for low disorder and on a single site for high disorder can clearly be observed. To precisely identify the phase boundary is a challenge for all known methods, and this one is no exception. While the measure we propose here may not give a reliable quantitative estimate of the transition, it nevertheless provides a clear qualitative one. Furthermore, it strengthens the intuition of the nature of the phase transition, giving rise to a broadening of qLCOMs.

Using the constructed qLCOMs, we now turn to the effective model and investigate its properties in detail. We would like to point out that this is only possible since our set of qLCOMs fulfills properties (i)–(iii) exactly and not only approximately and hence offers the algebraic structure necessary to exactly construct the effective description. We compute the weights ω_μ in energy space as explained before using the orthogonality of the $\{\tau_i^z\}$ operators and show their decay in Fig. 7. While the ω_μ decay with increasing spatial extension $d(\cdot)$, there is no apparent inter-order decay. Moreover, there is an apparent saturation for higher orders. This allows two explanations: Either the qLCOMs can be further optimized to fit the expectations of the effective description better or the Heisenberg model cannot be mapped to the effective model with strongly decaying couplings. A possible measure of where to set an effective cutoff N_{eff} is the operator norm distance of the Hamiltonian H and its effective description $H_{\text{eff}}^{(N_{\text{eff}})}$. Figure 6 shows the scaling of $\|H - H_{\text{eff}}^{(N_{\text{eff}})}\|/\|H\|$ in the dependence on the disorder strength Δ with N_{eff} as a parameter. Here, we observe that indeed all orders do decay with an exponential trend for larger disorder. However, to get the norm error small, a rather large N_{eff} has to be chosen. This seems to put the validity of the effective description as a full solution in question. However, note that we cannot rule out that qLCOMs can be found that allow a better effective model as also stated previously. For a brute force approach, 2^L many

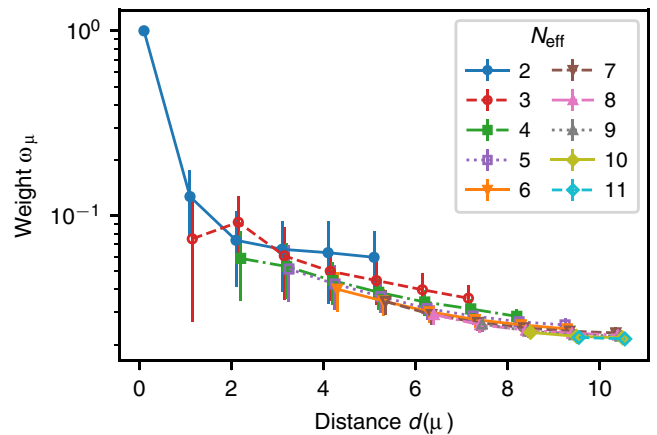


FIG. 7. Average coupling strength ω_μ on $L = 13$ with random disorder of strength $\Delta = 20$ on a log scale. Different colors indicate the order of the approximation N_{eff} . Error bars show statistical deviations of the average over 300 realizations and per realization over all operators with support of extension $d(\mu)$. Lines are a guide to the eye.

configurations have to be checked, which quickly out scales any computational resources. Hence it will be necessary to work with a heuristic such as the one presented in this work. Devising new heuristics which can better fit the effective model will be part of future research.

However, imposing such strict global constraints as done by the operator norm difference of the exact and effective Hamiltonian may not be required to recover the essential physical behavior of the system. Hence we will investigate the predictions of the effective model on a local scale in the following.

VII. OBTAINING LOCAL DYNAMICS FROM THE EFFECTIVE DESCRIPTION

To provide more substance to this discussion, we investigate the nonequilibrium quench dynamics of local observables akin to recent experiments [8]. We compare the dynamical evolution of the *imbalance*

$$\mathcal{I} = \frac{1}{L} \sum_i (-1)^i \sigma_i^z, \quad (11)$$

where the initial state is a real space *Neel state vector* $|1, 0, \dots, 1, 0, 1\rangle$ for the Heisenberg Hamiltonian and the effective description truncated to order $N_{\text{eff}} = 4$. In Fig. 8 we pick three realizations based on the norm difference $\|H - H_{\text{eff}}^{(4)}\|$, namely, the worst, intermediately good, and best one. We find quantitative agreement of the dynamical evolution when the low-order effective description is close in operator norm to the true Hamiltonian; however, there may exist realizations where the phenomenological model would demand many higher-order terms as seen for the bad realization (red in Fig. 8). Notably, the effective description fails to reproduce quantitatively fast oscillations of the imbalance, but the qualitative behavior, e.g., the average imbalance value, is still captured. For realizations that work intermediately well, the quantitative agreement is lost over time.

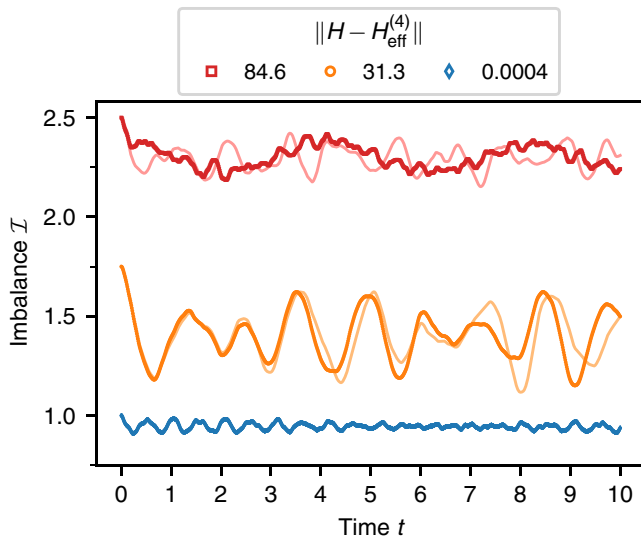


FIG. 8. Dynamics of the imbalance in the Neel state of $L = 13$ spins with periodic boundary conditions with disorder strength $\Delta = 20$. The plot shows a comparison of the exact dynamics (solid lines) in three realizations (picked by norm difference $\|H - H_{\text{eff}}^{(4)}\|$ of 30 realizations) with the evolution generated by the truncated effective Hamiltonian $H_{\text{eff}}^{(4)}$ (symbols).

VIII. SUMMARY AND OUTLOOK

In this work, we have proposed an algorithm for numerically constructing exact constants of motion in the localized phase of models exhibiting MBL, with an emphasis on the random field Heisenberg chain. In contrast to previous attempts of

numerically tackling MBL systems, we have put strong emphasis on exactly fulfilling all desired commutation relations as well as obtaining a Pauli- z spectrum of the constructed operators. Based on this paradigm, our algorithm finds operators which furthermore act quasilocally in real space in the localized regime. Equipped with a full set of exact qLCOMs, we are able to explicitly calculate the effective description of localized systems to all orders. It is the hope that this tool to construct exact effective Hamiltonians can help to satisfactorily explore the rich phenomenology of many-body localized systems. For future work, it appears a natural question to investigate whether the equilibrium state of MBL systems can as anticipated be described by *generalized Gibbs ensembles* featuring the qLCOM. As MBL systems can be tuned between “ergodicity” and “integrability,” progress in this direction may also shed light on thermalization in more general models. Moreover, we aim at elevating the present method to a tensor network consisting of many subsystems, iterating steps, to give rise to a two-layer quantum cellular automaton, reminiscent of the tensor network of Ref. [19]. It is the hope that equipped with exact constants of motion and effective models, the present work can contribute to resolving the remaining puzzles on many-body localization in one spatial dimension.

Note added. Recently we became aware of the independent similar work presented in Refs. [42–44].

ACKNOWLEDGMENTS

We thank J. Behrmann, D. Litinski, and H. Wilming for helpful comments. This work has been supported by the ERC (TAQ), the DFG (CRC 183, A2, EI 519/7-1, and EI 519/14-1), the Templeton Foundation, and the EC (AQuS).

- [1] J. Eisert, M. Friesdorf, and C. Gogolin, *Nat. Phys.* **11**, 124 (2015).
- [2] A. Polkovnikov, K. Sengupta, A. Silva, and M. Vengalattore, *Rev. Mod. Phys.* **83**, 863 (2011).
- [3] C. Gogolin and J. Eisert, *Rep. Prog. Phys.* **79**, 56001 (2016).
- [4] P. W. Anderson, *Phys. Rev.* **109**, 1492 (1958).
- [5] D. M. Basko, I. L. Aleiner, and B. L. Altshuler, *Ann. Phys. (NY)* **321**, 1126 (2006).
- [6] V. Oganesyan and D. A. Huse, *Phys. Rev. B* **75**, 155111 (2007).
- [7] D. J. Luitz, N. Laflorencie, and F. Alet, *Phys. Rev. B* **91**, 081103 (2015).
- [8] M. Schreiber, S. S. Hodgman, P. Bordia, H. P. Lüschen, M. H. Fischer, R. Vosk, E. Altman, U. Schneider, and I. Bloch, *Science* **349**, 842 (2015).
- [9] J.-Y. Choi, S. Hild, J. Zeiher, P. Schauß, A. Rubio-Abadal, T. Yefsah, V. Khemani, D. A. Huse, I. Bloch, and C. Gross, *Science* **352**, 1547 (2016).
- [10] M. Znidaric, T. Prosen, and P. Prelovsek, *Phys. Rev. B* **77**, 064426 (2008).
- [11] J. H. Bardarson, F. Pollmann, and J. E. Moore, *Phys. Rev. Lett.* **109**, 017202 (2012).
- [12] B. Bauer and C. Nayak, *J. Stat. Mech.* (2013) P09005.
- [13] J. Eisert, M. Cramer, and M. B. Plenio, *Rev. Mod. Phys.* **82**, 277 (2010).
- [14] M. Friesdorf, A. H. Werner, W. Brown, V. B. Scholz, and J. Eisert, *Phys. Rev. Lett.* **114**, 170505 (2015).
- [15] X. Yu, D. Pekker, and B. K. Clark, *Phys. Rev. Lett.* **118**, 017201 (2017).
- [16] V. Khemani, F. Pollmann, and S. L. Sondhi, *Phys. Rev. Lett.* **116**, 247204 (2016).
- [17] F. Pollmann, V. Khemani, J. I. Cirac, and S. L. Sondhi, *Phys. Rev. B* **94**, 041116 (2016).
- [18] D. M. Kennes and C. Karrasch, *Phys. Rev. B* **93**, 245129 (2016).
- [19] T. B. Wahl, A. Pal, and S. H. Simon, *Phys. Rev. X* **7**, 021018 (2017).
- [20] D. A. Huse, R. Nandkishore, and V. Oganesyan, *Phys. Rev. B* **90**, 174202 (2014).
- [21] M. Serbyn, Z. Papić, and D. A. Abanin, *Phys. Rev. Lett.* **111**, 127201 (2013).
- [22] M. Serbyn, Z. Papić, and D. A. Abanin, *Phys. Rev. Lett.* **110**, 260601 (2013).
- [23] M. Friesdorf, A. H. Werner, M. Goihl, J. Eisert, and W. Brown, *New J. Phys.* **17**, 113054 (2015).
- [24] J. Z. Imbrie, *J. Stat. Phys.* **163**, 998 (2016).
- [25] R. Vosk and E. Altman, *Phys. Rev. Lett.* **110**, 067204 (2013).
- [26] L. Rademaker and M. Ortuño, *Phys. Rev. Lett.* **116**, 010404 (2016).
- [27] L. Rademaker, M. Ortuño, and A. M. Somoza, *Ann. Phys. (NY)* **529**, 1600322 (2017).
- [28] C. Monthus, *J. Phys. A* **49**, 305002 (2016).

- [29] D. Pekker, B. K. Clark, V. Oganesyan, and G. Refael, *Phys. Rev. Lett.* **119**, 075701 (2017).
- [30] W. De Roeck, F. Huveneers, M. Müller, and M. Schiulaz, *Phys. Rev. B* **93**, 014203 (2016).
- [31] D. J. Luitz, F. Huveneers, and W. De Roeck, *Phys. Rev. Lett.* **119**, 150602 (2017).
- [32] A. Chandran, I. H. Kim, G. Vidal, and D. A. Abanin, *Phys. Rev. B* **91**, 085425 (2015).
- [33] T. E. O'Brien, D. A. Abanin, G. Vidal, and Z. Papić, *Phys. Rev. B* **94**, 144208 (2016).
- [34] R.-Q. He and Z.-Y. Lu, *Chin. Phys. Lett.* **35**, 027101 (2018).
- [35] J. Z. Imbrie, V. Ros, and A. Scardicchio, *Ann. Phys. (NY)* **529**, 1600278 (2017).
- [36] E. Ilievski, M. Medenjak, T. Prosen, and L. Zadnik, *J. Stat. Mech.* (2016) 064008.
- [37] M. Mierzejewski, P. Prelovšek, and T. Prosen, *Phys. Rev. Lett.* **114**, 140601 (2015).
- [38] M. Mierzejewski, T. Prosen, and P. Prelovšek, *Phys. Rev. B* **92**, 195121 (2015).
- [39] A. Montanaro and T. J. Osborne, *Chicago J. Theoret. Comput. Sci.* **1**, 1 (2010).
- [40] R. De Wolf, *Th. Comp.* **1**, 1 (2008).
- [41] N. Linden, S. Popescu, A. J. Short, and A. Winter, *Phys. Rev. E* **79**, 061103 (2009).
- [42] A. K. Kulshreshtha, A. Pal, T. B. Wahl, and S. H. Simon, [arXiv:1707.05362](https://arxiv.org/abs/1707.05362).
- [43] S. J. Thomson and M. Schiró, *Phys. Rev. B* **97**, 060201 (2018).
- [44] M. Mierzejewski, M. Kozarzewski, and P. Prelovsek, *Phys. Rev. B* **97**, 064204 (2018).

CONSTRUCTING EDGE MODE OPERATORS FOR SYSTEMS
EXHIBITING SYMMETRY PROTECTED ORDER

Let us take a step back from many-body localised systems and broaden our scope to a class of systems which also feature local constants of motion. In particular we would like to focus on spin chains with symmetry protected edge modes. These are a subclass of topological systems, a field that combines intriguing physics with high level mathematics, while still allowing for experimental realisations, i. e. in Majorana nanowires [58]. We consider a spin chain with a global symmetry that decouples bulk and boundary degrees of freedom which leads to the formation of edge modes whose commutator with the Hamiltonian vanishes in the thermodynamic limit. Products of edge modes supported on both ends of the chain do exactly commute with the Hamiltonian even for finite chains. This allows us to use a variation of the algorithm presented in the previous chapter to numerically construct these edge modes as well. Since much of the knowledge about symmetry protected spin chains is based on analytical results for exactly solvable models and extensions with weak perturbations, this is a fruitful application as our method works in the interacting regime as well. Because our approach is not limited by interaction strength, we will investigate the stability of edge modes in the presence of disorder and interactions in this final chapter.

6.1 THE XZX-CLUSTER HAMILTONIAN

The model we will consider in this chapter, is the XZX-cluster Hamiltonian, a prototypical, exactly solvable model for symmetry protected order which takes the form

$$H_{\text{XZX}} = - \sum_{j=2}^{L-1} \sigma_{j-1}^x \sigma_j^z \sigma_{j+1}^x,$$

where σ^a are again Pauli matrices. The accompanying symmetry is time reversal which can be formalised as $\mathcal{T} = \prod_{j=1}^L \sigma_j^z \mathcal{K}$, where \mathcal{K} is the complex conjugation operation. By defining the model this way, it necessarily has open boundary conditions and furthermore supports exactly local spin-1/2 degrees of freedom at the edge spanned by the following edge mode operators

$$\mathcal{E}_0 = \left\{ \begin{array}{ll} \mathcal{X}_L = \sigma_1^x, & \mathcal{X}_R = \sigma_L^x, \\ \mathcal{Y}_L = \sigma_1^y \sigma_2^x, & \mathcal{Y}_R = \sigma_{L-1}^x \sigma_L^y, \\ \mathcal{Z}_L = \sigma_1^z \sigma_2^x, & \mathcal{Z}_R = \sigma_{L-1}^x \sigma_L^z \end{array} \right\}.$$

We would like to point out that while these exactly commute with H_{XZX} , only their products commute with the time reversal symmetry \mathcal{T} as well. This will be of importance as our algorithm introduced in the previous chapter constructs exactly commuting operators.

As defined above, the XZX-cluster Hamiltonian is well studied analytically. However, little is known about the stability of the edge modes when additional interactions and disorder are present in the system. Such questions are particularly relev-

ant for experimental realisations where stray interactions and disorder potentials are ubiquitous. The model we use to include these is the following

$$H_{\text{XZX}}^{\text{int}} = - \sum_{j=2}^{L-1} (1 + h_j) \sigma_{j-1}^x \sigma_j^z \sigma_{j+1}^x - J \sum_{k=1}^{L-1} (\sigma_k^x \sigma_{k+1}^x + \sigma_k^y \sigma_{k+1}^y + \eta \sigma_k^z \sigma_{k+1}^z),$$

where η is the anisotropy which we either set to zero to obtain a non-interacting model or to one to investigate the effect of many-body interactions. The disorder fields are drawn from $h_j \in [-\Delta/2, \Delta/2]$ in order to have a gapped model at all times.

The edge modes liken the quasi-local constants of motion in that they are local subspaces defined by local operators. It is expected that introducing interactions to the system delocalises the edge mode operators, similarly to our discussion of the Anderson model. Even though the model is not exactly in the class of many-body localisation, it is expected, that additional disorder will localise the bulk degree of freedoms in similar fashion [59]. To investigate the influence of these perturbations on the edge mode locality, we will construct the edge mode operators numerically. In the absence of interactions, the edge modes can be found via a singular value decomposition directly. For the interacting system, we will use a variant of the algorithm presented in chapter 5 with some adjustments to also deal with the degeneracies caused by the symmetry. We use products of the unperturbed edge modes \mathcal{E}_0 as an ansatz for our heuristic.

In this last work, we use this specialised method to study the locality of the emergent edge modes of the perturbed XZX-cluster Hamiltonian.

CLIMATE FOOTPRINT ESTIMATE

Total Kernel hours [h]	230400
Total Energy consumption [kWh]	2648
Total CO ₂ -emission [kg]	1484

Table 6.1: Estimated climate footprint of the numerical calculations performed for the paper “Edge mode locality in perturbed symmetry protected topological order”. Estimates are based only on the data for the interacting system presented in the manuscript and exclude prototyping. CO₂-emission estimates are based on the German average emission of 0.56 kg/kWh. Calculations were performed on the tron cluster equipped with Intel® Xeon® Processor E5-2680 v2 nodes with a thermal design power of 115 W. Further details on the estimation can be found in Appendix A

Edge mode locality in perturbed symmetry protected topological order

Marcel Goihl*, Christian Krumnow, Marek Gluza,
Jens Eisert and Nicolas Tarantino

Dahlem Center for Complex Quantum Systems,
Freie Universität Berlin, 14195 Berlin, Germany

* mgoihl@physik.fu-berlin.de

Abstract

Spin chains with a symmetry-protected edge zero modes can be seen as prototypical systems for exploring topological signatures in quantum systems. However in an experimental realization of such a system, spurious interactions may cause the edge zero modes to delocalize. To combat this influence beyond simply increasing the bulk gap, it has been proposed to harness disorder which does not drive the system out of a topological phase. Equipped with numerical tools for constructing locally conserved operators that we introduce, we comprehensively explore the interplay of local interactions and disorder on localized edge modes in such systems. Contrary to established heuristic reasoning, we find that disorder has no effect on the edge mode localization length in the non-interacting regime. Moreover, disorder helps localize only a subset of edge modes in the truly interacting regime. We identify one edge mode operator that behaves as if subjected to a non-interacting perturbation, i.e., shows no disorder dependence. This implies that in finite systems, edge mode operators effectively delocalize at distinct interaction strengths despite the presence of disorder. In essence, our findings suggest that the ability to identify and control the best localized edge mode trumps any gains from introducing disorder.



Copyright M. Goihl *et al.*

This work is licensed under the Creative Commons

[Attribution 4.0 International License](https://creativecommons.org/licenses/by/4.0/).

Published by the SciPost Foundation.

Received 14-01-2019

Accepted 06-06-2019

Published 21-06-2019

doi:[10.21468/SciPostPhys.6.6.072](https://doi.org/10.21468/SciPostPhys.6.6.072)



Check for updates

Contents

1	Introduction	1
2	SPT chains with spatial disorder	3
3	Edge mode construction	4
3.1	Edge modes under free fermion perturbations	4
3.2	Edge modes under perturbative many-body interactions	6
3.3	Measure of locality	7
4	Numerical Results	9
4.1	Free fermionic perturbation	9

4.2 Many-body interacting perturbation	10
5 Conclusions	11
6 Acknowledgements	11
A Fractionalization	12
B Operator norm decay of edge modes for $\eta = 0$	12
C Scaling behaviour of support results for $\eta = 0$	13
D Finite size scaling and cross validation	14
E Additional numerical data	15
References	16

1 Introduction

Topological states of matter have been the focus of intense research over the past 30 years. Within systems of *condensed matter physics*, topological effects are known to occur in quantum Hall systems of the electron gas [1] and topological insulators [2]. Experiments on wires with proximity induced superconductors gave compelling evidence for Majorana zero modes [3]. Cold atomic gases and photonic devices offer possibilities of creating synthetic topological properties [4]. These new phases of matter by definition have no local order parameter but can be detected via their entanglement properties [5] and are classified by topological invariants [6]. When considering one-dimensional spin chains, these invariants give rise to protected gapless edge modes [7–14], which survive only if perturbations do not break the symmetries of the Hamiltonian.

Such edge modes are interesting from the perspective of quantum information science as well: They are one of many proposed candidates to encode quantum information robustly using topology [6, 9, 15]. However, the localization of the edge modes can be compromised by the onset of interactions allowing them to delocalize by hybridizing with delocalized bulk states. This will have deleterious effects on ones ability to encode and faithfully extract quantum information well before the topological to trivial phase transition. As we can only expect to operate on a finite number of edge qubits to operate the quantum memory, the likelihood that a read-in/read-out procedure introduces errors increases with localization length, as more and more of the protected quantum information leaks into the bulk of the chain. To counteract this effect, it has been suggested that topological quantum information can be stabilized by disorder [16–18], which is supposed to inhibit transport by localizing the bulk. These works have given rise to the narrative that disorder is expected to always be beneficial when it comes to enhancing the localisation of the edge states.

The interplay of topological features, interactions and disorder is far from being fully understood. While there is evidence that disorder can drive a system into a topologically insulating phase [19–21], these do not in and of themselves support that any logical qubit is further localized by disorder. What is known rigorously is that, for topologically ordered systems, sufficiently weak local perturbations do not lift the ground-state degeneracy [22–24]

– but this kind of statement shows that small noise levels do not drive a phase transition, rather than making explicit constructive use of them. While this implicitly defines a coherence length for the edge modes, it is far from clear how the local structure of these operators is deformed in the presence of interactions and disorder. These seemingly basic questions should be addressed before more sophisticated scenarios can be meaningfully studied. This work sets out to do exactly that by studying the deformation of edge modes under disorder in a comprehensive fashion, laying the ground for a more general picture of the interplay of topological features and disorder.

In this work, we study the XZX cluster Hamiltonian, a topological chain which hosts one qubit at each edge and analyze if disorder can help localize them [17, 18] in the presence of weak interactions. We devise algorithms capable of calculating the support of the edge operators of the disordered XZX cluster Hamiltonian perturbed by either XX or XXZ type interactions. Equipped with this tool, we are in a position to determine the sensitivity of the edge mode localization length to each perturbation type. Contrary to previous expectations, we find that disorder only aids localization slightly, and only in the presence of interaction terms which are non-quadratic in the fermionic dual. Furthermore, and surprisingly, we also find that some edge modes are completely insensitive to disorder. Building on these findings, we elaborate on the lessons to be learned on the interplay of disorder and topological features.

2 SPT chains with spatial disorder

Our main focus is on the interplay of disorder, interactions and SPT order. Take for example a spin chain hosting a XZX cluster Hamiltonian

$$H_0(h) = - \sum_{j=2}^{N-1} (1 + h_j) X_{j-1} Z_j X_{j+1}, \quad (1)$$

where the h_j are drawn uniformly from $[-\frac{\Delta}{2}, \frac{\Delta}{2}]$ and X_j, Y_j, Z_j are the Pauli operators acting at site j . This system is known to be in a symmetry protected topological (SPT) phase, and thus supports localized, spin 1/2, edge zero modes. The choice of disorder model here may seem unphysical to readers familiar with many-body localization, where a disordered local magnetic field is commonplace. Such a field competes with the SPT order, driving a transition to a topologically trivial phase. By disordering the cluster terms directly, we are implementing an ideal version of disorder, in that it breaks the degeneracies in the excited state spectrum while preserving the ground state manifold. Thus, if we should fail to observe increased localization in this circumstance we do not expect any improvement by moving to a more physical model of disorder.

Without any extra interaction terms, the two edge zero modes enforce a four-fold degeneracy at every energy level in the spectrum, and are perfectly localized on the two sites nearest to the boundary. By inspection, we can find local operators which exactly commute with the Hamiltonian (1)

$$\mathcal{E}_0 = \left\{ \begin{array}{ll} \mathcal{X}_L = X_1, & \mathcal{X}_R = X_N, \\ \mathcal{Y}_L = Y_1 X_2, & \mathcal{Y}_R = X_{N-1} Y_N, \\ \mathcal{Z}_L = Z_1 X_2, & \mathcal{Z}_R = X_{N-1} Z_N \end{array} \right\}, \quad (2)$$

that are located at the left and right edge. Apart from these local conserved quantities, the Hamiltonian in (1) also commutes with the time reversal operator

$$\mathcal{T} = \prod_{j=1}^N Z_j \mathcal{K}, \quad (3)$$

where \mathcal{K} is complex conjugation. Note that all local edge operators fail to commute with time reversal and thus cannot be used to split the degeneracy without breaking the symmetry. Each set of these operators describe a spin-1/2 Hilbert space. Although $\mathcal{T}^2 = 1$ on the full Hilbert space, $\mathcal{T}^2 = -1$ when restricted to these spin-1/2 Hilbert spaces, i.e. these edge states transform projectively under the global time reversal (see Appendix A).

To perturb H_0 , we will introduce a translationally invariant XXZ-coupling to our spin chain of the form

$$H_{\text{int}}(J, \eta) = -J \sum_{j=1}^{N-1} (X_j X_{j+1} + Y_j Y_{j+1} + \eta Z_j Z_{j+1}), \quad (4)$$

which, for $J \ll 1$, is representative of interactions typically found in real solid-state material where Heisenberg-type interactions are ubiquitously present as a result of exchange interactions. Since we will only be investigating the effects of either an XX or a Heisenberg perturbation, we have included a parameter η which interpolates between the two, and leave J as the overall interaction strength. Specifically, we consider the following Hamiltonian defined on N lattice sites

$$H(h, J, \eta) = H_0(h) + H_{\text{int}}(J, \eta), \quad (5)$$

where we choose $\eta = 0$ or $\eta = 1$. By choosing $\Delta \neq 0$ we can switch on the presence of local disorder that can have the effect of diminishing the influence of the perturbation added to the exact Hamiltonian.

Note that $H_{\text{int}}(J, \eta)$ commutes with the time reversal operator for any values of J and η , so if it is sufficiently weak it will only lift the degeneracy by an amount exponentially suppressed in system size [7–9, 25]. This occurs because, as soon as $J \neq 0$, the edge modes will no longer be perfectly localized at the edges and are in fact expected to be smeared within an exponential envelope [7–14]. With the degeneracy lifted, the edge mode operators will no longer commute exactly with the Hamiltonian, since the existence of operators which anticommute with \mathcal{T} (a feature of the edge modes in (2)) and commute with Hamiltonian would require *exact* degeneracies due to Kramer’s theorem. The failure of the edge mode operators to commute exactly with play an important role in informing our algorithm in Section 3.2.

From here, we set out to understand this interplay of topology, interactions and disorder by explicitly constructing edge modes for this perturbed XZX cluster Hamiltonian. For Anderson and many-body localized systems, the localization length of all local conserved quantities depends on the disorder strength. Thus, one would expect that localizing the bulk of the SPT chain should stabilize the edge modes as excitations cannot traverse the full system to allow the hybridization of opposite edges [17, 18]. We devise methods capable of computing the edge mode support in presence of both non-interacting and many-body interacting perturbations. Contrary to the previously stated heuristic argument, we find numerous cases where the edge modes are completely insensitive to disorder.

3 Edge mode construction

In this section, we describe two methods employed to construct the edge mode operators \mathcal{E} in the perturbed XZX cluster Hamiltonian. Computing the broadening of the edge modes is a particularly daunting task, precisely because the operator encodes information about states throughout the entire spectrum, and thus cannot be studied using low energy techniques such as DMRG. The first method assumes that the perturbed Hamiltonian represents non-interacting fermions and yields an efficient solution in terms of Majorana eigenmodes, which

allows for a direct computation of the edge modes. The second approach tackles the generic interacting case, where no Bogoliubov transformation will suffice and hence the construction of the edge modes becomes more intricate. In this case we rely on a method developed to construct conserved operators called "l-bits" for a many-body localized system [26, 27]. The construction of these conserved quantities from first principles is difficult, but algorithms which can construct them using various methods do exist [28–40].

3.1 Edge modes under free fermion perturbations

After a Jordan-Wigner transformation, the choice of $\eta = 0$ is equivalent to a non-interacting fermionic problem whereas $\eta \neq 0$ maps to an interacting fermionic model with quartic interactions. Introducing the Majorana operators $\tilde{\gamma}_j, \gamma_j$ for $j = 1, \dots, N$ as

$$\gamma_j = Z_1 \dots Z_{j-1} X_j \quad \text{and} \quad \tilde{\gamma}_j = Z_1 \dots Z_{j-1} Y_j, \quad (6)$$

with

$$\{\gamma_j, \gamma_k\} = \{\tilde{\gamma}_j, \tilde{\gamma}_k\} = 2\delta_{j,k}, \quad \{\tilde{\gamma}_j, \gamma_k\} = 0, \quad (7)$$

the Hamiltonian (5) becomes

$$H(h, J, \eta) = -i \sum_{j=2}^{N-1} (1 + h_j) \tilde{\gamma}_{j-1} \gamma_{j+1} - J \sum_{j=1}^{N-1} (i \tilde{\gamma}_j \gamma_{j+1} + i \gamma_j \tilde{\gamma}_{j+1} - \eta \gamma_j \tilde{\gamma}_j \gamma_{j+1} \tilde{\gamma}_{j+1}), \quad (8)$$

which is non-interacting if and only if $\eta = 0$. Written in terms of the Majorana operators, the edge modes for $J = 0$ take the form

$$\begin{aligned} \mathcal{X}_L &= \gamma_1, & \mathcal{Y}_L &= i\gamma_1 \gamma_2, & \mathcal{Z}_L &= \gamma_2, \\ \mathcal{X}_R &= -iP \tilde{\gamma}_N, & \mathcal{Y}_R &= -i\tilde{\gamma}_{N-1} \tilde{\gamma}_N, & \mathcal{Z}_R &= -iP \tilde{\gamma}_{N-1}, \end{aligned} \quad (9)$$

with $P = Z_1 \dots Z_N$ being the global parity operator which commutes with H . For this we note that (8) can be written as

$$H(h, J, \eta = 0) = i \sum_{j,k=1}^N \gamma_j C_{j,k} \tilde{\gamma}_k, \quad (10)$$

with the coupling matrix

$$C_{i,j} = \begin{cases} J & \text{if } i = j + 1 \\ -J & \text{if } i = j - 1 \\ -(1 + h_{i+1}) & \text{if } i = j - 2. \end{cases} \quad (11)$$

As $C \in \mathbb{R}^{N \times N}$ is real, the singular value decomposition of C takes the specialized form $C = Q^T \Sigma \bar{Q}$ with two orthogonal $Q, \bar{Q} \in O(N)$ and $\Sigma \in \mathbb{R}^{N \times N}$ a diagonal matrix with real non-negative entries. Using the two orthogonal matrices $Q, \bar{Q} \in O(N)$ we introduce new modes

$$m_j = \sum_{k=1}^n Q_{j,k} \gamma_k, \quad \bar{m}_j = \sum_{k=1}^N \bar{Q}_{j,k} \tilde{\gamma}_k, \quad (12)$$

which again fulfill the Majorana anti-commutation relations (7) and the Hamiltonian (10) becomes diagonal taking the form

$$H(h, J, \eta = 0) = i \sum_{l=1}^N \sigma_l m_l \bar{m}_l, \quad (13)$$

where we have defined the single particle energies $\sigma_j = \Sigma_{j,j}$ and assume without loss of generality that they are in increasing order.

For $J = 0$, we find that $\sigma_1 = \sigma_2 = 0$ with $m_1 = \gamma_1$, $m_2 = \gamma_2$, $\bar{m}_1 = \bar{\gamma}_n$, $\bar{m}_2 = \bar{\gamma}_{n-1}$ being the corresponding localized edge mode operators. At finite $J > 0$, $\sigma_1 \sim \sigma_2 \sim e^{-n/n_0}$ are not exactly zero anymore but decay exponentially with increasing system size [9] and hence much smaller compared to the next largest value σ_3 . Thus an approximate four-fold degenerate ground-state sector remains well defined. The operators $m_1, m_2, \bar{m}_1, \bar{m}_2$ hence correspond to perturbed edge mode operators which can be individually studied in the free fermionic setting via their single particle wavefunctions. Note however, that only their products $m_1 \bar{m}_1$ and $m_2 \bar{m}_2$, which are supported at both ends of the chain, are exact constants of motions of the Hamiltonian. This will also be a main difference to the interacting relaxation algorithm which from the outset seeks operators that exactly commute with the Hamiltonian.

3.2 Edge modes under perturbative many-body interactions

The intuition behind our approach to constructing edge modes of a system with many-body interactions is as follows: the edge modes \mathcal{E}_0 of the unperturbed model H_0 should deform smoothly to those of the full interacting Hamiltonian. Indeed, they turn out to be good starting points to obtain the actual edge mode operator \mathcal{E} which commutes with H exponentially well in the system size whilst remaining local to some degree.

The method requires an ansatz which is expected to resemble the conserved operators. Since we are perturbing away from a solvable point, we employ a natural choice, the exact edge modes obtained in the unperturbed fixed-point model. One might be inclined to use a single edge mode as an ansatz for finding the perturbed operators, but this approach will fail in general as the operators produced with this method necessarily commute exactly with the Hamiltonian by construction. This is not the case for single edge modes as they *cannot* commute with Hamiltonian, as discussed in Section 2. We can circumvent this problem by instead using products of edge modes supported on both the left and right ends of the chain which we call $\mathcal{B}_0 = \mathcal{E}_0^L \otimes \mathcal{E}_0^R$. Such products respect the time reversal symmetry and thus are not prevented from commuting exactly with the Hamiltonian. Due to the topological degeneracies present in our model, we have to make sure that the basis in any subspace also diagonalizes our edge mode guess \mathcal{E}_0 if we want to obtain the form in Eq. (15). This is reminiscent of standard degenerate perturbation theory and in fact requires by far the most resources of the total algorithm as we need to re-diagonalize 2^{N-2} many 4×4 matrices.

We will now detail how to construct the quasi-local conserved operators. By definition, these have a compact representation in the energy basis. This basis, which we label by $\{|k\rangle\}$, is obtained from full exact diagonalization. Consider a basis for diagonal operators in energy space fulfilling the Pauli-algebra. The minimal elements of this basis may take the following form

$$\Xi_i := 1_{2^{i-1}} \otimes Z \otimes 1_{2^{N-i}} = \sum_{k=1}^{2^N} (-1)^{\lfloor (k-1)/2^{N-i} \rfloor} |k\rangle\langle k|, \quad (14)$$

where Z is a Pauli-operator. This might look complicated at first glance, but it is really nothing but Pauli-operators defined in energy space. The full basis can be obtained by calculating all products of these N -many operators. These operators by construction exactly commute with the Hamiltonian. Hence, any constant of motion can be brought into the form of the Ξ operators. Their real space representation $U_D \Xi_i U_D^\dagger$ will however in general not be local. Their locality is completely dependent on the ordering of the eigenstates in the unitary U_D as this is the only freedom left. Due to the immense number of possible permutations – the order of the symmetric group S_{2^N} is $2^N!$ – a brute force approach is out of scope. We instead rely on a heuristic algorithm which dynamically relaxes an ansatz operator to obtain a good

permutation. Abstractly speaking, we bank on the time independent or equilibrium part of \mathcal{B}_0 to resemble the product of the perturbed edge modes \mathcal{B} already quite well. In cases where this is not given, the algorithm will fail to produce a local edge mode.

The unperturbed operator \mathcal{B}_0 and a diagonalization unitary U_D serve as inputs to our method. This unitary has an arbitrary ordering of eigenvectors at the start (for ED, usually determined by the size of the energies of the Hamiltonian). Upon mapping \mathcal{B}_0 to its equilibrium representation, we use it to obtain an ordering of the eigenstates that resembles the Pauli structure well. This representation is obtained by calculating the *infinite time average* of \mathcal{B}_0 , which stems from *equilibration theory*

$$\mathbb{E}(\mathcal{B}_0) := \lim_{T \rightarrow \infty} \frac{1}{T} \int_0^T dt \mathcal{B}_0(t) = \sum_k \langle k | \mathcal{B}_0 | k \rangle |k\rangle \langle k|, \quad (15)$$

the time average will hence be diagonal in the energy eigenbasis for non-degenerate spectra and is thus a constant of motion. However, since the infinite time average is not trace preserving, it in general causes \mathcal{B}_0 to lose its algebraic structure. We would like to point out that while localizing systems are in general not expected to thermalize, they do equilibrate which makes this ansatz meaningful [41].

Due to the topological degeneracies present in our model, we have to make sure that the basis in any subspace also diagonalizes our edge mode guess \mathcal{E}_0 if we want to obtain the form in Eq. (15). This is reminiscent of standard degenerate perturbation theory and in fact requires by far the most resources of the total algorithm as we need to rediagonalize 2^{N-2} many 4×4 matrices.

We then set out to find a permutation of the eigenvectors of H such that the time average of the \mathcal{B}_0 best resembles Ξ_1 which can be done by a sorting of the eigenvalues of $\mathbb{E}(\mathcal{B}_0)$. This permutation \mathcal{P} also gives rise to a new diagonalization unitary $\widetilde{U}_D = \mathcal{P}U_D$. Upon conjugating Ξ_1 with \widetilde{U}_D , we obtain an edge mode which fulfills all algebraic properties and commutes with the Hamiltonian. Since our sorting method is heuristic, we cannot rule out the existence of better localized edge modes. Nevertheless, the support that we find serves as a robust upper bound. Because of this, we note that a breakdown of our method, i.e. finding a non-local operator, does not necessarily imply that there are no localized edge modes.

The following pseudocode describes a possible way to implement this procedure numerically. We use a notation close to python.

```

1  input: diagonalizing unitary  $\widetilde{U}_D$  (as obtained from ED and
2  rediagonalization in degenerate subspaces)
3  input: edge modes of the unperturbed system  $\mathcal{E}_0^L, \mathcal{E}_0^R$ 
4  output: quasi-local diagonalization unitary  $U_D$ 
5
6  define infinite_time_average(V, O):
7      return diag(VOV†)
8
9  spec = infinite_time_average( $\widetilde{U}_D, \mathcal{E}_0^L \otimes \mathcal{E}_0^R$ )
10 perm = argsort(spec)
11
12 return  $\widetilde{U}_D[:, \text{perm}]$ 

```

This algorithm builds on a previously introduced method used in the context of many-body localized systems [40]. In this problem, the authors designed operators which commute exactly with the given Hamiltonian and are quasi-local. In a *many-body localized system*, one searches for extensively many quasi-local constants of motion and the system features a fully non-degenerate spectrum caused by the disordered potential landscape. In contrast, the SPT model is characterized by only constantly many edge mode operators which enforce degeneracies throughout the spectrum. These differences necessitated major modifications to the method from Ref. [40].

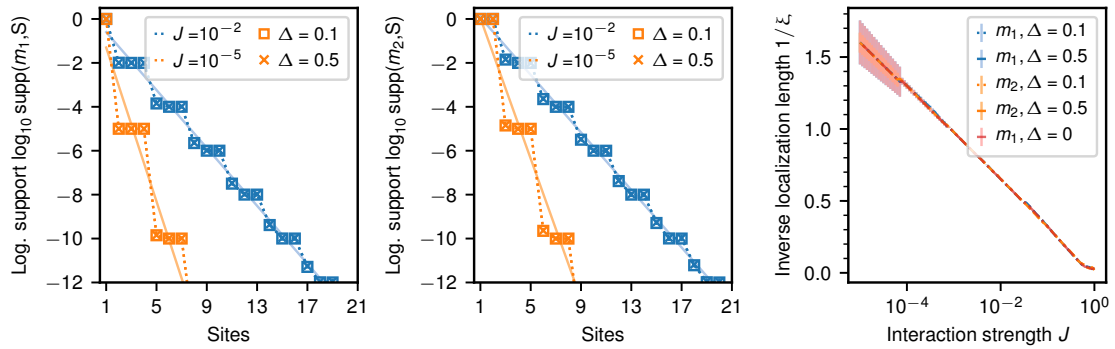


Figure 1: Left, Center: Logarithmic support $\log_{10}\text{supp}(\mathcal{B}, S)$ of the edge modes m_1 and m_2 for $\eta = 0$ on $N = 32$ sites, where S is a region starting from the left end of the system where sites starting from the right end have been removed. Color encodes the interaction (or hopping) strength J and markers indicate the disorder strength Δ . Each data point is an average over 100 realizations with error bars indicating the standard deviation of the data (smaller than symbols). Dotted lines are guides to the eye. Solid lines show linear fits of the data for $\Delta = 0.1$, which allow to extract the localization length ξ . Right: Interaction dependence of the inverse localization length $1/\xi$ for the edge modes. Here, color encodes the two modes and disorder strength Δ . Data for all interaction strengths and modes overlaps strongly. The lines shown have been extrapolated by using 100 values of interaction strengths in the shown interval. We also include data without disorder. Here, the errorbars show the quality of the fit in form of the least-squares error.

3.3 Measure of locality

In the following analysis we set out to assess the locality of the constructed edge mode operators. Therefore, we want to compare the action of the full operator to a itself truncated to a local region only. As a first step, we will need to specify a reduction map, which reduces our operators to such operators with local support in a region S

$$\Gamma_S(A) := \frac{1}{2^{S^c}} \text{tr}_{S^c}(A) \otimes 1_{S^c}, \tag{16}$$

where support is defined using site indices. This map truncates an operator down to its local support on S and afterwards embeds it into the full real space again by tensoring identities on S^c . This operator can now be compared to the original operator supported on the full system. The difference between the two will be a measure of the support

$$\text{supp}(A, S) = \|A - \Gamma_S(A)\|_\infty. \tag{17}$$

Due to the interacting procedure yielding products of edge modes, we expect their support to be mainly on both edges of the system. To assess their locality, we hence use an S which is centered in the middle of the chain and extends by increasing this block on its both ends by one site. We note that the norm used here is most sensitive and in many other applications operators which are expected to be local are so only in weaker norms than in operator norm [39, 40, 42, 43].

In the non-interacting case $\eta = 0$ we have access to the individual edge mode operators $m_1, m_2, \bar{m}_1, \bar{m}_2$ and we hence consider the sets $S_{L,k} = [k]$ and $S_{R,k} = [N - k]^c$ oriented at the left and right boundary of the system. The larger system size considered in this case, prohibits to use the full Hilbert-space representation of the operators. However, as we show in the appendix, one can exploit the algebraic properties of the non-interacting fermions in order

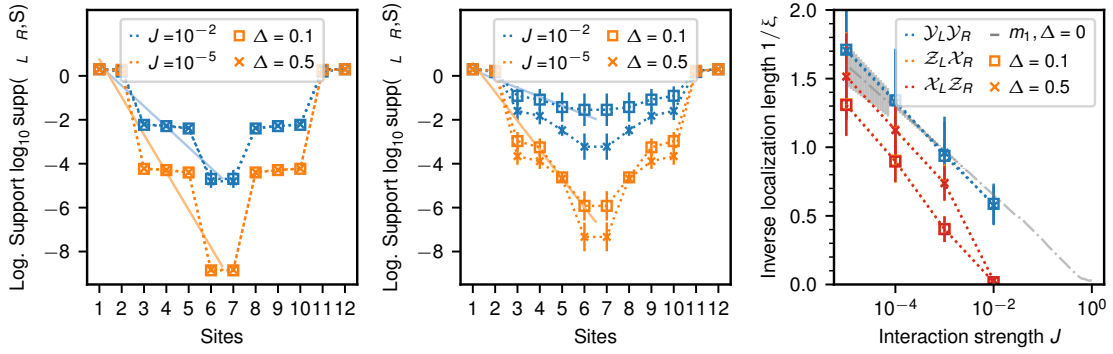


Figure 2: (Left, center) Logarithmic support $\log_{10}\text{supp}(\mathcal{B}, S)$ of the edge modes $\mathcal{Y}_L\mathcal{Y}_R$ and $\mathcal{Z}_L\mathcal{X}_R$ for $\eta = 1$ on $N = 12$ sites, where S is the left and right part of the system where blocks of even size centred around the middle of the chain have been removed. Colour encodes the used interaction strength J and markers encode the disorder strength Δ . Each data point is an average over 100 realizations with error bars indicating the standard deviation of the data. Dotted lines are a guide to the eye. Solid lines show linear fits of the data for $\Delta = 0.1$, which allow to extract the localization length ξ . Right: Interaction dependence of the localization length ξ for all three edge modes. Here, color encodes the three modes and markers again encode disorder strength Δ . The data for $\mathcal{Z}_L\mathcal{X}_R$ and $\mathcal{Z}_R\mathcal{X}_L$ overlaps completely which is why it is hard to spot the orange markers indicated in the legend. Again, the errorbars show the least-squares errors of the fit. The grey line is taken from the non-interacting results as a comparison.

to directly compute the reduction and norm of it within the fermionic picture which yields for $p = 1, 2$

$$\|m_p - \Gamma_{S_{L,k}}(m_p)\| = \sqrt{\sum_{l=k+1}^N Q_{l,p}^2}, \tag{18}$$

$$\|P\bar{m}_p - \Gamma_{S_{R,k}}(P\bar{m}_p)\| = \sqrt{\sum_{l=1}^{N-k} \bar{Q}_{l,p}^2}. \tag{19}$$

4 Numerical Results

In this section, we show and discuss the resulting operators for both models. We have worked with at least four interaction strengths $J \in \{10^{-2}, 10^{-3}, 10^{-4}, 10^{-5}\}$ and three disorder strengths $\Delta \in \{0.1, 0.3, 0.5\}$. For a clearer presentation, we only picked a subset of these results but the calculations not shown behave analogously.

4.1 Free fermionic perturbation

For $\eta = 0$, as described above, we show the support of the single edge modes supported on the left part of the chain. The system has a total size of $N = 32$ sites. While much larger systems are treatable and have been investigated by us with this algorithm, we find that this system size suffices to properly display the edge mode decay. For a system size scaling of this method, we refer interested reader to the Appendix D. Results can be found in Fig. 1. Left

and center plots show the logarithmic support $\log_{10}\text{supp}(\mathcal{E}, S)$ of the edge modes m_1, m_2 . We use the data of these plots to extract a localization length ξ , shown in the right plot. The errorbars indicating the least-squares error of the fit for small interactions stem from the fact that in these systems, the support of the edge mode falls off very strongly yielding only few non-zero points and therefore less accurate fits. We find that the inverse localization length ξ depends logarithmically on the interaction strength J .

The different modes m_1 and m_2 show the same qualitative behaviour. The support falls off in exponential fashion with the size of the support region. This aligns nicely with the intuition that additional interaction terms should only dress the original modes. Furthermore, the observed plateaus can be derived for the infinite system size limit as shown in Appendix C. With increasing interaction strength J , the edge modes become less local, as expected from perturbation theory.

A feature of particular note in these results is the insensitivity of the edge mode locality to the disorder strength Δ . As a comparison, we also show data without any disorder. This is surprising when contrasted with the intuition that disorder should help localize the edge modes [17, 18]. This suggests that the edge modes of this SPT do not couple to the bulk operators in circumstances of Anderson localization.

4.2 Many-body interacting perturbation

Now we resort to the calculations performed for $\eta = 1$, corresponding to the interacting system. Due to the size of the Hilbert space and the effort of the re-diagonalization of the topologically degenerate subspaces, we had to resort to system size $N = 12$. Fig. 2 again shows the logarithmic support $\log_{10}\text{supp}(\mathcal{E}, S)$ for $\mathcal{E} \in \{\mathcal{Y}_L\mathcal{Y}_R, \mathcal{X}_L\mathcal{Z}_R\}$ on the left and center panel. The right panel shows the extracted localization length. A more detailed discussion on the fitting procedure and cross validation of the code can be found in Appendix D. The symmetry of the plot is due to the choice of the system S as laid out in section 3.3.

The support again shows an exponential decay of operator support into the bulk. Moreover, this localization length ξ grows with increasing the interaction strength J as expected. The localization length observed for all edge modes is of the same order as the one found in much larger system sizes for the non-interacting perturbation (cp. gray dash-dotted line). However, when increasing the interaction strength to $J = 10^{-2}$ there is a sharp drop in the localization length for some operators which might be ascribed to a transition towards a topologically trivial phase. This transition point is far lower than the expected value of $J \sim 1$. This is an expected finite size effect as the edge modes are a priori closer together and thus able to hybridize more easily. Furthermore, the fit errors shown in this plot stem can also be ascribed to the finite size of the interacting system, since we are effectively fitting very few points. Nevertheless, the fit errors allow for distinguishing the different behavior of the modes. Nevertheless, the compatibility between non-interacting and many-body interacting localization lengths away from this transition indicates that the signal of SPT behaviour can still be reliably observed in system sizes tractable by exact diagonalization.

For the $\mathcal{Z}_L\mathcal{X}_R$ mode we find that the heuristic picture is recovered as increasing disorder strength aids localization. This contrasts strongly with our findings in the non-interacting case, indicating that many-body interactions are necessary to couple the edge modes to the bulk operators. Moreover, the localization length is generically longer than in the free fermion case with disorder strength pushing the length down towards the free fermion value. This suggests that the free fermion value represents the best localization of the edge modes for fixed interaction strength. The same behaviour is found for $\mathcal{X}_L\mathcal{Z}_R$ (cp. see appendix).

An exception to the behaviour reported above is displayed in the localization length of the $\mathcal{Y}_L\mathcal{Y}_R$ edge mode. Despite the presence of many-body interactions, it shows a disorder insensitivity akin to that of the non-interacting regime. This goes beyond mere analogy as

the value of the localization length of the $\mathcal{Y}_L\mathcal{Y}_R$ operator overlaps perfectly with the non-interacting results. We computed the localization behaviour for all six possible edge mode hybridization patterns and found that only the $\mathcal{Y}_L\mathcal{Y}_R$ operator displays free fermion localization behaviour. This suggests that this mode is subject to a selection rule which precludes the many-body interaction effects which delocalize the $\mathcal{Z}_L\mathcal{X}_R$ mode. The source of this selection rule is at this point mysterious, but we note that the $\mathcal{Y}_L\mathcal{Y}_R$ operator is unique among the choices of edge mode products in being local to the edges in both spin and fermionic variables, i.e. it does not feature a parity string across the whole chain. The absence of such a non-local feature in the fermionic picture may explain the reduced sensitivity to bulk localization behaviour.

Put succinctly, our results suggest that in the presence of many-body interactions, there may be a splitting of the modes into those which delocalize faster, i.e. $\mathcal{Z}_L\mathcal{X}_R$ and $\mathcal{X}_L\mathcal{Z}_R$ and are sensitive to disorder and one mode $\mathcal{Y}_L\mathcal{Y}_R$, which is insensitive to disorder and shows a stronger localization comparable to the one of non-interacting edge modes. We would like to point out, that since our method can only provide upper bounds to the localization behaviour, it is still conceivable that all three modes behave the same. Also, it is possible that the disorder sensitivity observed in all other products vanishes in larger systems than we are able to treat. However even if a finite size effect, this splitting constitutes an interesting result as it would be relevant for short synthetic chains or cold ion systems. In such circumstances where one seeks to improve edge mode locality in presence of many-body interactions to encode quantum information, the gains from disorder potentials are marginal compared to those from picking “better” edge modes.

5 Conclusions

In this work, we investigated the localization behavior of topological edge mode operators upon introducing both non-interacting and many-body interacting perturbations as well as disorder. Specifically, we started out from the disordered XZX cluster Hamiltonian which as a fixed-point model is exactly soluble and added XX and XXZ interactions which are expected to drive the transition towards a topologically trivial model. We introduce different methods of finding the topological edge mode operators, one based on the Majorana description which yields the lowest lying eigenmodes for non-interacting systems and a second one, which uses the relaxation of the fixed-point edge modes as an ansatz to heuristically find local edge modes for many-body interacting chains. While the support of the obtained edge operators with the interacting method is only an upper bound, the commutation with the Hamiltonian is exact.

Both perturbations considered delocalize as their strength is increased. However, the non-interacting model displays no disorder dependence whereas the interacting system does. Curiously, a single edge mode combination which in the fermionic language corresponds to the two density operators at both ends, namely $\mathcal{Y}_L\mathcal{Y}_R$, shows no disorder dependence even when adding many-body interactions. Our results suggest that for a finite size chain, one might find different localization behavior for different edge mode operators. Specifically, we find one edge mode that is most stable and completely insensitive to disorder, picking it out as the one best-suited to encode a logical qubit.

Since we fully diagonalize the Hamiltonian we are limited to small system sizes even for this one-dimensional problem. We hope to extend the method to larger systems by truncating to the ground state sector, which would possibly allow a tensor network implementation as well. The interacting method used in this work relies only on guessing a suitable ansatz edge mode operator. Hence, we plan to apply it to more physical models and other types of perturbations such as open dynamics. Here, one might hope to overcome the thermal instability of topological systems [44] with the help of disorder [45].

6 Acknowledgements

This work has been supported by the ERC (TAQ), the DFG (CRC 183, FOR 2724, EI 519/7-1), and the Templeton Foundation. This work has also received funding from the European Union’s Horizon 2020 research and innovation programme under grant agreement No 817482 (PASQuaS).

A Fractionalization

To see this, we must rewrite the time-reversal operator in a way that makes the edge action explicit. We can do this by re-expressing our time reversal operator using the cluster operators of our Hamiltonian,

$$\prod_{j=2}^{N-1} X_{j-1} Z_j X_{j+1} = (-1)^N X_1 X_2 \left(\prod_{j=2}^{N-1} Z_j \right) X_{N-1} X_N \quad (20)$$

$$= (-1)^N Y_1 X_2 \left(\prod_{j=1}^N Z_j \right) X_{N-1} Y_N \quad (21)$$

$$= \mathcal{Y}_L \left((-1)^N \prod_{j=1}^N Z_j \right) \mathcal{Y}_R, \quad (22)$$

which lets us recast \mathcal{T} as

$$\mathcal{T} = \mathcal{Y}_L \left(\prod_{j=2}^{N-1} X_{j-1} Z_j X_{j+1} \right) \mathcal{Y}_R \mathcal{K}. \quad (23)$$

If we decompose our Hilbert space into edge and bulk tensor factors, we can identify the emergent edge action

$$\mathcal{T} = \mathcal{Y}_L \mathcal{K}_L \otimes \left(\prod_{j=2}^{N-1} X_{j-1} Z_j X_{j+1} \mathcal{K}_{bulk} \right) \otimes \mathcal{Y}_R \mathcal{K}_R \quad (24)$$

and so we can see that the localized operators of time reversal on the edge states are

$$\mathcal{T}_{L/R} = \mathcal{Y}_{L/R} \mathcal{K}_{L/R} \quad (25)$$

which, curiously, these operators do not square to 1. Instead,

$$\mathcal{T}_{L/R}^2 = \mathcal{Y}_{L/R} \mathcal{K} \mathcal{Y}_{L/R} \mathcal{K}_{L/R}, \quad (26)$$

$$= \mathcal{Y}_{L/R} (-\mathcal{Y}_{L/R}) \mathcal{K}_{L/R}^2 = -1, \quad (27)$$

which demonstrates the symmetry fractionalization expected in an SPT phase.

B Operator norm decay of edge modes for $\eta = 0$

In the following we explicitly compute the norm of the edge mode operators m_p and $P\bar{m}_p$ with $p = 1, 2$ obtained in the case $\eta = 0$. Here, it is important to keep in mind, that we want to study

the effect of the reduction map on the level of the qubits in which the original Hamiltonian in (1) is defined. All following norms and traces are hence evaluated by reversing the Jordan-Wigner transformation and relating the fermionic operators to the Pauli operators. The results are then mapped again to the fermionic level as the expressions take a more compact form here.

Due to the non-interacting structure of the problem, the edge mode operators are linear combinations of the initial Majorana operators $\gamma_j, \bar{\gamma}_j$. In this case the result of the reduction map can be studied in detail. We find

$$\begin{aligned} \text{tr}_{S_{L,k}^c}(m_p) &= \sum_{l=1}^k Q_{p,l} \gamma_l, \\ \text{tr}_{S_{R,k}^c}(P\bar{m}_p) &= \sum_{l=N-k+1}^N \bar{Q}_{p,l} P \bar{\gamma}_l, \end{aligned} \tag{28}$$

where, as explained above, the trace is evaluated on the level of the qubits. The differences $A - \Gamma(A)$ are then given by

$$\begin{aligned} m_p - \Gamma_{S_{L,k}}(m_p) &= \sum_{l=k+1}^N Q_{p,l} \gamma_l, \\ P\bar{m}_p - \Gamma_{S_{R,k}}(P\bar{m}_p) &= \sum_{l=1}^{N-k} \bar{Q}_{p,l} P \bar{\gamma}_l, \end{aligned} \tag{29}$$

and again essentially only linear combinations of γ_j and $\bar{\gamma}_j$.

We can however compute easily the norm of any linear combination of Majorana operators. Let $S \subset [N]$ and define

$$A = \sum_{j \in S} a_j \gamma_j \tag{30}$$

to be any linear combination of the γ_j operators with $a_j \in \mathbb{R}$ for $j \in S$. One finds that the square of A is given by

$$\begin{aligned} A^2 &= \sum_{j,k \in S} a_j a_k \gamma_j \gamma_k \\ &= \sum_{j \in S} a_j a_j 1 + \sum_{j,k \in S: j < k} a_j a_k \gamma_j \gamma_k + \sum_{j,k \in S: k < j} a_j a_k \gamma_j \gamma_k \\ &= \sum_{j \in S} a_j^2 1. \end{aligned} \tag{31}$$

From this we can directly conclude, that A has only two degenerate eigenvalues $\pm(\sum_{j \in S} a_j^2)^{1/2}$ such that

$$\|A\|^2 = \sum_{j \in S} a_j^2 \tag{32}$$

can be directly computed. The same argument holds for the operators $P\gamma_j$. Hence, we obtain

$$\begin{aligned} \|m_p - \Gamma_{S_{L,k}}(m_p)\|^2 &= \sum_{l=k+1}^N Q_{p,l}^2, \\ \|P\bar{m}_p - \Gamma_{S_{R,k}}(P\bar{m}_p)\|^2 &= \sum_{l=1}^{N-k} \bar{Q}_{p,l}^2. \end{aligned} \tag{33}$$

C Scaling behaviour of support results for $\eta = 0$

Some features of the edge mode support can be inferred from analytical results computed for $N \rightarrow \infty$. Starting with

$$H = -i \sum_{j=2}^{N-1} \Delta_j \tilde{\gamma}_{j-1} \gamma_{j+1} - J \sum_{j=1}^{N-1} (i \tilde{\gamma}_j \gamma_{j+1} + i \gamma_j \tilde{\gamma}_{j+1}), \quad (34)$$

we can attempt to construct the edge modes iteratively. We can infer from the structure of the Hamiltonian that the left edge modes will be of the form

$$m_p = \sum_{j=1}^N \alpha_{p,j} \gamma_j. \quad (35)$$

In the thermodynamic limit, the edge zero modes are expected to be exact. This imposes a condition on the coefficients of the zero modes via the commutator

$$\frac{1}{2i} [m_p, H] = \tilde{\gamma}_1 (J \alpha_{p,2} + \Delta_2 \alpha_{p,3}) + \sum_{j=2}^{\infty} \tilde{\gamma}_j (J \alpha_{p,j+1} + \Delta_{j+1} \alpha_{p,j+2} - J \alpha_{p,j-1}) = 0, \quad (36)$$

from which we can construct a recurrence relation

$$\alpha_{p,j+1} = -\frac{J}{\Delta_j} (\alpha_{p,j} - \alpha_{p,j-2}), \quad (37)$$

that will allow us to produce two linearly independent edge mode operators. Since we assume that these should be smoothly related to the perfectly localised operators when $J = 0$, we choose to begin the recurrence relation with either $\alpha_1 = 1$ and $\alpha_2 = 0$, which we identify with m_1 , or vice versa, which we identify with m_2 . In the case of m_1 , a clear scaling behaviour emerges from $j = 4$ onward

$$\alpha_{1,3k+1} \sim J^{-k}, \quad \alpha_{1,3k+2} \sim J^{-(k+1)}, \quad \alpha_{1,3k+3} \sim J^{-(k+2)}, \quad k \in \mathbb{N}, \quad (38)$$

while the coefficients of m_2 exhibit a similar scaling behaviour from $j = 3$ onward

$$\alpha_{2,3k} \sim J^{-k}, \quad \alpha_{2,3k+1} \sim J^{-(k+1)}, \quad \alpha_{2,3k+2} \sim J^{-(k+2)}, \quad k \in \mathbb{N}, \quad (39)$$

which predicts a significant amount of structure in our support measure plots. Since we can compute our support measure exactly in the free fermion context, we see that

$$\text{supp}(m_1, S_{L,j}) \sim J^{-\lfloor \frac{j-1}{3} \rfloor}, \quad (40)$$

$$\text{supp}(m_2, S_{L,j}) \sim J^{-\lfloor \frac{j}{3} \rfloor}, \quad (41)$$

from which we infer that the support measure should have descending plateaus of width 3, all of which fall within an exponential envelope, which is precisely what is observed in Figure 1. The analysis for the right edge modes is identical, and we expect these to also show a plateau structure, which is also seen.

D Finite size scaling and cross validation

In this appendix, we discuss the finite size scaling of the non-interacting code and also explain the cross validation between the two methods.

The data for the finite size scaling for the non-interacting ($\eta = 0$) code is shown in Fig. 3. The color encodes support data of m_0 for different different system sizes and the gray line is machine precision. Each point is an average over 100 realizations for interaction and disorder values similar to the main text. We find that the different system sizes agree quite well in the parameter regime investigated here. Moreover, the data indicates that at a size of 24 sites the support decays to the machine precision, which is why we settled for a system size of that order for the main text material despite the availability of even larger systems.

For the interacting code things are quite different, as here 12 sites is the maximal system size that can be reached due to the effort needed for the sorting procedure. Furthermore, the emergent plateau structure which can be demonstrated in the infinite system limit for the non-interacting case (see App.,C) still persists in the interacting model. Thus, we are forced to effectively fit the exponential envelope to only three points, which unfortunately renders a system size scaling towards smaller systems meaningless. Nevertheless, the interacting procedure naturally also works if the Hamiltonian is actually non-interacting so we used this to at least cross validate results between both algorithms for small systems where they agree.

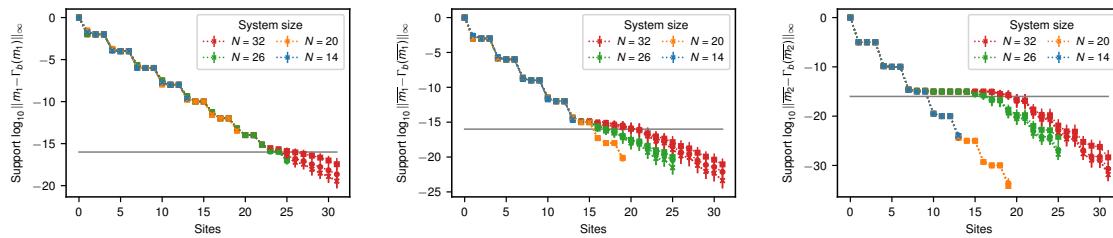
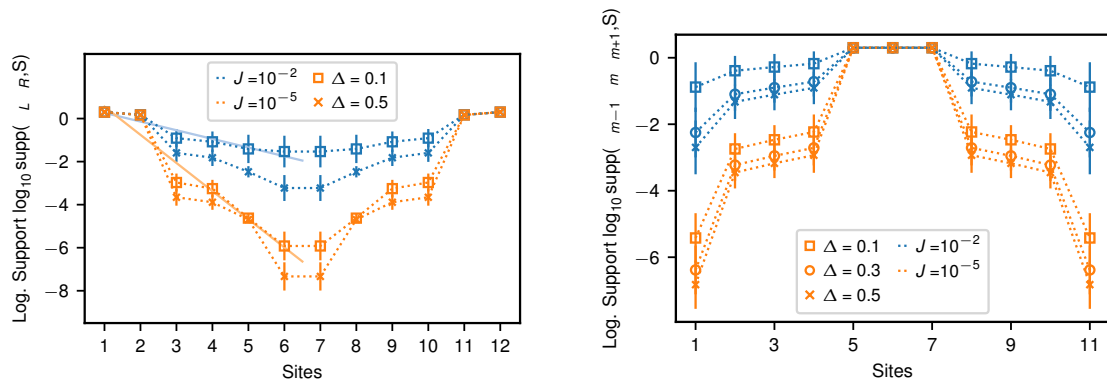


Figure 3: Finite size scaling for the non-interacting ($\eta = 0$) algorithm and the m_0 mode. Color encodes system size, the gray line indicates machine precision. Each point is an average over 100 realizations. The different panels show interaction strength $J = 10^{-2}, 10^{-3}, 10^{-5}$ from left to right. The three values of disorder $\Delta = 0.1, 0.3, 0.5$ are indicated by markers and either lie on top of one another or are below machine precision.

E Additional numerical data

In this appendix, we show additional numerical data obtained for the $\mathcal{X}_L \mathcal{Z}_R$ edge mode and a bulk operator. Fig. 4a shows the support of $\mathcal{X}_L \mathcal{Z}_R$ edge mode on the same scale as in the main text. It shows the same disorder dependence and has the same localization length as $\mathcal{Z}_L \mathcal{X}_R$. Fig. 4b shows the localization behaviour of a bulk operator in a chain of length $N = 11$. Here again, the disorder strength decreases the localization length.



(a) Logarithmic support $\log_{10}\text{supp}(\mathcal{X}_L \mathcal{Z}_R, S)$ for $\eta = 1$ on $N = 12$ sites. , where S is the left and right part of the system where blocks of even size centered around the middle of the chain have been removed. Color encodes the used interaction strength J and markers encode the disorder strength Δ . Each data point is an average over 100 realizations. Dotted lines are a guide to the eye. Solid lines show linear fits of the data for $\Delta = 0.1$, which allow to extract the localization length ξ .

(b) Logarithmic support $\log_{10}\text{supp}(\mathcal{X}_{m-1} \mathcal{Z}_m \mathcal{X}_{m+1}, S)$ for $\eta = 1$ on $N = 11$ sites. , where S is the middle of the system where sites to the left and right were successively removed. Color encodes the used interaction strength J and markers encode the disorder strength Δ . Each data point is an average over 100 realizations. Dotted lines are a guide to the eye.

Figure 4: Additional numerical data.

References

- [1] S. D. Sarma and A. Pinczuk, *Perspectives in quantum Hall effects*, Wiley-VCH, Weinheim (1996), doi:[10.1002/9783527617258](https://doi.org/10.1002/9783527617258).
- [2] M. Z. Hasan and C. L. Kane, *Colloquium: Topological insulators*, Rev. Mod. Phys. **82**, 3045 (2010), doi:[10.1103/RevModPhys.82.3045](https://doi.org/10.1103/RevModPhys.82.3045).
- [3] R. M. Lutchyn, E. P. A. M. Bakkers, L. P. Kouwenhoven, P. Krogstrup, C. M. Marcus and Y. Oreg, *Majorana zero modes in superconductor–semiconductor heterostructures*, Nat. Rev. Mater. **3**, 52 (2018), doi:[10.1038/s41578-018-0003-1](https://doi.org/10.1038/s41578-018-0003-1).
- [4] N. R. Cooper, J. Dalibard and I. B. Spielman, *Topological bands for ultracold atoms*, Rev. Mod. Phys. **91**, 015005 (2019), doi:[10.1103/RevModPhys.91.015005](https://doi.org/10.1103/RevModPhys.91.015005).
- [5] A. Kitaev and J. Preskill, *Topological entanglement entropy*, Phys. Rev. Lett. **96**, 110404 (2006), doi:[10.1103/PhysRevLett.96.110404](https://doi.org/10.1103/PhysRevLett.96.110404).
- [6] A. Yu. Kitaev, *Fault-tolerant quantum computation by anyons*, Ann. Phys. **303**, 2 (2003), doi:[10.1016/S0003-4916\(02\)00018-0](https://doi.org/10.1016/S0003-4916(02)00018-0).
- [7] F. D. M. Haldane, *Nonlinear field theory of large-spin Heisenberg antiferromagnets: Semi-classically quantized solitons of the one-dimensional easy-axis Néel state*, Phys. Rev. Lett. **50**, 1153 (1983), doi:[10.1103/PhysRevLett.50.1153](https://doi.org/10.1103/PhysRevLett.50.1153).
- [8] I. Affleck, T. Kennedy, E. H. Lieb and H. Tasaki, *Rigorous results on valence-bond ground states in antiferromagnets*, Phys. Rev. Lett. **59**, 799 (1987), doi:[10.1103/PhysRevLett.59.799](https://doi.org/10.1103/PhysRevLett.59.799).

- [9] A. Y. Kitaev, *Unpaired Majorana fermions in quantum wires*, Physics-Uspekhi **44**, 131 (2001), doi:[10.1070/1063-7869/44/10S/S29](https://doi.org/10.1070/1063-7869/44/10S/S29).
- [10] A. Roy and T. Quella, *Chiral Haldane phases of $SU(N)$ quantum spin chains*, Phys. Rev. B **97**, 155148 (2018), doi:[10.1103/PhysRevB.97.155148](https://doi.org/10.1103/PhysRevB.97.155148).
- [11] R. Verresen, R. Moessner and F. Pollmann, *One-dimensional symmetry protected topological phases and their transitions*, Phys. Rev. B **96**, 165124 (2017), doi:[10.1103/PhysRevB.96.165124](https://doi.org/10.1103/PhysRevB.96.165124).
- [12] X. Chen, Z.-C. Gu, Z.-X. Liu and X.-G. Wen, *Symmetry protected topological orders and the group cohomology of their symmetry group*, Phys. Rev. B **87**, 155114 (2013), doi:[10.1103/PhysRevB.87.155114](https://doi.org/10.1103/PhysRevB.87.155114).
- [13] N. Schuch, D. Pérez-García and I. Cirac, *Classifying quantum phases using matrix product states and projected entangled pair states*, Phys. Rev. B **84**, 165139 (2011), doi:[10.1103/PhysRevB.84.165139](https://doi.org/10.1103/PhysRevB.84.165139).
- [14] F. Pollmann and A. M. Turner, *Detection of symmetry-protected topological phases in one dimension*, Phys. Rev. B **86**, 125441 (2012), doi:[10.1103/PhysRevB.86.125441](https://doi.org/10.1103/PhysRevB.86.125441).
- [15] B. M. Terhal, *Quantum error correction for quantum memories*, Rev. Mod. Phys. **87**, 307 (2015), doi:[10.1103/RevModPhys.87.307](https://doi.org/10.1103/RevModPhys.87.307).
- [16] J. R. Wootton and J. K. Pachos, *Bringing order through disorder: Localization of errors in topological quantum memories*, Phys. Rev. Lett. **107**, 030503 (2011), doi:[10.1103/PhysRevLett.107.030503](https://doi.org/10.1103/PhysRevLett.107.030503).
- [17] D. A. Huse, R. Nandkishore, V. Oganesyan, A. Pal and S. L. Sondhi, *Localization-protected quantum order*, Phys. Rev. B **88**, 014206 (2013), doi:[10.1103/PhysRevB.88.014206](https://doi.org/10.1103/PhysRevB.88.014206).
- [18] Y. Bahri, R. Vosk, E. Altman and A. Vishwanath, *Localization and topology protected quantum coherence at the edge of hot matter*, Nat. Commun. **6**, 7341 (2015), doi:[10.1038/ncomms8341](https://doi.org/10.1038/ncomms8341).
- [19] H. Jiang, L. Wang, Q.-f. Sun and X. C. Xie, *Numerical study of the topological Anderson insulator in $HgTe/CdTe$ quantum wells*, Phys. Rev. B **80**, 165316 (2009), doi:[10.1103/PhysRevB.80.165316](https://doi.org/10.1103/PhysRevB.80.165316).
- [20] J. Li, R.-L. Chu, J. K. Jain and S.-Q. Shen, *Topological Anderson insulator*, Phys. Rev. Lett. **102**, 136806 (2009), doi:[10.1103/PhysRevLett.102.136806](https://doi.org/10.1103/PhysRevLett.102.136806).
- [21] C. W. Groth, M. Wimmer, A. R. Akhmerov, J. Tworzydło, C. W. J. Beenakker, *Theory of the topological Anderson insulator*, Phys. Rev. Lett. **103**, 196805 (2009), doi:[10.1103/PhysRevLett.103.196805](https://doi.org/10.1103/PhysRevLett.103.196805).
- [22] S. Bravyi, M. B. Hastings and S. Michalakis, *Topological quantum order: Stability under local perturbations*, J. Math. Phys. **51**, 093512 (2010), doi:[10.1063/1.3490195](https://doi.org/10.1063/1.3490195).
- [23] S. Bravyi and M. B. Hastings, *A short proof of stability of topological order under local perturbations*, Commun. Math. Phys. **307**, 609 (2011), doi:[10.1007/s00220-011-1346-2](https://doi.org/10.1007/s00220-011-1346-2).
- [24] M. B. Hastings, *The Stability of free Fermi Hamiltonians* (2017), [arXiv:1706.02270](https://arxiv.org/abs/1706.02270).

- [25] I. Affleck, T. Kennedy, E. H. Lieb and H. Tasaki, *Valence bond ground states in isotropic quantum antiferromagnets*, in *Condensed Matter Physics and Exactly Soluble Models*, Springer, 253 (1988), doi:[10.1007/978-3-662-06390-3_19](https://doi.org/10.1007/978-3-662-06390-3_19).
- [26] M. Serbyn, Z. Papić and D. A. Abanin, *Local Conservation laws and the structure of the many-body localized states*, *Phys. Rev. Lett.* **111**, 127201 (2013), doi:[10.1103/PhysRevLett.111.127201](https://doi.org/10.1103/PhysRevLett.111.127201).
- [27] D. A. Huse, R. Nandkishore and V. Oganesyan, *Phenomenology of fully many-body-localized systems*, *Phys. Rev. B* **90**, 174202 (2014), doi:[10.1103/PhysRevB.90.174202](https://doi.org/10.1103/PhysRevB.90.174202).
- [28] R. Vosk and E. Altman, *Many-body localization in one dimension as a dynamical renormalization group fixed point*, *Phys. Rev. Lett.* **110**, 067204 (2013), doi:[10.1103/PhysRevLett.110.067204](https://doi.org/10.1103/PhysRevLett.110.067204).
- [29] L. Rademaker and M. Ortuño, *Explicit local integrals of motion for the many-body localized state*, *Phys. Rev. Lett.* **116**, 010404 (2016), doi:[10.1103/PhysRevLett.116.010404](https://doi.org/10.1103/PhysRevLett.116.010404).
- [30] L. Rademaker, M. Ortuño and A. M. Somoza, *Many-body localization from the perspective of Integrals of Motion*, *Ann. Phys.* **529**, 1600322 (2017), doi:[10.1002/andp.201600322](https://doi.org/10.1002/andp.201600322).
- [31] C. Monthus, *Flow towards diagonalization for many-body-localization models: adaptation of the Toda matrix differential flow to random quantum spin chains*, *J. Phys. A* **49**, 305002 (2016)., doi:[10.1088/1751-8113/49/30/305002](https://doi.org/10.1088/1751-8113/49/30/305002).
- [32] D. Pekker, B. K. Clark, V. Oganesyan and G. Refael, *Fixed points of Wegner-Wilson flows and many-body localization*, *Phys. Rev. Lett.* **119**, 075701 (2017), doi:[10.1103/PhysRevLett.119.075701](https://doi.org/10.1103/PhysRevLett.119.075701).
- [33] D. J. Luitz, F. Huveneers and W. De Roeck, *How a small quantum bath can thermalize long localized chains*, *Phys. Rev. Lett.* **119**, 150602 (2017), doi:[10.1103/PhysRevLett.119.150602](https://doi.org/10.1103/PhysRevLett.119.150602).
- [34] A. Chandran, I. H. Kim, G. Vidal and D. A. Abanin, *Constructing local integrals of motion in the many-body localized phase*, *Phys. Rev. B* **91**, 085425 (2015), doi:[10.1103/PhysRevB.91.085425](https://doi.org/10.1103/PhysRevB.91.085425).
- [35] T. E. O'Brien, D. A. Abanin, G. Vidal and Z. Papić, *Explicit construction of local conserved operators in disordered many-body systems*, *Phys. Rev. B* **94**, 144208 (2016), doi:[10.1103/PhysRevB.94.144208](https://doi.org/10.1103/PhysRevB.94.144208).
- [36] R.-Q. He and Z.-Y. Lu, *Interaction-induced characteristic length in strongly many-body localized systems**, *Chinese Phys. Lett.* **35**, 027101 (2018), doi:[10.1088/0256-307X/35/2/027101](https://doi.org/10.1088/0256-307X/35/2/027101).
- [37] A. K. Kulshreshtha, A. Pal, T. B. Wahl and S. H. Simon, *Behavior of l -bits near the many-body localization transition*, *Phys. Rev. B* **98**, 184201 (2018), doi:[10.1103/PhysRevB.98.184201](https://doi.org/10.1103/PhysRevB.98.184201).
- [38] S. J. Thomson and M. Schiró, *Time evolution of many-body localized systems with the flow equation approach*, *Phys. Rev. B* **97**, 060201 (2018), doi:[10.1103/PhysRevB.97.060201](https://doi.org/10.1103/PhysRevB.97.060201).
- [39] M. Mierzejewski, M. Kozarzewski and P. Prelovšek, *Counting local integrals of motion in disordered spinless-fermion and Hubbard chains*, *Phys. Rev. B* **97**, 064204 (2018), doi:[10.1103/PhysRevB.97.064204](https://doi.org/10.1103/PhysRevB.97.064204).

- [40] M. Goihl, M. Gluza, C. Krumnow and J. Eisert, *Construction of exact constants of motion and effective models for many-body localized systems*, Phys. Rev. B **97**, 134202 (2018), doi:[10.1103/PhysRevB.97.134202](https://doi.org/10.1103/PhysRevB.97.134202).
- [41] M. Serbyn, Z. Papić and D. A. Abanin, *Quantum quenches in the many-body localized phase*, Phys. Rev. B **90**, 174302 (2014), doi:[10.1103/PhysRevB.90.174302](https://doi.org/10.1103/PhysRevB.90.174302).
- [42] M. Mierzejewski, P. Prelovšek and T. Prosen, *Identifying local and quasilocal conserved quantities in integrable systems*, Phys. Rev. Lett. **114**, 140601 (2015), doi:[10.1103/PhysRevLett.114.140601](https://doi.org/10.1103/PhysRevLett.114.140601).
- [43] M. Mierzejewski, T. Prosen and P. Prelovšek, *Approximate conservation laws in perturbed integrable lattice models*, Phys. Rev. B **92**, 195121 (2015), doi:[10.1103/PhysRevB.92.195121](https://doi.org/10.1103/PhysRevB.92.195121).
- [44] S. Roberts, B. Yoshida, A. Kubica and S. D. Bartlett, *Symmetry-protected topological order at nonzero temperature*, Phys. Rev. A **96**, 022306 (2017), doi:[10.1103/PhysRevA.96.022306](https://doi.org/10.1103/PhysRevA.96.022306).
- [45] A. Chandran, V. Khemani, C. R. Laumann and S. L. Sondhi, *Many-body localization and symmetry-protected topological order*, Phys. Rev. B **89**, 144201 (2014), doi:[10.1103/PhysRevB.89.144201](https://doi.org/10.1103/PhysRevB.89.144201).

CONCLUSIONS

As any healthy relationship thrives on harmony but also dissonance, the relationship between quantum mechanics and thermodynamics is no difference. The former, much younger theory describes the universe with a breathtaking level of detail while the latter predicts the collective behaviour of an innumerable number of particles without even knowing their positions. Yet both of them agree that systems - quantum or classical - dynamically find their way to equilibrium and furthermore thermal ensembles in most circumstances. In the realm of quantum mechanics, the underlying reasons for thermalisation are still subject of heated debates. A necessary condition for thermalisation is prior equilibration, which provably happens for generic systems but it is unclear what the associated time scales are. Since exact solutions of many-body systems scale unfavourably in the system size, such questions are not easily accessible.

Many-body localisation is an effect that localises the constituent particles of a system causing it to refrain from thermalisation altogether in a wide range of regimes while still equilibrating. It can be explained by an emerging quasi-integrability in terms of local constants of motion. In this thesis, we set out to elucidate questions in many-body localisation in the more general context of out-of-equilibrium dynamics addressing its stability, its experimental measurability and the computability of its theory.

Firstly, we addressed whether many-body localisation is stable to small regions which are thermal in one-dimensional spin chains. In spirit of the Griffiths effect, we constructed a small many-body localised system with a thermal inclusion that competes with localisation. This can be seen as a constituent part of a larger chain. If the thermal inclusion is not able to thermalise its localised surroundings, it will also not destabilise larger chains. We calculated localisation properties for two scenarios: In the first, the thermal region is of constant size, whereas in the second it scales extensively with system size. The results suggest that many-body localisation is stable for finite inclusions, but extensive thermal regions do drive the system towards thermalisation.

One of the most fascinating aspects of many-body localisation is that it can actually be realised in state-of-the-art analogue quantum simulators. Focusing specifically on ultra-cold atoms in optical lattices, we devised measurements that allow to probe the theoretically established phenomenology in an experiment using only technology that is available in such a setup. We put emphasis on the question of how to witness interactions which are crucial for many-body localisation and showed that those can be detected measuring density-density correlators with the in-situ measurement as well as with equilibration of local particle densities.

Another direction we investigated in this thesis are local constants of motion. Basically the full phenomenology of many-body localisation can be explained using such operators. As their occupation does not change in time, they are also the reason for the non-thermalising behaviour. We introduced an algorithm which constructs exact constants of motion for many-body localised systems. Since the operators we found constitute an operator basis by construction, we can decompose

the Hamiltonian to find a low order approximation of it in terms of these local constants of motion. While global quantities such as the norm difference between the approximation and the full Hamiltonian suggest that the approximation is not reliable, we also show that it can faithfully reproduce local dynamics.

In the last part, we broadened the scope and devised an extension of our algorithm to construct edge modes of spin chains with symmetry protected order. These are also constants of motion due to the structure of the Hamiltonian and are expected to be stabilised by a global symmetry. We investigated the influence of disorder and interactions as perturbations to the original model and found that for non-interacting perturbations, the disorder does not change the localisation properties of the edge modes at all. This is intriguing, as the mechanism for delocalisation is hybridisation via the bulk and the disorder should cause Anderson localisation in the bulk making it far less likely to hybridise the ends of the chain. When subjected the system with additional many-body interactions, the disorder did help stabilise two out of three edge mode operators, while the remaining one is ignorant of the disorder and in other words behaves like the non-interacting case.

To put in a nutshell what we have learned in the course of this thesis, we think it is fair to say that local constants of motions are powerful objects that allow to simplify and understand the complex dynamics of quantum many-body systems. They are essential for the breakdown of thermalisation and can be put to use in effective models with significantly simpler structures than real space Hamiltonians. Nevertheless, we are only beginning to understand their origin and full impact. The proposed algorithm in this work is capable of finding exact constants of motion, but their locality is only heuristic. It can be generalised to other systems, if a suitable heuristic or ansatz operators exists. What is lacking is a generalised, maybe even analytical framework that allows to compute local constants of motion for arbitrary systems, given that there are any. Such a method could potentially consist of an extended perturbation theory on the Hamiltonian level taking into account the locality of the generated terms. We think it is crucial to obtain an in-depth understanding of local constants of motion to make progress on the longstanding question of the whereabouts of thermalisation.

BIBLIOGRAPHY

- [1] D. Wallace. Recurrence theorems: A unified account. *Journal of Mathematical Physics*, 56(2):022105, 2015.
- [2] C. Gogolin and J. Eisert. Equilibration, thermalisation, and the emergence of statistical mechanics in closed quantum systems. *Reports on Progress in Physics*, 79(5):056001, 2016.
- [3] M. Gluza, C. Krumnow, M. Friesdorf, C. Gogolin, and J. Eisert. Equilibration via gaussification in fermionic lattice systems. *Phys. Rev. Lett.*, 117:190602, 2016.
- [4] M. Gluza, J. Eisert, and T. Farelly. Equilibration towards generalized gibbs ensembles in non-interacting theories. *arXiv:1809.08268*, 2018.
- [5] N. Linden, S. Popescu, A. J. Short, and A. Winter. Quantum mechanical evolution towards thermal equilibrium. *Phys. Rev. E*, 79:061103, 2009.
- [6] A. J. Short. Equilibration of quantum systems and subsystems. *New Journal of Physics*, 13(5):053009, 2011.
- [7] H. Wilming, M. Goihl, I. Roth, and J. Eisert. Entanglement-ergodic quantum systems equilibrate exponentially well. *arXiv:1802.02052*, 2018.
- [8] J. Eisert, M. Friesdorf, and C. Gogolin. Quantum many-body systems out of equilibrium. *Nature Phys.*, 11:124--130, 2015.
- [9] S. Goldstein, T. Hara, and H. Tasaki. Time scales in the approach to equilibrium of macroscopic quantum systems. *Phys. Rev. Lett.*, 111:140401, 2013.
- [10] A. S. L. Malabarba, L. P. García-Pintos, N. Linden, T. C. Farrelly, and A. J. Short. Quantum systems equilibrate rapidly for most observables. *Phys. Rev. E*, 90:012121, 2014.
- [11] M. C. Banuls, J. I. Cirac, and M. B. Hastings. Strong and weak thermalization of infinite nonintegrable quantum systems. *Phys. Rev. Lett.*, 106:050405, 2011.
- [12] H. Wilming, M. Goihl, C. Krumnow, and J. Eisert. Towards local equilibration in closed interacting quantum many-body systems. *arXiv:1704.06291*, 2017.
- [13] T. R. de Oliveira, C. Charalambous, D. Jonathan, M. Lewenstein, and A. Riera. Equilibration time scales in closed many-body quantum systems. *New Journal of Physics*, 20(3):033032, 2018.
- [14] W. Beugeling, R. Moessner, and M. Haque. Off-diagonal matrix elements of local operators in many-body quantum systems. *Phys. Rev. E*, 91, 2015.
- [15] I. Arad, T. Kuwahara, and Z. Landau. Connecting global and local energy distributions in quantum spin models on a lattice. *Journal of Statistical Mechanics: Theory and Experiment*, 2016(3):033301, 2016.
- [16] E. Leviatan, F. Pollmann, H. Bardarson, J. A. Huse, D. and E. Altman. Quantum thermalization dynamics with matrix-product states. *arXiv:1702.08894*.

- [17] P. Reimann. Foundation of statistical mechanics under experimentally realistic conditions. *Phys. Rev. Lett.*, 101(19):190403, 2008.
- [18] P. Reimann and P. Kastner. Equilibration of isolated macroscopic quantum systems. *New J. Phys.*, 14:043020, 2012.
- [19] P. Reimann. Typical fast thermalization processes in closed many-body systems. *Nature Comm.*, 7:10821, 2016.
- [20] J. von Neumann. Proof of the ergodic theorem and the h-theorem in quantum mechanics. *The European Physical Journal H*, 35(2):201--237, 2010.
- [21] M. Gring, M. Kuhnert, T. Langen, T. Kitagawa, B. Rauer, M. Schreitl, I. Mazets, D. A. Smith, E. Demler, and J. Schmiedmayer. Relaxation and prethermalization in an isolated quantum system. *Science*, 337(6100):1318--1322, 2012.
- [22] J. M. Deutsch. Quantum statistical mechanics in a closed system. *Physical Review A*, 43(4):2046, 1991.
- [23] M. Srednicki. Chaos and quantum thermalization. *Physical Review E*, 50(2):888, 1994.
- [24] M. Rigol, V. Dunjko, and M. Olshanii. Thermalization and its mechanism for generic isolated quantum systems. *Nature*, 452(7189):854, 2008.
- [25] A. Polkovnikov, K. Sengupta, A. Silva, and M. Vengalattore. Nonequilibrium dynamics of closed interacting quantum systems. *Rev. Mod. Phys.*, 83(3):863--883, 2011.
- [26] N. de Beaudrap, T. J. Osborne, and J. Eisert. Ground states of unfrustrated spin hamiltonians satisfy an area law. *New Journal of Physics*, 12(9):095007, 2010.
- [27] J.-S. Caux and J. Mossel. Remarks on the notion of quantum integrability. *Journal of Statistical Mechanics: Theory and Experiment*, 2011(02):P02023, 2011.
- [28] F. H. L. Essler and M. Fagotti. Quench dynamics and relaxation in isolated integrable quantum spin chains. *Journal of Statistical Mechanics: Theory and Experiment*, 2016(6):064002, 2016.
- [29] P. W. Anderson. Absence of diffusion in certain random lattices. *Physical review*, 109(5):1492, 1958.
- [30] C. K. Burrell, J. Eisert, and T. J. Osborne. Information propagation through quantum chains with fluctuating disorder. *Physical Review A*, 80(5):052319, 2009.
- [31] D. M. Basko, I. L. Aleiner, and B. L. Altshuler. Metal--insulator transition in a weakly interacting many-electron system with localized single-particle states. *Annals of physics*, 321(5):1126--1205, 2006.
- [32] A. Abanin, D. E. Altman, I. Bloch, and M. Serbyn. Colloquium: Many-body localization, thermalization, and entanglement. *Rev. Mod. Phys.*, 91:021001, 2019.
- [33] M. Schreiber, S. S. Hodgman, P. Bordia, H. P. Lüschen, M. H. Fischer, R. Vosk, E. Altman, U. Schneider, and I. Bloch. Observation of many-body localization of interacting fermions in a quasirandom optical lattice. *Science*, 349(6250):842--845, 2015.

- [34] S. Trotzky, Y.-A. Chen, A. Flesch, I. P. McCulloch, U. Schollwoeck, J. Eisert, and I. Bloch. Probing the relaxation towards equilibrium in an isolated strongly correlated one-dimensional Bose gas. *Nature Phys.*, 8:325, 2012.
- [35] M. Serbyn, Z. Papić, and D. A. Abanin. Quantum quenches in the many-body localized phase. *Phys. Rev. B*, 90:174302, 2014.
- [36] E. H. Lieb and D. W. Robinson. The finite group velocity of quantum spin systems. In *Statistical mechanics*, pages 425--431. Springer, 1972.
- [37] M. Cheneau, P. Barmettler, D. Poletti, M. Endres, P. Schauß, T. Fukuhara, C. Gross, I. Bloch, C. Kollath, and S. Kuhr. Light-cone-like spreading of correlations in a quantum many-body system. *Nature*, 481(7382):484, 2012.
- [38] P. Jurcevic, B. P. Lanyon, P. Hauke, C. Hempel, P. Zoller, R. Blatt, and C. F. Roos. Quasiparticle engineering and entanglement propagation in a quantum many-body system. *Nature*, 511(7508):202, 2014.
- [39] M. Znidaric, T. Prosen, and P. Prelovsek. Many-body localization in the Heisenberg XXZ magnet in a random field. *Phys. Rev. B*, 77:064426, 2008.
- [40] J. H. Bardarson, F. Pollmann, and J. E. Moore. Unbounded growth of entanglement in models of many-body localization. *Phys. Rev. Lett.*, 109:017202, 2012.
- [41] M. Serbyn, Z. Papić, and D. A. Abanin. Local conservation laws and the structure of the many-body localized states. *Phys. Rev. Lett.*, 111:127201, 2013.
- [42] D. A. Huse, R. Nandkishore, and V. Oganesyan. Phenomenology of fully many-body-localized systems. *Phys. Rev. B*, 90(17):174202, 2014.
- [43] M. Žnidarič. Entanglement in a dephasing model and many-body localization. *Physical Review B*, 97(21):214202, 2018.
- [44] J. Z. Imbrie. On many-body localization for quantum spin chains. *Journal of Statistical Physics*, 163(5):998--1048, 2016.
- [45] J.-Y. Choi, S. Hild, J. Zeiher, P. Schauß, A. Rubio-Abadal, T. Yefsah, V. Khemani, D. A. Huse, I. Bloch, and C. Gross. Exploring the many-body localization transition in two dimensions. *Science*, 352(6293):1547--1552, 2016.
- [46] W. De Roeck and F. Huveneers. Stability and instability towards delocalization in many-body localization systems. *Physical Review B*, 95(15):155129, 2017.
- [47] J. Šuntajs, J. Bonča, T. Prosen, and L. Vidmar. Quantum chaos challenges many-body localization. *arXiv:1905.06345*, 2019.
- [48] J. Smith, A. Lee, P. Richerme, B. Neyenhuis, P. W. Hess, P. Hauke, M. Heyl, D. A. Huse, and C. Monroe. Many-body localization in a quantum simulator with programmable random disorder. *Nature Physics*, 12(10):907, 2016.
- [49] P. Roushan, C. Neill, J. Tangpanitanon, V. M. Bastidas, A. Megrant, R. Barends, Y. Chen, Z. Chen, B. Chiaro, A. Dunsworth, A. Fowler, B. Foxen, M. Giustina, E. Jeffrey, J. Kelly, E. Lucero, J. Mutus, M. Neeley, C. Quintana, D. Sank, A. Vainsencher, J. Wenner, T. White, H. Neven, D. G. Angelakis, and J. Martinis. Spectroscopic signatures of localization with interacting photons in superconducting qubits. *Science*, 358(6367):1175--1179, 2017.

- [50] K. Agarwal, E. Altman, E. Demler, S. Gopalakrishnan, D. A. Huse, and M. Knap. Rare-region effects and dynamics near the many-body localization transition. *Annalen der Physik*, 529(7):1600326, 2017.
- [51] D. J. Luitz, F. Huveneers, and W. De Roeck. How a small quantum bath can thermalize long localized chains. *Physical review letters*, 119(15):150602, 2017.
- [52] A. Fehske, J. Malmodin, G. Biczók, and G. Fettweis. The global carbon footprint of mobile communications - the ecological and economic perspective. *IEEE Communications Magazine*, 49, 2011.
- [53] I. Bloch, J. Dalibard, and W. Zwerger. Many-body physics with ultracold gases. *Reviews of modern physics*, 80(3):885, 2008.
- [54] A. Chandran, I. H. Kim, G. Vidal, and D. A. Abanin. Constructing local integrals of motion in the many-body localized phase. *Phys. Rev. B*, 91:085425, 2015.
- [55] T. E. O'Brien, D. A. Abanin, G. Vidal, and Z. Papić. Explicit construction of local conserved operators in disordered many-body systems. *Phys. Rev. B*, 94:144208, 2016.
- [56] L. Rademaker and M. Ortuño. Explicit local integrals of motion for the many-body localized state. *Phys. Rev. Lett.*, 116:010404, 2016.
- [57] Umweltbundesamt. Treibhausgas-emissionen in der europäischen union, <https://www.umweltbundesamt.de/daten/klima/treibhausgas-emissionen-in-der-europaeischen-union#textpart-1>, 2018.
- [58] R. M. Lutchyn, E. P. A. M. Bakkers, L. P. Kouwenhoven, P. Krogstrup, C. M. Marcus, and Y. Oreg. Realizing majorana zero modes in superconductor-semiconductor heterostructures. *Nature Rev. Mater.*, 3:52--68, 2018.
- [59] D. A. Huse, R. Nandkishore, V. Oganesyan, A. Pal, and S. L. Sondhi. Localization-protected quantum order. *Phys. Rev. B*, 88:014206, 2013.

ADDENDUM

I cannot tell which scientific breakthroughs will make it into history school books in 200 years. Quantum computers or the quantum internet paraphrased as the quantum revolution or the discovery of room temperature superconductivity are potential candidates. I am however sure, that the history books in 200 years will include a chapter on how we successfully prevented climate change. It is either that or no history books at all.

It is my firm belief that any other problem will soon be outweighed in importance and gravity by the global climate change. It is a serious problem not only because it does threaten the very existence of mankind, but furthermore it has transpired that only global solutions with the participation of virtually every living human on this planet stand any chance of changing our fate.

In this light, I think it is a valid and useful question to investigate what changes are necessary and realisable in the scientific community. Throughout this thesis, I calculated the CO₂-emission of the numerical simulations presented. In total, even if they are divided by the number of authors, they make up roughly 10% of the annual German CO₂-emission per capita. It is very hard if not impossible to compare this to the results achieved but what I would like to suggest is to raise awareness of the climate resources which are needed for numerical projects. Maybe sometimes it is not worth advancing the field incrementally if the climate costs are soaringly high. My feeling is that scientists do not really know how much CO₂ is actually emitted when they submit a flood of jobs to a high performance cluster and that this awareness could help to design numerics in a more climate friendly way. The far more devastating impact however is the offset of CO₂ for flights around the globe to visit other groups or attend conferences. A single flight to another continent easily makes up the largest share of a scientist's annual CO₂-emissions. Yet, the technology for having virtual conferences is already available and an investment in a meeting room equipped with cameras and screens would probably pay off in no time given the costs of hotels and flights.

So why are we still not changing our ways? I think climate change is a very uncomfortable topic for many people as its solution appears to be a massive transformation of society and lifestyle as we know it. It appears as if little changes we make have no meaning and even if we devote our lives to living carbon neutral, our neighbour can simply ruin our endeavours with their next business trip or holiday. This incentivises people to take a fatalistic stance in this question which evidently is also not helping.

I would like to stress that it very important to take the small steps first or at least make steps instead of sitting and waiting, which is obviously not a winning strategy here. Since the transformation we need extends to all facets of our lives, we should also change our ways as scientists - and this should happen rather sooner than later.

CO ₂ -emission of this thesis [kg]	10803
Total number of citations	18

ACKNOWLEDGEMENTS

First of all, let me thank **Jens Eisert** for granting me the opportunity to work in his group - a chance that came with great freedom and the concomitant responsibility. Not only did Jens trust me with such a great topic for my dissertation, he also brought me into contact with world-leading experimenters in Garching from whom I have learned so much. Being part of the group already since my Bachelor thesis, I always enjoyed the relaxed working atmosphere and the wonderful co-workers in the group, that seemingly counterintuitively lead to a very productive time for me.

Furthermore, I would like to thank my collaborators, **Ingo Roth**, for numerous discussions on topic far away from the quantum world, such as wine, jazz, typesetting and electronic devices of all kind, **Henrik Wilming**, enlightening me with his sheer endless knowledge about literally anything in physics, while still being one of the most down-to-earth people I know, **Albert Werner**, founding member of the many-body localisation part of the group, **Winton Brown**, for his crazy ideas on everything, **Marek Gluza**, whom I have gone to hell with and come back, **Christian Krumnow**, helping and supporting me in every aspect of my thesis, **Nicolas Tarantino**, for allowing me a glimpse of the unthinkable and lastly **Mathis Friesdorf**, who I am eternally indebted for his caring support during my graduate studies.

This thesis would not be what it is without the help of the ZEDV and especially **Jens Dreger** and **Jörg Behrmann**, who patiently helped me with stupid questions regarding numerics and IT problems. I would also like to thank **sheldon**[†], **yoshi**[†], **leonard**[†] and **tron** for their loyal services.

I would furthermore like to thank **Annette Schumann-Welde** and **Marianne Braun**, **Nathan Walk**, **Laura Baez**, **Dominik Hangleiter** and **Jonas Haferkamp** and **Frederik Hahn**, enduring members of men yoga, **Juani Bermejo-Vega** and **Ryan Sweke** and **Carlos Riofrio**, the best office mates ever and **Daniel Litinski** and **Philip Loche** as the last remnants of the honey table crew, for the great time I was allowed to spend with you at this department.

Lastly, I wish to thank **my family** and my partner **Carolin Lindemann** for the unlimited support and understanding.

CLIMATE FOOTPRINT CALCULATION

When we estimate the CO₂-emission of the performed numerical calculations, we use the following approach. The total hours are estimated using the wall time request for the cluster jobs - naturally this number is slightly higher than the actual runtime. To obtain the energy consumption, we use the thermal design power given by the manufacturer of the CPUs. We do not add any other energy consumption for cooling or other applications, which makes us confident that this should account for the overestimation of the runtime. Most importantly, we only base the calculation on the data that actually ended up in the paper or even a subset thereof. In practise, most of the CPU time is actually spent on prototyping. Also in many cases, more calculations were performed that did not end up in the final version of the paper. We think that the estimates given are hence very conservative and probably even an order of magnitude away from the actual CO₂-emission of the whole doctoral research.